Julia Woitischek,BSc

Geochemical and isotopic evolution of thermal waters in São Miguel, Azores (Portugal): Evidence for gas-water-rock interactions

MASTER'S THESIS

to achieve the university degree of

Master of Science

Master's degree programme: Earth Sciences

submitted to

Graz University of Technology

Supervisor

Univ.-Prof. Dipl.-Min. Dr.rer.nat., Martin Dietzel

Institute of Applied Geosciences

Graz, October 2015

AFFIDAVIT

I declare that I have authored this thesis independently, that I have not used other than the declared sources/resources, and that I have explicitly indicated all material which has been quoted either literally or by content from the sources used. The text document uploaded to TUGRAZonline is identical to the present master's thesis dissertation.

Date

Signature

First I would like to thank the European Community Action Scheme for Mobility of University Students (ERASMUS) supporting me financially with scholarships for conducting research on the Azores and in Palermo, and the KUWI Programme (TU Graz). I am also very grateful for the generous support of my family. Furthermore, I would like to thank my supervisor Martin Dietzel for his helpful comments and the possibility of working independently on the Azores, Santorini and in Palermo. I also want to thank José Virgilio de Matos Figueira Cruz for the invaluable help during the field work in São Miguel 2013. I would also like to acknowledge Andre Baldermann, Judith Jernej and Andrea Wolf for providing high quality data from solid as well as liquid solutions and Maria Hierz, Dorothee Hippler, Dietmar Klammer for helpful advice. I would also like to express gratitude to Albrecht Leis, Michael Böttcher and Mathias Gehre for the isotope measurements.

Abstract

Thermal water of São Miguel has been investigated to decipher its geochemical and isotopic evolution as a case study for the development of a geothermal system in an evolving basaltic ocean island. Besides water, precipitates and local volcanic rocks were sampled for analyses. From isotope, geochemical, microstructural and mineralogical data a conceptual model for water evolution in São Miguel (Furnas, Fogo, and Ferraria) was developed.

Thermal discharges were divided into springs (up to 75 °C) and boiling pools, and classified by dominant dissolved ions in Na-SO_4, Na-HCO_3 and Na-Cl types. In Furnas, at higher temperature the concentrations of $Si(OH)_4$, K^+ and Sr^{2+} increased through intensive alteration of basaltic rocks, whereas in contrast Al^{3+} and ∑Fe concentrations decreased by precipitation of e.g. alunite. In Fogo, at higher altitude in particular CO_2 rich water at T ≈ 20 °C occurs. In this case, the extent of basaltic rock leaching rather depends on uptake of volcanic CO_2 than on temperature. HCO_3^- concentration and its isotopic composition ($\delta^{13}C_{DIC}$ = -5 ± 3 ‰ V-PDB) reflect evolved CO_2 uptake and subsequent leaching progress. High SO_4 concentration of up to 16.5 mmol L^{-1} with $\delta^{34}S_{SO4}$= 0.35 ± 0.3 ‰ (V-CDT) are reflecting magmatic origin which mainly controls water chemistry of boiling pools of both, Fogo and Furnas. Lowest $\delta^{34}S_{SO4}$ = -3.7 ‰ (V-CDT) are accompanied by stromatolite-like microstructures in the precipitates. In Ferraria, water is discharging from a basal aquifer and belongs to the Na-Cl type, where stable hydrogen and oxygen isotopes reveal mixing of meteoric and sea water. The molar Mg/Ca ratio (≈ 0.77) of all thermal discharges reflects leaching of analysed local basalt (Mg/Ca ≈ 0.78).

Table of contents

Acknowledgement ii
Abstract iv
1. Introduction 6
2. Fundamentals 6
2.1 Water-rock interaction 6
2.2 Hydrothermal Alteration 10
2.3 Influence of volcanic gasses on fluids 12
2.4 Isotopic compositions of fluids 13
3. Sampling Site 17
3.1 Geological setting and the origin of the islands 19
3.2 Azores triple junction and hydrothermal vent fields 19
3.3 Plateau and hot spot 22
3.4 São Miguel 23
4. Methodology 26
4.1 Sampling 26
4.2 Analytics 29
5. Results 31
5.1 Mineralogical and chemical composition of the solids 31
5.2 Hydrogeochemistry of thermal water 32
5.3 Isotopic composition 35
6. Discussion 38
7. Summary and conclusion 63
8. References 67
9. Appendix 75

1. Introduction

Hydrothermal processes comprise of dissolution of natural rocks and re-precipitation of solids by the circulation of thermal fluids within geochemical cycling in hydro-, atmo-, bio- and lithosphere (e.g. Yardley and Bodnar, 2014). Hydrothermal activities are suggested to be linked to the development of early life and are known to control various mineral formations, in particular in respect to ore deposits (e.g. Guidry and Chafetz 2003, Hoffmann, 1973, Jones and Renaut, 2003, Konhauser et al., 2003, Phoenix et al., 2000, Piranjo, 2009). Moreover, a huge number of studies exists about the development of hydrothermal systems and their connection with alteration patterns of natural rocks and tectonic settings (e.g. Boyce et al., 2007, Cioni et al., 1992, Cruz et al., 1999, Cruz, 2003, Cruz et al., 2010, Delalande et al., 2001, German et al., 1996, Inguaggiato et al., 2005). These studies include aspects like the impact of volcanic gases, sea water contamination and/or rock leaching on the composition of thermal water. Although the general reaction mechanisms of hydrothermal systems are known, significant gaps of knowledge still exist in respect to the coupled influence of (i) compositions and sources of volcanic/magmatic gases on rock leaching, (ii) inorganically controlled precipitation versus biological activity, and (iii) the impact of sea water on thermal fluid composition versus volcanic rock alteration.

São Miguel, as an island of the Azores (Portugal), is an excellent case to study the development of a locally restricted thermal system and related geochemical cycles because, as a part of the Azores Archipelago in the Atlantic Ocean, it is almost isolated from continental impacts and composed of young volcanic rocks with still pronounced volcanic activities. In the present study, 33 natural solutions and 8 local volcanic rocks and precipitates were sampled in São Miguel, belonging to three different volcanoes, named Furnas, Fogo and Sete Cidades (Ferraria area) volcano, for mineralogical, geochemical, isotopic, and microstructural analyses. The aims of the present study are (i) to decipher the geochemical and isotopic evolution of the thermal water of São Miguel and (ii) to develop from this case study a conceptual model for a hydrogeothermal system in an evolving basaltic ocean island.

2. Fundamentals

2.1 Water-rock interaction

Water as a critical solvent contains dissolved components like hydrogen ions, hydroxyl ions, inorganic salts as well as dissolved gases like CO_2 and O_2 and organic molecules. These components interact with each other and with the mineral surface. Moreover, fluid-solid interaction influences the surface layer of crystals as well as the boundary layer of the fluid. A boundary layer signifies the direct contact with fluid and mineral

surface. Furthermore, its thickness is a function of the bulk fluid and the advection transport velocity (Figure 1) (Lüttge and Arvidson, 2008).

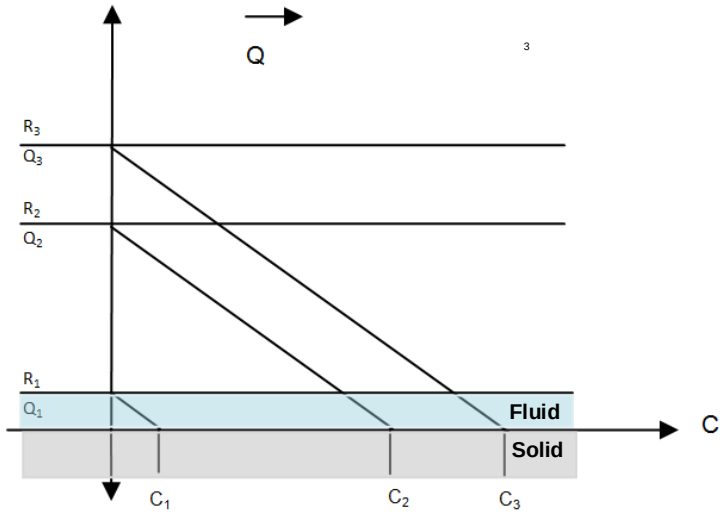

Figure 1 Schematic boundary layer (solid: surface layer of crystal, fluid: liquid) and its various thickness as a function of advection velocity and dissolved components. R is an abbreviation for dissolution rate of a mineral, Q is the advection velocity of the overlying bulk fluid and C gives information about the centration at the interface. R1-Q1 shows a slow dissolution rate of an undersaturated solution with respect to a given mineral; R2-Q2 stands for an intermediate dissolution rate with at moderate undersaturation state; R3-Q3 implies a rapid dissolution rate (modified after Lüttge and Arvidson, 2008).

The structure of crystal surfaces has to be distinguished from bulk crystal structure itself. Those differences imply a force for reorganisation and exchange of the surface with the fluid, which is driven by hydration and adsorption of dissolved components (Lüttge and Arvidson, 2008). Hence, micro- and macroscopic structures give information about the environment of formation as well as prevailing thermodynamic and kinetic conditions of the process: for instance, the distribution of dislocations, and development during crystallisation and grow. These features are important for dissolution processes because they act like weakness points of a crystal lattice. Surfaces with a high density of dislocations will have a higher reactivity than surfaces with less dislocations.

2.1.1 Sorption-Desorption Reactions

The process of sorption includes adsorption and absorption. Adsorption implies the accumulation of substances and the development of an interface between two phases e.g. combination of the surface of solid particles, air or water interface, but without the formation of three-dimensional crystal structures (Chorover and Brusseau, 2008). The inverse process is desorption and refers to the loss of matter. Sorption-desorption processes effect the concentration of components in fluids and at mineral surfaces. These processes control also the structure and reactivity of particles surfaces. Moreover, transport processes are important for these reactions, which include advection and diffusion in a liquid, solid phase diffusion, surface diffusion, intraparticle

diffusion and diffusion in liquid filled meso- and/or macropores (Chorover and Brusseau, 2008).
Adsorption can be expressed by a chemical reaction, proceeding from the left to the right (see Figure 2). Desorption reacts from the right to the left:

$$SFG(s) + x(aq) \leftrightarrow SFG - x(s) \quad (1)$$

In Eq. 1 SFG implies a surface functional group, x is a shortcut for the adsorptive species in a fluid and SFG – x(s) reflects the adsorbent-adsorbate surface product. Examples for SFG are surface hydroxyl groups of Al^{3+}, Fe^{3+}, Mn^{2+} or Si^{4+} oxides as well as hydroxides and natural organic components. The development of surface complexes, inner and outer surface complexes, and diffuse ion swarms reflected the adsorbent and adsorbate specificity (Figure 2). These complexes differ in the rate of reversibility of sorption reactions, for instance, inner-sphere complex formations are slower and less reversible compared to outer-sphere complex formations (Chorover and Brusseau, 2008).

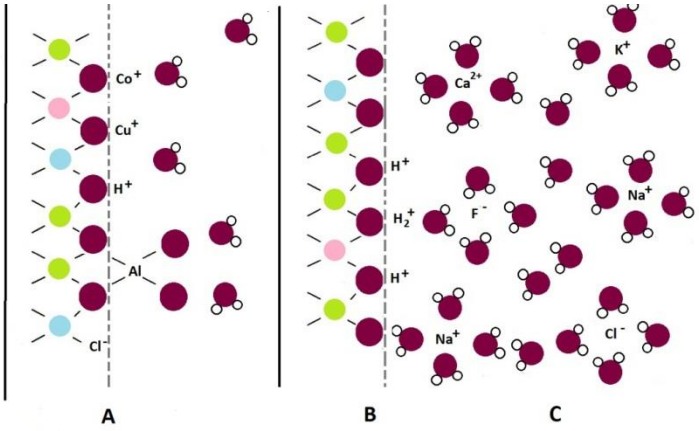

Figure 2 Schematic illustration of inner-sphere complexation (A), outer-sphere complexation (B) and diffuse swarm adsorption at a hydroxylated mineral surface.

2.1.2 Dissolution Reactions

Mineral dissolution processes affect the physical and chemical nature of sceneries as well as the quality of water. In general, dissolution is reducing the connectivity of network atoms caused by processes like precipitation and hydrolysis. Dissolution of a mineral $A_{\xi a}B_{\xi b}$ described by:

$$A_{\xi a}B_{\xi b(s)} \rightarrow \xi a A^{q_A}_{(aq)} + \xi b B^{q_B}_{(aq)} \quad (2)$$

and the rate of reaction r':

$$r' = -\frac{d[A_{\xi a}B_{\xi b}]}{dt} = \frac{1}{\xi a}\frac{d[A_{aq}]}{dt} = \frac{1}{\xi b}\frac{d[B_{aq}]}{dt} \quad (3)$$

[x] implied the concentration of species x, ξ_x is the stoichiometric coefficient of the reaction, t stands for time and q_x is the charge of the aqueous species in the solution.
Equation 3 describes the mineral dissolution with the increase in concentration of solutes as a function of time. During long term experiments, dissolution rates decrease as a function of time (Brantley, 2008). Two types of dissolution mechanisms exist, the stoichiometric and the nonstoichiometric or incongruent one. In the second case, the stoichiometry of the solution, where dissolution takes place, is not equal compared to the dissolving mineral, which implies secondary solid phases formation, adsorption phenomena or/and different leaching behaviour of elements from mineral surface. Nonstoichiomeric dissolution is common for dissolving silicates at moderate pH-values (Brantley, 2008). Besides pH, an influence factor for the development of leaching layers is the Al^{3+}/Si^{4+} ratio e.g. of feldspar. The dissolution-rate of plagioclase increases with the Al^{3+}/Si^{4+} ratio.
Alteration layers grow on silicate mineral surfaces through dissolution processes of silicates, where the release of $Si(OH)_4$ is less compared to that of cations (Brantley, 2008). Furthermore, simple diffusion across a leaching layer cannot be explained by the sharp interface between surface layer and bulk material. Processes like reprecipitation and reconstruction also have to be considered.

Dissolution could also have an effect on pH distribution according to sorption of protons and on bridging oxygens (Furrer and Stumm, 1983; Brantley, 2008); for instance the development of positively and negatively charged surface components like $[\equiv SOH_2^+]$ and $[\equiv SO^-]$. The dissolution rate r' according to Brantley (2008):

$$r' = k_H[\equiv SOH_2^+]^{q1} + = k_{OH}[\equiv SO^-]^{q2} \quad (4)$$

with q_1 and q_2 as constants. This model suggested that the dissolution rate of metal oxides is slowest at pH_{ppzc} (pH of pristine point of zero charge) (Brantley, 2008).
Moreover, dissolved cation concentration in a solution has an effect of further mineral dissolution; for instance, amount of dissolved inorganic salts like halite for gibbsite dissolution because of ionic strength effect on Al^{3+} activity. Moreover, feldspar dissolution in acidic liquids related to the aspiration of H^+ and other cations on the surface of it. In contrast to feldspars, low concentration of alkaline earth and alkali cations increase the dissolution rate of quartz and amorphous silica (Brantley, 2008).

The CO_2 concentration has a direct effect on pH value as well as on dissolution-rate. The adsorption of inorganic carbon species on mineral surfaces can influence the dissolution behaviour of Ca^{2+} and Mg^{2+} silicates and Fe^{3+} oxides (Wogelius and Walther, 1991; Berg and Banwart, 2000; Brantley, 2008). Temperature is also an important parameter for the mineral dissolution behaviour and the distribution of aqueous species. In most cases: the higher the temperature the more can be dissolved. Nevertheless, exceptions exist, and among them are carbonates. Another point to be made, the dissolution behaviour depends on the formation of an isotropic or anisotropic crystal lattice, therefore, amorphous solids dissolve easier compared to crystalline phases, even though they have the same composition e.g. SiO_2(amorph) vs. quartz (Sigg and Stumm, 2011).

To check if the thermodynamic equilibrium between host rock and water is reached, the saturation index (SI) is used. The saturation index gives information whether given solid phases can be dissolved or precipitated:

$$SI = log(IAP|Ksp) \tag{5}$$

Accordingly, the SI is defined as the ratio of the ion activity product (IAP) and the solubility product (Ksp) of a solid phase. If the SI is 0 thermodynamic equilibrium between solid and water is reached. SI below 0 reflects undersaturation. In contrast positive SI values correspond to supersaturation and the given solid phase could be precipitate.

2.2 Hydrothermal Alteration

2.2.1 Epithermal alterations

Chemical alterations are forming petrologically and chemically different hydrothermal mineral phases. Epithermal systems and their mineral assemblages vary as the result of rock type, fluid type (acidic, neutral, near neutral chloride), temperature, pressure, time, permeability and rock/water ratio. High– sulfidication (HS^-) epithermal systems are developed in two stages: (1) an early stage with advanced argillic alteration with acidic conditions and a second ore forming phase (2) with acid high mineralisation fluids circulating in pores (Boyce et al., 2007). At lower temperature (<180 °C) main mineral phases that precipitate in acid-sulphate geothermal fluids are kaolinite, alunite, gypsum, sulphides and different kind of SiO_2 (Piranjo, 2009).

Hydrothermal alteration of potash feldspar to kaolinite:

$$4K[AlSi_3O_8] + 4H^+ + 4HCO_3^- + 2H_2O \rightarrow Al_4((OH)_8|Si_4O_{10})) + 8SiO_2 + 4K^+ + 4HCO_3^- \quad (6)$$

H^+ is consumed and K^+ is released.

Acid leaching is responsible for the hydrothermal alteration of kaolinite to alunite (Piranjo, 2009):

$$3Al_2Si_2O_5(OH)_4 + 2K^+ + 6H^+ + 4SO_4^{2-} \rightarrow 2KAl_3(SO_4)_2(OH)_6 + 6SiO_2 + 3H_2O \quad (7)$$

Alunite is often associated with intense leaching zone, which is porous and siliceous (Piranjo, 2009).

Dissolution and precipitation of silica is one of the most common characteristics of active hydrothermal systems. The solubility of silica in water increases with temperature as follows (Piranjo, 2009). Silica supersaturated fluids tend to precipitate amorphous silica and with time chalcedon or fine grained quartz can be formed. At 250 °C e.g. pyrophylite, diaspor and andalusite can be formed (Piranjo, 2009). All these mineral phases belong to advanced argillic alteration.

2.2.2 Hot spring siliceous sinter

Precipitation of siliceous sinter in hot springs is controlled by organic and inorganic processes. The dominant mineral of the modern hot springs is opal- A ($SiO_2 \cdot nH_2O$) (Jones and Renaut, 2003). Biotic processes can be divided into active and passive microbial precipitation. Bacterial taxa, which have the ability to precipitate silica, include cyanobacteria, chemoorganotrophic bacteria (Krumbein and Werner, 1983; Guidry and Chafetz, 2003) as well as sulphate reducing bacteria (Birnbaum and Wireman, 1984), green bacteria and diatoms (Fernandez-Turiel et al., 2005).
Active precipitation is limited by vital effects of organism. As a result, these effects induce precipitation of amorphous silica (Guidry and Chafetz, 2003). In general, the silicification process of organisms is very fast e.g. 0.75 mm/month (Xiaotong and Jones, 2012). Consequently, bacteria are still alive during this process (Guidry and Chafetz, 2003). Apart from that, sulphate reducing microbes are able to change pH values and these modifications can induce silica precipitation (Birnbaum and Wireman, 1984). However, there are studies, which prove the ability of organisms to bind metal ions in a solution and precipitate them. Although the precipitation process has already started, some bacteria can be cultured

(Phoenix et al., 2000; Guidry and Chafetz, 2003). On the other hand, the passive organic precipitation needs a template for precipitation or an organic substrate (Guidry and Chafetz, 2003) and the silicification process continues without any control of the microorganism. Apart from that, inorganic processes like the cation effect, rapid cooling, evaporate conditions and the change of pH value influence the formation of sinter precipitates (Guidry and Chafetz, 2003).

Siliceous sinters also provide insights into the primeval earth and the associated biofacies, like the Precambrian cherts because present day hydrothermal deposits are similar to ancient ones and to the Archean oceans (Siever, 1992; Konhauser et al., 2003).

The reason why the present day organisms in siliceous precipitation are identified as stromatolites is the loss of details of cytoplasm as well as cell wall structure with the silicification process (Konhauser et al., 2003). According to Walter (1976) such structures are named “Geyserite”.

During the sinter evolvement various kinds of opal-A can be formed in silica supersaturated fluids. It includes, for instance, processes of replacement of organic substrates, precipitation as cement, deposition and redeposition with several accessory minerals (Jones and Renaut, 2003).

2.3 Influence of volcanic gasses on fluids

Volcanic gases emit at the Earth`s surface and have their origin in magma degassing processes. Main components of these gases are carbon dioxide, carbon monoxide, hydrogen sulphide, sulphur dioxide, trace components and halogen gases. The SO_4^{2-}, Cl^- ,F^-, HCO_3^-, and B contents of water are linked to fluxes of magmatic outgassing (Martin-Del Pozzo et al., 2002). The emitted gases differ from each other as a function magma type, its differentiation and activity of volcanoes, for instance, chlorine derived from andesitic magma (Edmonds et al., 2001). They also show differences in their solubility behaviour and react with liquids to form acids or bases. The dissolution of gases depends on temperature for instance an increase of temperature causes a decrease in the saturation value of oxygen (Dietzel, 2014).

The behaviour of sulphur bearing components depends on their speciation in vapour (Di Liberto et al., 2002). Oxidation/Hydration processes are important to create sulphurous acid described in Eq. (8):

$$SO_2 + 1/2\ O_2 + H_2O \leftrightarrow H^+ + HSO_4^- \quad (8)$$

The formation of sulphurous acid lowers the pH-value.

Due to the hydration of CO_2 the pH values decrease because of the development of H_2CO_3. However, acidic water, as a result of dissolved acid gases in water, interacts

with rocks as a neutralisation process and therefore cations are released (Armienta et al., 2008). Lowest degree of neutralisation implies still a high percentage of H^+. The concentration of release of rock derived cations is generally higher at low pH values.

2.4 Isotopic compositions of fluids

As a result of the water-rock interaction, some isotopic tracers are non-diagnostic, for instance, in terms of sources of fluids and metals (Piranjo, 2009). In addition, especially in costal volcanic areas, seawater is involved during water-rock interaction, which leads to an isotopically and chemically unique thermal system (Saki and Matsubaya, 1977). Other useful stable isotope systems would be noble gases like He, Ar and Ne to get information about the role of the mantle as the source of volatile components in hydrothermal discharges (Piranjo, 2009).

2.4.1 Hydrogen and Oxygen

Hydrogen has three isotopes, including two stable and one radiogenic. Among the stable ones are ^1H (protium) and ^2H (deuterium) which is also known as D. They occur naturally and their abundances are (Rossmann and Tylor, 1998; Hoefs, 2009):

^1H: 99.9885 %
D: 0.0115 %

^3H, tritium, is radiogenetic with a half-life of 12.5 years (Hoefs, 2009). The international reference standard is Vienna Standard Mean Ocean Water abbreviated to V-SMOW. The δD-values for natural waters on Earth are mostly negative because of the high D/H ratio of the V-SMOW.

δ is given by the formula:

$$\delta = (R_{sample}/R_{standard} - 1) * 1000 \quad (9)$$

R is the ratio of respective isotopes. In addition, negative or positive δ values represent depletion or enrichment in respect of the standard (given in ‰). These variations are the result of fractionating processes, which have their origin mostly in mass difference of the two isotopes. Responsible mechanisms for isotopic fractionation are (Misra, 2000; Piranjo, 2009):

- Isotope exchange reactions between phases that contain the same element
- Bacteriogenic mediated reactions

- Mass differences caused by phase transition like evaporation, melting, condensation and crystallisation. Other processes are diffusion processes and adsorption.

Hydrogen isotope fractionation processes are explained by phase transitions like precipitation/evaporation and/or condensation/boiling. Differences in the isotopic composition are related to differences in vapour pressure of water and their freezing points. For example, the vapour pressure of HDO is lower than of H_2O (Hoefs, 2009). In respect of the differences in vapour pressure, the concentration of D is higher in the liquid phase than in the vapour phase (Hoefs, 2009). With reference to a study of Horita and Wesolowski (1994) it is shown that isotope fractionation at equilibrium decreases rapidly, concerning to increasing temperatures and become nearly zero at about 250 °C (Hoefs, 2009).

Oxygen has three isotopes too, but all of them are stable. Furthermore, it is the most abundant element on Earth. The three isotopes with their abundances (Rossmann and Tylor, 1998; Hoefs, 2009) are:

^{16}O: 99.757 %
^{17}O: 0.038 %
^{18}O: 0.205 %

Common reference standards for the oxygen isotope system are V-SMOW and V-PDB (Vienna Pee Dee Belemnite). In general, the V-PDB scale is used mainly for studies of carbonates while VSMOW is used for most other applications.

Most isotopic signature of geothermal water indicates a meteoric origin. In particular the $\delta^{18}O$ values are different compared to the meteoric water due to evaporation and also because of the water-rock exchange of oxygen isotopes (Aguilera et al., 2005). Thus, the isotopic composition depends also on the original rock type and on the water-rock interaction in past. In the case of magmatic water the isotopic signature is strongly influenced by the source of magma and the interaction with the wall rocks during cooling processes (Figure 3).

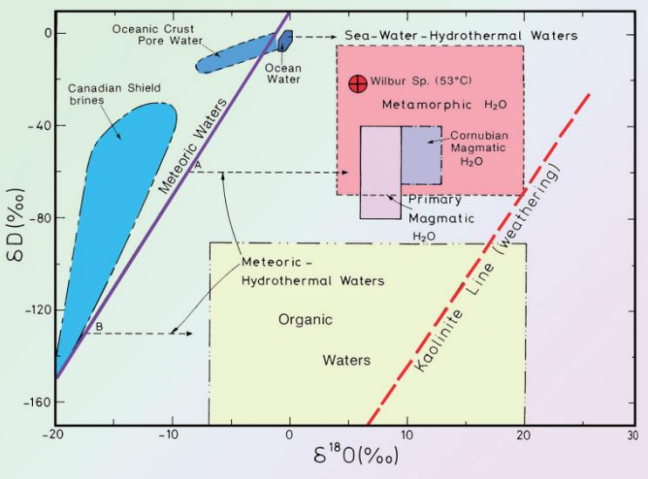

Figure 3 Stable isotopic compositions of natural waters of different origins e.g. magmatic, metamorphic and ocean waters. Noticeable is that magmatic waters are enriched in $\delta^{18}0$ as well as metamorphic water. However, hydrothermal fluids occur on the right side of the global meteoric waterline and therefore show enrichment in $\delta^{18}O$ (Yardley and Bodnar. 2014; modified from Sheppard, 1986).

2.4.2 Sulphur

Sulphur has four stable isotopes and one radiogenic isotope. The four stable isotopes with their abundances (Rossmann and Tylor, 1998):

^{32}S: 95.05 %
^{33}S: 0.75 %
^{34}S: 4.2 %
^{36}S: 0.017 %

^{35}S is the radiogenic one with its short-time life of 85 days. $\delta^{34}S$ values show the ratio of $^{34}S/^{32}S$ of sulphur-bearing components like sulphate, sulphide, SO_2 as well as H_2S. The iron meteorite, named Canyon Diablo Troilite, is used as the international standard. The S-bearing components can be found in magmatic and hydrothermal waters, when they originate e.g. from the mantle ($\delta^{34}S \approx 0‰$) or modern seawater ($\delta^{34}S \approx 20‰$) or have sedimentary origin (wide range of negative values) (Piranjo, 2009). In general, enriched $\delta^{34}S$ values of dissolved SO_4^{2-} have their origin in the dissolution of marine calcium sulphate rocks consisting of e.g. gypsum or anhydrite. In contrast, $\delta^{34}S$ values triggered by magmatic or microbial processes are difficult to distinguish, which is caused by their overlap with each other (Szynkiewicz et al., 2012). Also both processes (organic and inorganic) can be found in modern hydrothermal active settings. Areas of hot acid discharges tend to have a higher biomass but a lower bacterial diversity and it is mainly dominated by thermoacidophic S- metabolizing microbes, which are responsible for the reduction of elemental S and the oxidation of H_2S (Szynkiewicz et al., 2012). However, $\delta^{34}S$ of S- bearing components like sulphate

and sulphide in hydrothermal systems are controlled by temperature, pH-value and activity of bacteria.

2.4.3 Carbon

The most important carbon reservoirs on Earth are marine carbonates and organic material. Carbon occurs in a widespread spectrum of organic and inorganic compounds. It has two stable isotopes and their abundances are (Rossmann and Tylor, 1998; Hoefs, 2009):

^{12}C: 98.93 %

^{13}C: 1.07 %

Carbon stable isotope ratios are commonly expressed as $\delta^{13}C$ values versus the international reference standard for carbon isotope measurements VPDB (Vienna Pee Dee Belemnite) $\delta^{13}C$ of dissolved inorganic carbon ($\delta^{13}C_{DIC}$) is used for hydrothermal water to determine if a source of carbon has its origin in igneous or organic processes (Piranjo, 2009).

As a result of kinetic effects during photosynthesis, organic material increases the light ^{12}C isotope. Their $\delta^{13}C$ values range between -15 to -40 ‰, so the mean $\delta^{13}C$ is around -25 ‰ (Hoefs, 2009). The isotopic values for magmatic CO_2 and mantle carbon range between -4 and -8 ‰ (Deines and Gold, 1973; Kyser, 1986; Aguilera et al., 2005 Hoefs, 2009). $\delta^{13}C$ values of DIC can be locally affected by the input of external carbon from distinct isotopes sources and/or by secondary processes like precipitation, dissolution as well as CO_2 degassing (Delalande et al., 2011).

To estimate the $\delta^{13}C$ of gaseous CO_2 from $\delta^{13}C$ values of DIC the fractionation factors for carbonate species for different temperatures following equations were used considering isotopic equilibrium Eq. 10 and 11:

$$\delta^{13}C_{GAS} = \frac{(\delta^{13}C_{DIC}+10^3)}{\alpha_{DIC}} - 10^3 \quad (10)$$

$$\alpha_{DIC} = x_{H2CO3*} * \alpha_{\mathrm{H2CO3*}} + x_{HCO3-} * \alpha_{HCO3-} + x_{CO32-} * \alpha_{CO32-} \quad (11)$$

(e.g. Dietzel et al., 1997). α denotes the fractionation factor, which is defined as the quotient of the $^{12}C/^{13}C$ ratio of $CO_{2(g)}$ and of H_2CO_3*, HCO_3^- and CO_3^{2-}, respectively. x is the molar fraction of $CO_{2(aq)}$,HCO_3^- and CO_3^2 in the particularly case of DIC.

3. Sampling Site

The Azores Archipelago is located in the North Atlantic Ocean between latitudes of 36°55'43''N and 39°43'23''N and longitudes of 24°46'15''W and 31°16'24''W (Cruz et al., 2010). The distance to the European Continent, for instance the west-coast of the Portuguese mainland, is about 1500 km (Cruz and França, 2006) (Figure 4). The Azores are divided into nine islands, which build up a chain. These islands are divided into three groups (Figure 4).

- The Western Group: Flores and Corvo islands
- The Central Group: Terceira, Graciosa, São Jorge, Pico and Faial islands
- The Eastern Group: São Miguel and Santa Maria islands

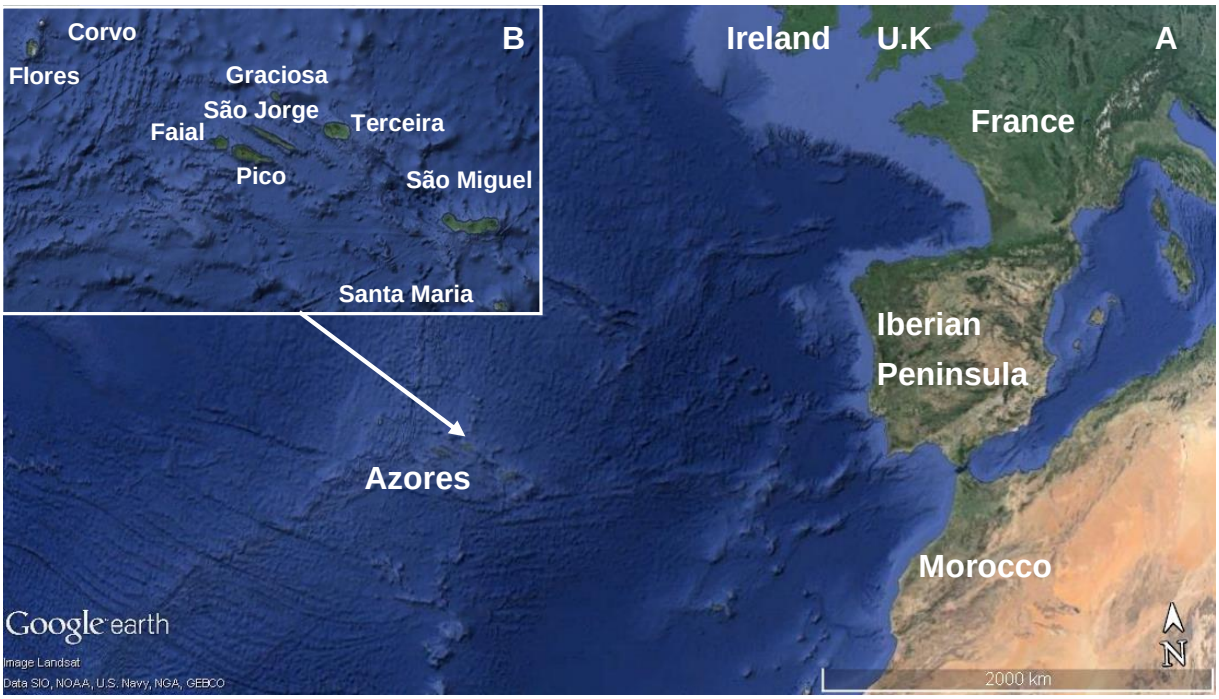

Figure 4 A: Geographic position of Azorean Archipelago (white arrow) in the North Atlantic. (Google Inc, 2015) ; B: Azorean Islands. Between the Western and Eastern Group is the Central Group with Terceira, Graciosa, São Jorge, Pico and Faial islands (modified after http://upload.wikimedia.org/wikipedia/commons/e/e3/AzoresLocation.png, May 2015).

The whole area of these islands covers about 2333 km^2 with approximately 240 000 inhabitants (Cruz and França, 2006). All nine islands are coming up from depths about 2000 m and rise over time 2000 m above sea level (Luis and Neves, 2006). The ages of the Azorean Archipelago are varying (Figure 5). The island of Santa Maria is the oldest one and evolved during the Miocene in contrast to São Miguel, which has its origin in Pliocene, and all the others emerged during the Quaternary (Madeira,1990). The youngest of all islands is Pico with 0.037 My (Trota, 2013).

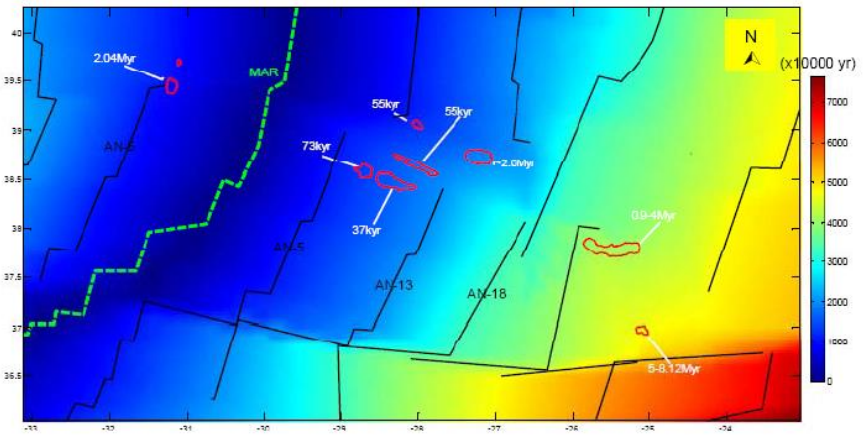

Figure 5 Ages of the Azorean Archipelago (Trota, 2013). Isotopic age (K-Ar) from rocks of the islands shows for Santa Maria 8.12 My, São Miguel 4.01 My, Terceira 2 My, Graciosa 0.62 My, São Jorge 0.55 My, Pico 0.04 My and Flores 2.04 My (Abel- Monem et al., 1968; Madeira, 1990)

Since the settlement of the islands in the 15th century volcanic activity has been reported. From 1439 to the present there were about 33 inland volcanic eruptions (Zbyszewski, 1963; Madeira,1990) (Figure 6) as well as several offshore ones.

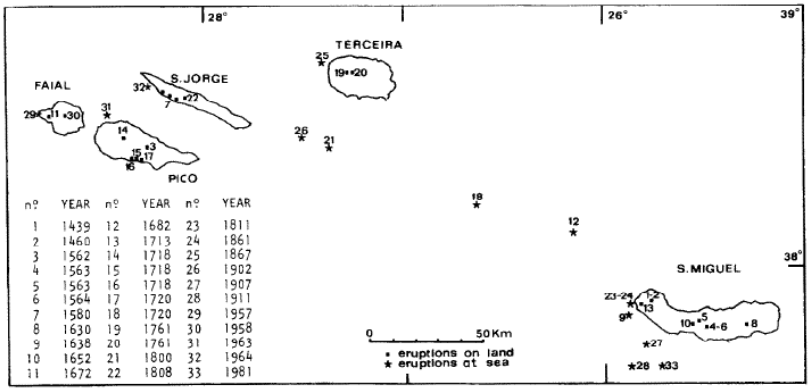

Figure 6 Volcanic eruptions since 1439 in the Azorean islands (modified from Weston1963, 1964; Madeira, 1990).

The Azorean climate can be divided into a wet and a warmer dry season (Ferreira, 1980). Wet season is characterised by lower temperatures (average temperature is approximately 17 °C) and by 75 % of the annual precipitation (DROTRH/ING, 2001). Because of the position of the Azores (open to tropics and North Pole) there is an interaction between the marine and the cold air masses from the pole (Ferreira, 1980). Accordingly, the climate can be described as marine temperate (Cruz, 2003) with a high air humidity that could reach 100 %. In addition, the average value of annual precipitation is about 1930 mm and for evapotranspiration 510 mm (DROTRH/INAG, 2001). To sum up, the annual precipitation exceeds the evapotranspiration.

3.1 Geological setting and the origin of the islands

All of these islands are located at the Mid-Atlantic Ridge. Dynamic processes are responsible for the elevation of the ocean floor such as surface expression of a mantle plume (White et al., 1976, McKenzie and O'Nions, 1995). The archipelago is located at the triple point of American, Eurasian and African lithospheric plates. In addition to this, there are three main tectonic features (Guest et al., 1999) (Figure 7):

- The Mid-Atlantic Ridge (MAR) between the Western and the Central Groups; it separates Eurasia and Africa from the American plate
- The East Azores Fracture Zone (EAFZ) which extends east–west from the MAR to Gibraltar
- The Terceira-Rift from Santa Maria island to MAR

In general, all fracture systems have a WNW-ESE trend (Guest et al., 1999).

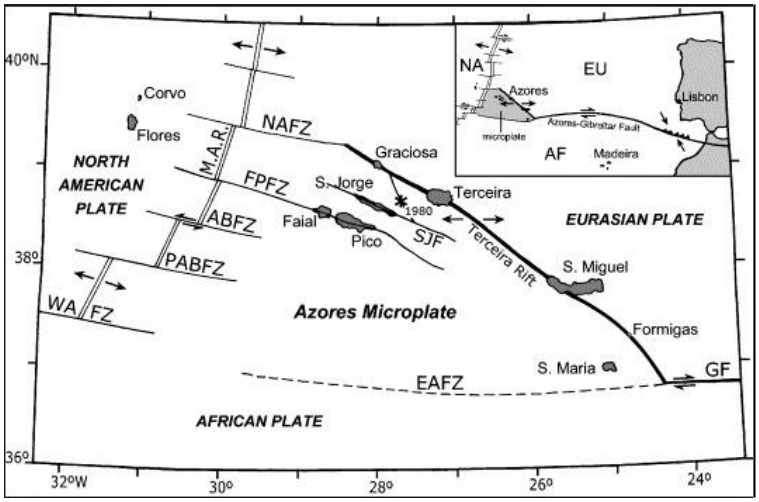

Figure 7 Geotectonic framework of the Azores Triple Junction of the Eurasian, African and North American plates. Between the Western Group and the Central Group runs the Mid- Atlantic Ridge (M.A.R). . Furthermore, it also separates Eurasia and Africa from the American plate (Guest et al., 1999).

Volcanic activity varies from effusive eruption characterised by a steady outpouring of lava to explosive events with magma fragmentation. Therefore, on the islands, several hydrothermal solutions are discharged, including mineral and thermal spring water. Moreover, fumarolic grounds occur all over the archipelago.

3.2 Azores triple junction and hydrothermal vent fields

The Azores triple junction (ATJ) is located, where the American, Eurasian and African (Nubia) lithospheric plates meet (Figure 7) with coordinates of 39°N and 30°W (Madeira, 1990). It is marked by a ca. 15 % decrease in MAR seafloor spreading rates (Marques et al., 2013). Marques identified that the spreading rates decrease from 22.5 mm/yr N of 40°N to 19.5 mm/yr S of 38°N. All nine islands move relative to the African plate with 1 ± 0.5 mm/yr. There was a triple junction jump, although it is still

unclear if it was triggered by the mantle plume (Luis and Neves, 2006). The movement started about 36 MA from the Mid Atlantic Ridge (MAR) and the East Azores Fracture Zone (EAFZ) to its current location (Luis et al., 1994; Yang et al., 2006).
Three different geodynamic models exist (Madeira, 1990):

- Terceira Ridge model (Figure 8)
- Azores microplate model (Figure 9)
- Leaky transform model (Figure 10).

However, the plate boundary between the African and the European plate is still not defined (Neves et al., 2013). Forjaz (1988) and Madeira (1990) believe that this boundary crosses São Miguel.

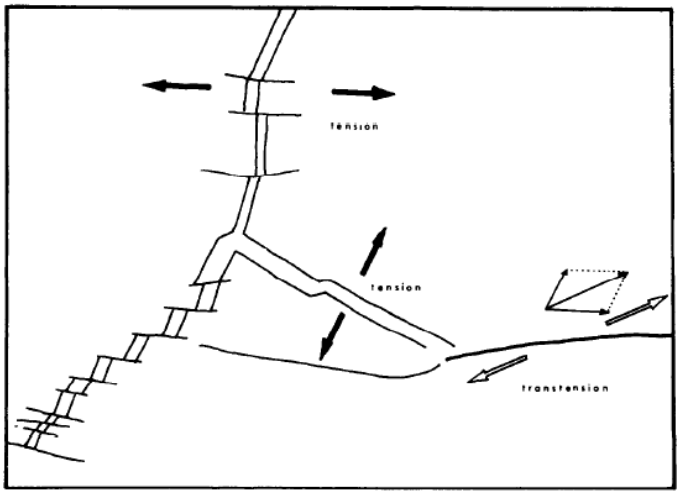

Figure 8 Terceira Ridge model: northeast movement of the Eurasian lithospheric plate with respect to the African one is triggered by seafloor spreading in MAR and Terceira Rift (modified from Buforn et. al., 1988; Madeira, 1990).

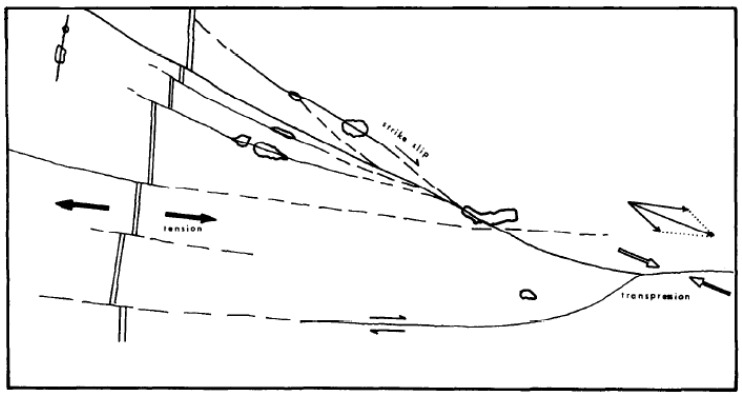

Figure 9 Azores microplate model: Forjaz suggested triangular shape of the microplates with several borders like MAR and EAFZ (after Forjaz, 1988; Madeira, 1990).

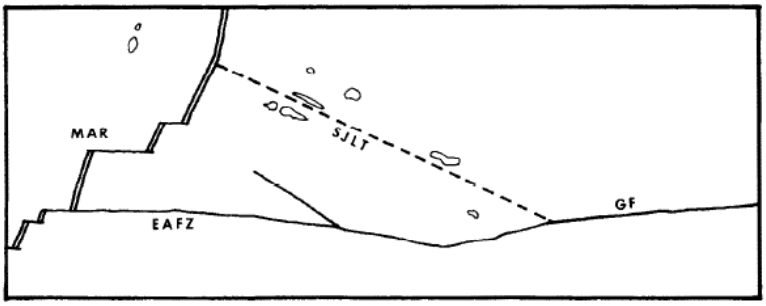

Figure 10 Leaky transform model: result of the east-west spreading of the MAR is a leaky transform structure (Madeira, 1990).

German (1996) identified along a distance of 200 km of the MAR between coordinates of 36° and 38° N seven signs for the existence of hydrothermal activity. Tectonic features such as cross cutting faults, MAR and its spreading rate are suggested to be the controlling factors for hydrothermal vents. To conclude, the numbers of hydrothermal vents increase as a result of the increase-rate of ridge spreading (Desbruyères et al., 2001). Therefore, in the vicinity of the hydrothermal fields the ridge axis is getting shallower. There are three famous hydrothermal vent fields close to the ATJ: Mendez Gwen (840 m), Lucky Strike (1700 m) and Rainbow (2300 m) (Desbruyères et al., 2001; Colaço et al., 2006) (Figure 11). All fields can be distinguished by their anomalously thick crust, different depths and temperatures, elemental composition of the hydrothermal fluids, biogeography as well as bioaccumulation of metals. The variability of hydrothermal waters in different vents also affects the bioaccumulation of elements in many marine animals. For instance, the same species at Mendez Gwen shows a higher Hg but lower lower Cu and Zn content compared to individuals of Lucky Strike and Rainbow sites (Colaço et al., 2006).

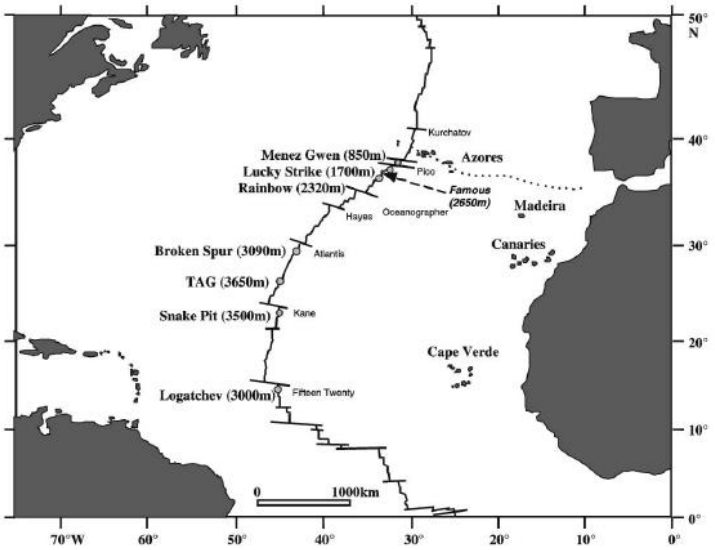

Figure 11 Map for hydrothermal vent fields between 0° and 50° N. Mendez Gwen, Lucky Strike and Rainbow fields are located next to the Azores triple junction (Desbruyères et al., 2001).

3.3 Plateau and hot spot

The volcanic Azorean plateau is about 20 My old and was formed during a high melt production supplied by a hotspot in the area of the Mid-Atlantic Ridge (MAR) (Cannat et al., 1999). Moreover, the production of melt is controlled by the interaction of the hot spot and the ridge melting zones. For this reason, a volcanic archipelago has been formed on the top of the plateau that evolved around 7 My ago. In this region of the North Atlantic, the hot-spot-ridge interaction has taken place since 85-95 Ma (Gente et al., 2003). The surface of the plateau was formed by magmatic and tectonic activities (Silveira et al., 2006). In addition, the geometry of the triple junction had an effect on its evolution (Georgen and Sankar, 2010). Apart from that, it consists mainly of alkaline basalts, which are very heterogeneous in their isotopic composition with a high volatile content (Silveira et al., 2006).
In contrast to moving plates, hot spots are a relatively fixed source of volcanism. The origin of plumes could be deep in the mantle, either the core mantle boundary or the transition zone. Due to their origin, hot spots are associated with temperature, topographic, gravimetric anomalies and differences in basalt geochemistry compared to normal Mid Ocean Ridge Basalts. Apart from that, there are two types of hot spots along the MAR (Montagner, 2001; Silveira et al., 2006):

- Hot spots with negative seismic signature, which is not deeper than 300 km
- Hot spots with an origin in the transition zone or even deeper, like the one in Iceland

The hot spot of the Azores is quite young indicated by a high volume of volcanism on a slow moving plate. Compared to the plume of Hawaii the melting conditions are different, for instance, it is not as hot as Hawaii (Beier et al., 2012). Furthermore, the size of the Azorean hot spot is smaller compared to the hot spots of Hawaii and Iceland. As a result of the classification of Montagner, the Azorian hot spot belongs to the first type. Moreover, beneath the Azores is a deep vertical anomaly. It is clearly visible at 100 km depth and it disappears around 300 km caused by differences in S- wave velocities (Figure 12).

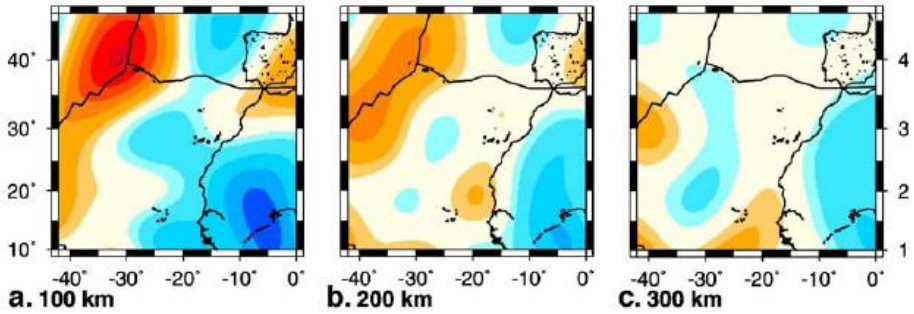

Figure 12 Different body wave travel time velocities for different depths between 100 and 300 km. For 100 km the negative anomaly increases more than 5 % (compared to others depths), at 200 km the anomaly is still in evidence and at 300 km the anomaly disappears (Grand, 1994).

Calculated mantle temperatures beneath the Azores range between 1350 and 1480 °C (Herzberg and Asimow, 2008). For this reason, the U- Th-Pa disequilibrium can be used as an indicator for the upwelling velocity. The U- Th-Pa disequilibrium of Terceira is higher than underneath all other islands. This suggested that the plume is situated under Terceira (Beier et al., 2012). Another argument for the plume situation in the vicinity of Terceira could be the $^{187}Os/^{188}Os$ ratios that vary from 0.128 to 0.198 compared to the range for the whole Azorean archipelago with 0.122 to 0.195 (Widom and Shirey, 1996). Also the lowest $^{3}He/^{4}He$ with a minimum value of 64 000 (Moreira et al., 1999; Bourdon et al., 2005) and the highest $^{20}Ne/^{22}Ne$ ratios are indicators that the plume is situated nowadays under Terceira (Madureira, 2005). In spite of this, another model suggests that the plume is located northeast of Terceira island (Yang et al., 2006) (Figure 13), because of its higher upwelling velocity with 30-40 mm/yr compared to the surrounding vicinity (Yang et al., 2006). Nevertheless, Schilling (1991) considered the plume should be somewhere near Faial.

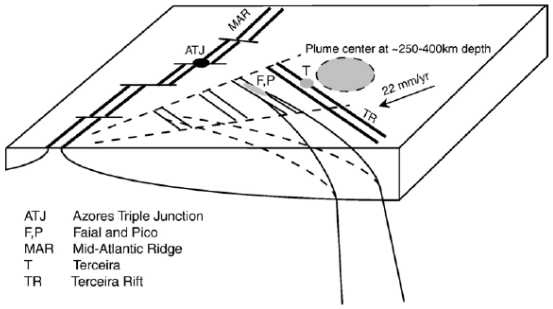

Figure 13 Model for a plume centred northeast of Terceira with its plume centre at about 250-400 km depth (Gripp and Gordon, 2002; Yang et al., 2006).

3.4 São Miguel

The three active centres of São Miguel are the main trachytic central volcanoes (Figure 14). These zones are linked by rift zones. On the one hand, there was explosive volcanism, which related to trachytic centres and, on the other hand, there were basaltic effusive events attended by strombolian cone buildings.

At the west end of the island, Sete Cidades Volcano is located. It was built up from several active phases, for example, explosive eruptions or production of a lava shield. Nowadays, it is a caldera complex, which contains two lakes and several domes as well as cones linked by the caldera infilling. Between Sete Cidades and Fogo Volcano, the 'waist' region is located. It is about 18 km long and has many cinder cones including shatter and scoria cones, and has its origin in lava flows.
Fogo Volcano consists at least of pyroclastic deposits close to the surface. During the last 5000 years there had been four eruptions that formed the caldera complex (Guest et al., 1999). The most recent eruption was in 1563 AD (Guest at al., 1999). Between Fogo Volcano and Furnas, another trachytic centre, known as the Achada das Furnas, is about six km long and consists of cinder cones and lava flows.
The oldest caldera belongs to the region of Nordeste and is partly open to the sea.

Figure 14 Map of São Miguel showing the three active centres of São Miguel which are the main trachytic central volcanoes named Sete Cidades, Fogo and Furnas (Google Inc, 2015).

First of all, there are two concepts of volcanoes, which are responsible for the hydrogeological setting of the islands and also for the aquifer systems (Cruz and França, 2006):

- *The Hawaii type*: perched water bodies
- *The Canary archipelago* type: a basal water body

The basal water systems occur in the area of coastal regions and correspond to freshwater lenses floating on underlying saltwater. In general, it has a very low hydraulic gradient and is limited to a small area (Cruz et al., 2010). Perched water bodies discharge in altitude and release water to basal units. Usually this kind of aquifer system discharges at a large number of springs on volcano flanks and corresponds to confined layers or leaky aquifers. The majority of mineral and thermal springs belongs to perched water systems at altitude, close to a slope of active volcanic structures. In spite of this, the springs close to the coastline are related to basal aquifer systems, which are influenced by the mixing with seawater. But only in few cases discharges belong to basal bodies.

3.4.1 Furnas

Furnas volcano is the most eastern of all three volcanoes. In the west it is bounded by the Povoação caldera, which belongs to an inactive volcano, and in the east Fogo volcano raises as border. Furnas central volcano has been active for more than 100 000 years and is a result of trachytic eruptions (Moore, 1991). Nowadays, instead of the central volcano of Furnas, there exist two calderas, which are the result of several collapses (Figure 15). The older one is approximately 7 x 5 km and 290 m deep, compared to the younger caldera with a diameter of 5 km (Cruz, 2003).

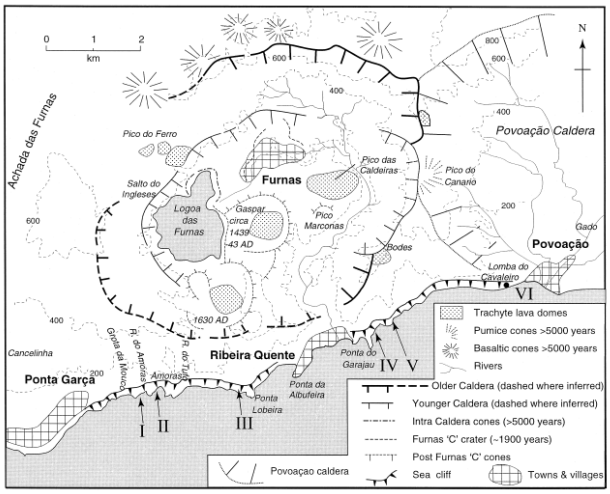

Figure 15 Geological map of central Furnas with its 2 caldera and lakes as well as the surrounding areas with the caldera of Povoação march upon its right side (Guest et al., 1999).

During the last 5000 years 10 explosive eruptions took place within the caldera and built up the Furnas Village (Booth, 1978; Cruz, 2003) as well as the Furnas Lake (Zbyszweski, 1963; Cruz, 2003). The last eruption happened 1630 A.D. in the southern part of the caldera (Cruz, 2003).

In addition to this, the petrology of Furnas volcano is mildly alkaline and consists of basanite, alkali olivine basalt, potassic trachybasalt, basaltic trachyandesite, trachandesite and trachyt according to the classification of Le Maitre (Guest et al., 1990). Furthermore, the mineralogical composition within the caldera is trachytic in contrast to the flank. Compared to the other two central volcanoes the composition is more potassic (Guest et al., 1999).

The major thermal appearances are connected to a W-E trending tectonic lineament that cuts the Furnas caldera. Due to this tectonic lineament two fumarolic grounds can be entirely distinguished from each other, Furnas lake, 290 m.a.s.l., and Furnas village, 200 m.a.s.l (Cruz, 2003). Discharges such as hot springs, carbonated and cold mineral waters are related to these hydrothermal fields. Also the gaseous compositions of the fields differ from each other as a result of the tectonic, for instance, at Furnas lake the CO_2 content is a bit higher than in Furnas village (Furnas lake: 92,5 – 99,22 % ; Furnas village: 91,6- 99,0 %) (Ferreira, 1994). The most important minor components are H_2S

and N_2 with concentration lower than 2 % (Cruz, 2003). Ferreira (1994) assumed that minor components of Fogo volcano are responsible for the Furnas Fumaroles (Ferreira and Okársson, 1999; Cruz, 2003).

3.4.2 Fogo

Fogo volcano is located in the central part of São Miguel with a caldera, 3 x 3.5 km diameter (Cruz, 2003). The caldera within a lake, called Fogo Lake, is surrounded by walls as high as 300 m (Moore, 1991). Furthermore, the age of the volcano is about 180 000 ± 15 000 years (Moore, 1991; Cruz, 2003). The central volcano consists of lava flows and pyroclastic deposits. In general, Fogo shows a decrease in K_2O concentration with a peralkine tendency (Guest et al., 1999) compared to the other active volcanoes. Mainly, most of the eruption took place on the slopes of the volcano. Moreover, the most recent explosive event happened in its flanks at Pico de Sapateiro in 1563 and 1564 A.D. During the last 5000 years there were about seven explosive eruptions (Booth, 1978; Wallenstein and Duncan 1998; Cruz, 2003). In addition, one fumarolic ground exists at Caldeira Velha (320 m.a.s.l) and the others occur east of Caldeiras da Ribeira Grande (250 m.a.s.l) (Cruz, 2003). Furthermore, in both fumarolic fields is CO_2 the main component of the outgassing (Caldeira Velha: 88.68 – 99.56 mol%; Caldeira da Ribeira Grande: 98.54- 99.39 mol%). However, minor constituents are H_2S and N_2 with not even 1 % (Cruz, 2003). There are two major fumarolic grounds linked to the northern flank of Fogo volcano. Thermal features, besides fumaroles grounds, are thermal and cold mineral water, especially cold CO_2 rich discharges, which are associated with an NW-SE tectonic lineament (Forjaz, 1986; Cruz, 2003).

3.4.3 Ferraria

Ferraria spring discharges at the west flank of the Sete Cidades volcano into the Atlantic Ocean. The petrology of Sete Cidades shows a more sodic trend compared to Furnas and Fogo volcano (Guest et at., 1999).

4. Methodology

4.1 Sampling

4.1.1 Solutions

During the rain period in October 2013 in total 33 water samples from different locations in São Miguel, including Ferraria (Figure 16), Furnas (Figures 17 and 18) and Fogo (Figure 19) were collected. Among them are also samples from Sete Cidades (blue lake, Figure 17) from the surface and from depth at 23 m, tap water und seawater

samples. The abbreviation Fu implies samples from Furnas, Fo is an abbreviation for samples from Fogo and Fe stands for Ferraria. AS, SW and DW denotes solution samples from Sete Cidades, the ocean and local drinking water, gained from groundwater. 18 samples were used for the hydrochemical analyses of Furnas water from Furnas village as well as Furnas lake. For the analysis of water of Fogo area altogether ten samples from different locations, including Caldeira Velha, Caldeiras da Ribeiras Grande and Lombadas were collected.

Figure 16 Sampling side Ferraria is at the west end of São Miguel (Google Inc, 2015). Thermal water of Ferraria (Fe) discharges at the west flank of Sete Cidades volcano into the Atlantic Ocean. Furthermore, the Azorean sea water (SW) sample was taken close to the Ferraria spring. Also 2 samples of the blue lake exists (AS). One was taken at the lakes surface and one at the same location but at the depth of 23 m.

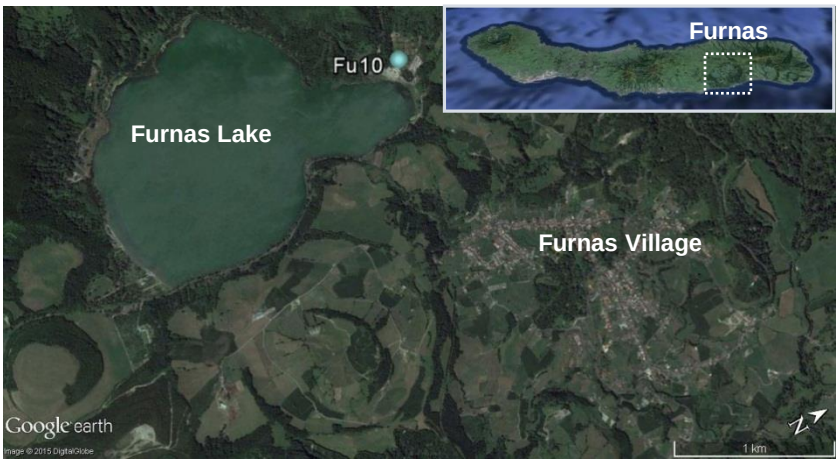

Figure 17 Sampling side of Furnas is in the Caldera of Furnas volcano and includes 2 sampling sides: Furnas Lake and Furnas Village (Google Inc, 2015). Sample Fu10 comes from a boiling pool located in a fumarolic field is close to Furnas lake.

Figure 18 Sampling side Furnas Village which is located in Furas' Volcanoes younger caldera at the south east part of São Miguel (Google Inc, 2015). Abbreviations in the map are sampling points for fluids and rocks. Altogether, 18 samples had been taken directly in the village. These samples include a huge variety of different spring discharges among them thermal water and mineral water as well as boiling pools Boiling pools like sample Fu9 and Fu17 are located in an fumarolic field.

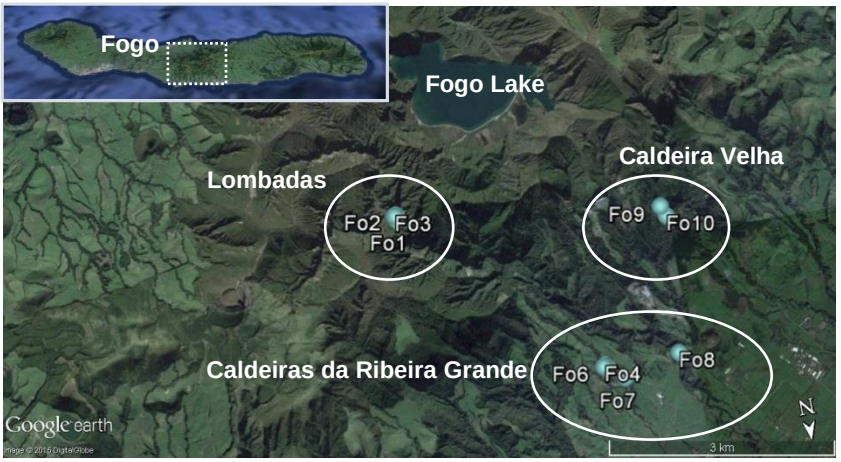

Figure 19 Map of Fogo sampling area with its sampling points for solids and solutions (Google Inc, 2015). Fogo volcano is located in the central part of the island with a caldera lake called Fogo Lake. Sampling area of Fogo can be divided into 3 locations: Caldeira Velha, Caldeira da Ribeira Grande and Lombadas. In total 10 samples were taken, among them are thermal water, cold mineral water and boiling pools. Samples Fo9 and Fo10 belong to Caldeira Velha, Fo4 - Fo8 were taken in Ribeira Grande (Caldeiras da Ribeira Grande). The abbreviations Fo1, Fo2 and Fo3 denote samples from Lombadas.

4.1.2 Solids

In total eight rock samples were taken for analyses. These samples originate from the fumarolic ground or thermal discharges, which are in relation to one of three main active volcanoes in São Miguel. Solid samples abbreviations are given in italics compared to liquid samples. The sample *SW* was taken close to the thermal water of Ferreira, directly in the area of Atlantics breakers. The geology of this area is influenced by the eruptions of Sete Cidades and the erosive force of the Atlantic. Sample *Fo9* belongs to the thermal discharge of Caldeira Velha in the area of Fogo volcano. *Fo10* is an abbreviation for the sample from the fumarole ground in Caldeira Vehla, at the north flank of Fogo volcano. *Fu9* belongs to Caleira Grande and is one of the biggest boiling pools with gaseous emission in the fumarolic ground (Figure 20). Sample *Fu10*

was taken from the fumarolic fields in Lagoa das Furnas (Furnas Lake). There are three samples for *Fu10*:

- directly from the rim of a pool which was covered by stromatolitic structured material (*Fu10_1*)
- behind the rim, but still in an area where host rock interacts with hydrothermal water and gaseous emissions (*Fu10_2*)
- fine grained material which was covered by a thick crust

Fu17 is an abbreviation for all samples that were taken from Caldeira do Asmodeu located in the fumarolic field of Furnas village. Additional samples from this Caldeira were gathered at the rim of a domal mound, made of organism (*Fu17_2*) and behind the pool margin, where thermal water still affects the rock (*Fu17_1*).

Figure 20 Caldeira Grande in Funras village, the diameter of the boiling pool varies between 2 and 3 m (A), and the process of taking solid samples during fieldwork at Caldeira Grande which was taken for the analyses of Fu9. The black arrow points to the sample taken. Remarkable are the alternate reddish and white layers as well as a thick black crust on the top of the sample (B).

4.2 Analytics

4.2.1 Solutions

Temperature, pH, electric conductivity (EC) as well as alkalinity were measured on-site. In case of each solution the following samples were taken: 50 ml filtrated (0.45 µm membrane), 50 ml filtrated and acidified (to yield 2 % HNO_3 solution), and 100ml unfiltrated in separate plastic flasks.

Alkalinity was measured by on-site by titration of 0.1 M HCl. Alkali, alkaline earth elements as well as ammonium, barium, bromine, chloride, fluorine, phosphor, nitrate and sulphate were analyzed by ion chromatography (Dionex ICS – 3000) with an analytical precision of ± 3 %. Silica, sulphur, aluminium, heavy metals and trace elements were measured by inductively coupled plasma optical emission spectrometer (Perkin Elmer Optima 4300 DV) with an analytical error ± 5%.
The isotopic composition of the water ($\delta^{18}O$, δD) and dissolved inorganic carbon ($\delta^{13}C$ value of DIC) and) was measured at the laboratory centre of Joanneum Research in

Graz. The oxygen and hydrogen isotope ratios of water were analysed by wavelength-scanned cavity ring-down spectroscopy (WS-CRDS), using a L2120-I system from Picarro. The samples had been injected into an evaporator and kept at 110°C. The analytical procedure that was used in this study is similar to the method described by Brand et al., (2009). For stable carbon isotope analyses (^{13}C-values of DIC) approximately 1 ml solution was injected into a 10 ml gas tight vial. Previously to sampling the vials were flushed with He gas and preloaded with six droplets of phosphoric acid in the Lab. Isotopic composition of DIC was analysed using Gasbench II device (Thermo), which was connected to a Finnigan DELTA^{plus} XP isotope ratio mass spectrometer. Analytical setup is comparable to that used in other studies (Spötl, 2005). Results of water and DIC measurements are given in permil (‰) with respect to Vienna Mean Ocean Water (V-SMOW) and Vienna Peedee Belemnite (V-PDB), respectively, using the standard delta notation. The analytical precision for stable isotope measurements is ±0.8 ‰ for δD, ±0.08 ‰ for δ^{18}O and ±0.1 ‰ for δ^{13}C.
$BaCl_2$ had been used for the precipitation of the dissolved sulphate as $BaSO_4$.1 liter of sample was used to precipitate $BaSO_4$. First steps included the addition of HCl (2 mol L^{-1}) to adjust a pH-value between 2 and 2.5 to remove carbonate. Subsequently $BaCl_2$ (0.3 mol L^{-1}) solution were added in surplus into the solution. The surplus value were calculated by considering previous hydrochemical results published by Cruz (2010). This mixture was heated at 60°C for 24 hours. Subsequently $BaCl_2$ solution was added again, but this time just one drop to verify that all sulphate had been precipitated quantitatively. The precipitated $BaSO_4$ was separated from the solution by filtration and dried at 30°C for 10 min. The isotopic composition of δ^{34}S for the precipitated $BaSO_4$ had been carried by using a C-irmMS (Thermo Finnigan MAT 253), coupled to a Thermo Flash Elemental analyser via a split interface at the Leibnitz Institute for Baltic Sea Research, Warnemünde. Calibration of isotope measurements to the V-CDT scale took place by using international intercomparison materials (Mann et al., 2009) and is given in the conventional δ -notation. Replicate measurements agreed within ± 0.2 ‰.
Collected data were processed with the computer code AquaChem (Schlummberger Water Sevice, 2007) and PHREEQC (Parkhurst and Appelo, 1999). For PHREEQC the database phreeqc.at were used for hydrochemical modeling, e.g. calculation of saturation indices among them quartz (SI_{Quartz}) and albite (SI_{Albite}).

4.2.2 Solids

For the mineralogical and chemical charactrization of each sample transmitted light microscopy of thin sections, X-ray diffraction (XRD), infrared spectroscopy(FTIR) as well as X-ray fluorescence (XRF spectroscopy) were applied. For the latter, fused beads were prepared, which consisted of a mixture of lithiumtetraborate ($Li_2B_4O_7$) and

powder at a ratio of 1:6. In this particular case not annealed sample had been used, not to lose the sulphur species. The annealing loss varies for all samples between 1.5 and 10.0 wt. % (Appendix, Table C1). At temperatures of 1050°C the $Li_2B_4O_7$ sampling mixture had been fused for 10 min by Perl'X3, PANalytical. For XRD analytics PW2404 X-ray spectrometer (Philips) was used. The instrument X'Pert Pro, PANalytical is equipped with a X-ray tube with Co- target tube operating at 40kV and at beam currents of 40 mA. Stretching and bending bands generated by IR vibration minerals can be identified by the FT-IR method. IR vibrations were detected by Spectrum 100, Perkin Elmer.

5. Results

5.1 Mineralogical and chemical composition of the solids

Volcanic rocks

All samples (from Furnas and Fogo) are dominated by SiO_2 content (Appendix, Table C 1) with elevated Na_2O and K_2O content (appearance of sanidine), and thus the solids occur in the field of rhyolite, quartz-trachyte or in the basalt field. Among volcanic rock samples are SW (Appendix, Figure B 1) and *Fo9* (Appendix, Figure B 2). *SW* is identified as weathered basalt. In the overview photo of the thin section a dark fine grained matrix, coarse minerals of orange colour as well as round opaque minerals are visible. However, remarkable for *Fo9* is its orange crust (even during sampling). The orange crust is also recognisable in the overview photo and varies in colour and thickness (Appendix, Figure B 2). The matrix is light coloured with coarse minerals with a feldspar-like habitus. It represents an altered basalt, where the microstructure is still detectable as microcrystalline porphyric.

Although *Fo9* and *Fo10* are located close to each other the thin sections show remarkable differences. In contrast to *Fo9*, in the *Fo10* sample the content of fine matrix increased while the size of the minerals in the thin sections decreased (Appendix, Figure B 3). Furthermore, the MgO content correlates with the potential placing of Mg^{2+} in amphibole. The observation of a higher content of volcanic glass in *Fo10* compared to *Fo9* goes hand in hand with elevated SiO_2 concentrations.

Precipitates

Samples *Fu9*, *Fu10* and *Fu17* built up this group of precipitates. The hand piece of *Fu9* shows alternating red and white layers (Appendix, Figure B 4), and especially its powdery occurrence was noticeable. On the top of the sample a hard dark nodular crust occurs. The hand sample of *Fu10_1* shows undulated surface structures (Appendix, Figure B 5). Moreover, there is a formation of a green crust directly below these structures. The light coloured thin section clearly reveals the undulated

structures. In contrast, *Fu10_2* shows a lack of these structures. The matrix of thin section *Fu10_2* is also more coarse and darker. It seems that there is just an undulated unconformity in the middle of the thin section (Appendix, Figure B 6). The surface of rock sample *Fu17_2* has a nodular and sharply acerous appearance (Appendix, Figure B 8) with erected slender columns without branching. The thin section shows also undulating and radial structures. However, the thin section of *Fu17_1* shows no radial or undulating structures (Appendix, Figure B 7). The content of matrix decreases and the size of minerals increase. Moreover, the highest SiO_2 belongs to sample *Fu17*. A way to differentiate between samples from Fogo and Furnas is due to the sulfur content, because of the appearance of alunite ($KAl_3(SO_4)_2(OH)_6$). Furthermore, this observation fits with the thin section as well as XRF pattern and IR vibrations (Appendix, Figure C 1- C 12). High Fe_2O_3 content in sample Fo9 is related to goethite. The concentration of Fe_2O_3 in Fu9 is referred to the red layers. To conclude, alunite is responsible for the sulfur content in the majority of the samples of Furnas in spite of *Fu10_1*. In addition to this, the small amount of MgO in Fu10_1 (inside) correlates with the occurrence of clinopyroxene. Despite the appearance of alunite and anorthite the sulfur and CaO content is low. Furthermore, the SiO_2 content fits with the silicification of the organisms (Chapter 2.2.2) and the high background of the XRF pattern (amorphous material).

5.2 Hydrogeochemistry of thermal water

Discharges in the Furnas caldera are heavily influenced by volcanic activity. For this reason, the water samples can be divided by their CO_2 content and temperature:

- hyperthermal water (Fu9, Fu10, Fu17)
- mesothermal water(Fu3,Fu6, Fu11, Fu12, Fu16)
- warm thermal water (Fu13, Fu14, Fu15, Fu16, Fu18)
- cold CO_2 rich water(Fu1, Fu2, Fu4, Fu5, Fu7, Fu8)
- carbonated water (Fu1, Fu7)

Hyperthermal waters are mainly thermal water from boiling pools with temperatures that ranged from 90.8 to 96.8 °C. It is obvious that thermal water from Furnas village has a higher salt content, in contrast to the Furnas lake sample. Also the pH- value was neutral to slightly basic in Furnas village compared to the acid discharges close to the lake.

Mixed thermal waters are warm thermal up mesothermal discharges with a widespread range of temperatures and electrical conductivity values. The temperature ranged from 20 to 86 °C. The pH value was slightly acid to neutral. Another point to be made is that the temperature of cold mineral water ranged from 15.8 to 16.1 °C with a pH-value around 5. Also a group of carbonated waters existed. All waters of this group had a CO_2 content of about 1000 mg L^{-1} regardless of the temperature.

Another possibility to classify different water types based on the major ionic composition. Furnas samples can be divided into 2 groups:

- $Na\text{-}HCO_3$ (Fu1, Fu2, Fu3, Fu4, Fu5, Fu6, Fu7, Fu8, Fu9, Fu11, Fu12, Fu13, Fu14, Fu15, Fu16, Fu17, Fu18)
- $Na\text{-}SO_4$ (Fu10)

According to this classification all the $Na\text{-}HCO_3$ type dominated across Furnas and according to Cruz and França (2006) across all islands.

Also Fogo samples can be distinguished by their different CO_2 content and temperature:

. warm thermal water (Fo7, Fo9)
. mesothermal water(Fo4, Fo5, Fo6, Fo10)
. cold CO_2 rich water and carbonated water(Fo1, Fo2, Fo8)
. cold CO_2 poor water (Fo3)

Warm thermal waters had temperatures around 30 °C with a slightly acid pH value, between 4.6 and 4.9. Mesothermal water was just samples from fumarolic boiling pools with temperatures from 45 to 57 °C. The pH-value as well as the total dissolved solids differ wildly in both of the fumarolic grounds. In Caldeiras da Ribeira Grande, the pH value was more acid (2.1 to 2.5) compared to the Caldeira Velha with a pH value of 4.7. All cold mineral water of Fogo can be found in Lombadas with one exception close to Caldeira da Ribeira Grande. The temperature varied from 13 to 20 °C and all pH values are slightly acid (4.6- 5.9). Two discharges from Lombadas even belonged to carbonated water type because of its CO_2 content which reaches nearly 1000 mg L^{-1}. Due to the ionic composition of Fogo samples, the discharges are grouped into 2 groups:

- $Na\text{-}HCO_3$ (Fo1,Fo2, Fo3, Fo8, Fo9,Fo10)
- $Na\text{-}SO_4$ (Fo4, Fo5, Fo6, Fo7)

Based on this classification it is obvious that the major ionic composition for cold CO_2 rich water is $Na\text{-}HCO_3$ type, in contrast to thermal water with a $Na\text{-}SO_4$ dominant composition.

In contrast to the already discussed discharges of Furnas and Fogo, thermal water of Ferraria is a result of the admixture with seawater which can be followed by a Na^+ content of 435 mmol L^{-1} and a Cl^- content of 502 mmol L^{-1}.

A more overall method to classify the different water types is referred to ternary plots with apexes of cations and silica (Figure 21) and anions (Figure 22).

The positive correlation between molar Ca and Mg in all thermal waters besides Ferraria resulted in a Ca/Mg ratio of 0.77 (Figure 21). This ratio was calculated by the molar ratio of Ca/(Mg+Ca) of 0.57 which is indicated by the arrow. Furthermore, the Si concentrations varied between 0.6 and 1 % apart from Ferraria and lake samples with very low Si content (Figure 21). Based on major anions, the second ternary plot displays basically three types for the samples sampled thermal waters: (1) sodium bicarbonate type, (2) sodium sulphate type and (3) sodium chloride type (Figure 22).

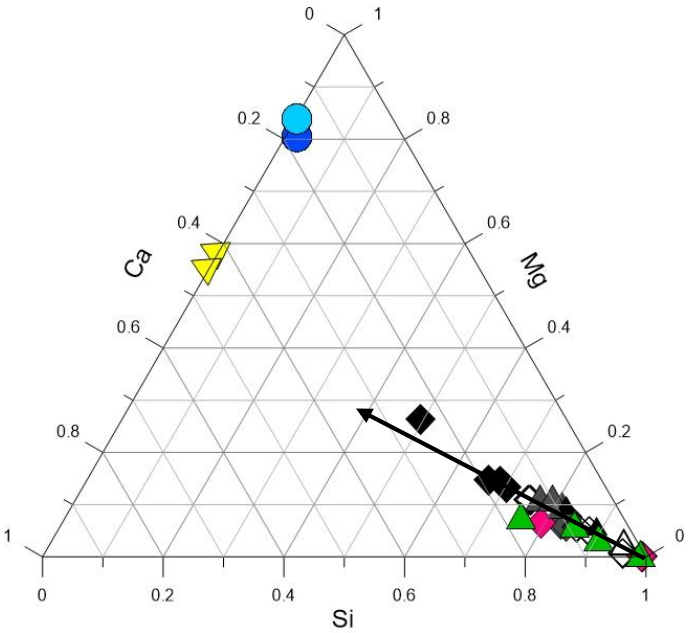

Figure 21 Ternary plot of Si, Mg and Ca, with concentrations given in mmol, of discharges in São Miguel shows that all samples are enriched in $Si(OH)_4$ besides lake samples and sea water influenced samples. All samples of Fogo and Furnas shows a similar evolution trend in case of a given Ca/Mg ratio of about 0.6. (Furnas: ◈: cold and CO_2 rich, ◆: warm type, ◇: mesothermal, ◆: boiling pools; Fogo: ▲: cold and CO_2 rich, △: Fo3 cold and decrease in CO_2, ▲: warm type, ▲: boiling pools , ▽: Sete Cidades, surface samples has a lower Mg content compared to the sample at 23 m depth, ●: Ferraria, ●: seawater).

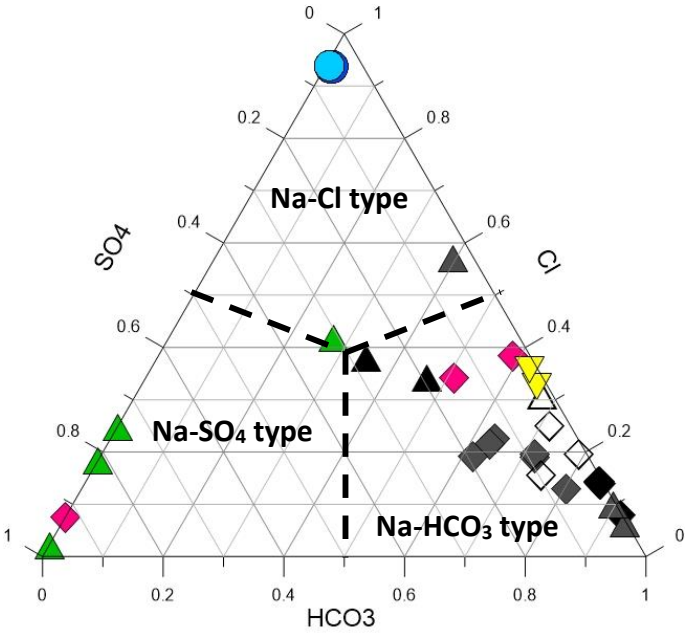

Figure 22 Ternary plot of HCO3, Cl and SO4 where concentrations in mmol L^{-1} are used, of discharges in São Miguel. It is obvious that boiling pools of Fogo and Furnas Lake are enriched in SO_4. However all other samples are enriched in HCO3. (Furnas: ◇: cold and CO_2 rich, ◆: warm type, ◇: mesothermal, ◆: boiling pools; Fogo: △: cold and CO_2 rich, △: Fo3 cold and decrease in CO_2, ▲: warm type, ▲: boiling pools, ▽: Sete Cidades, surface samples has a lower Mg content compared to the sample at 23 m depth, ●: Ferraria, ●: seawater).

The 33 sampled solutions have a broad range of stable hydrogen and oxygen Isotopic composition of values ranging from -20 to 20.4 ‰ for δD and $\delta^{18}O$ values from -4 to 5.2 ‰. Figure 23 shows the relationships between $\delta^{18}O$ and δD as well as the relationship between the Global Meteoric Water Line (GMWL), Local Meteoric Water Line (LMWL) and the sampled solutions. Sample Fo6 has the highest $\delta^{18}O$ values as well as the highest δD values. Fo7 has the lowest δD values and Fo1 shows the lowest $\delta^{18}O$ values. In conclusion, the highest and lowest δD and $\delta^{18}O$ values can be found in the area of Fogo. However, in the area of Furnas volcano the highest δD value is 12 ‰ and belongs to Fu10 and the highest $\delta^{18}O$ with 3 ‰ can be found in Fu17. Obviously, the highest values belong to the boiling pools.

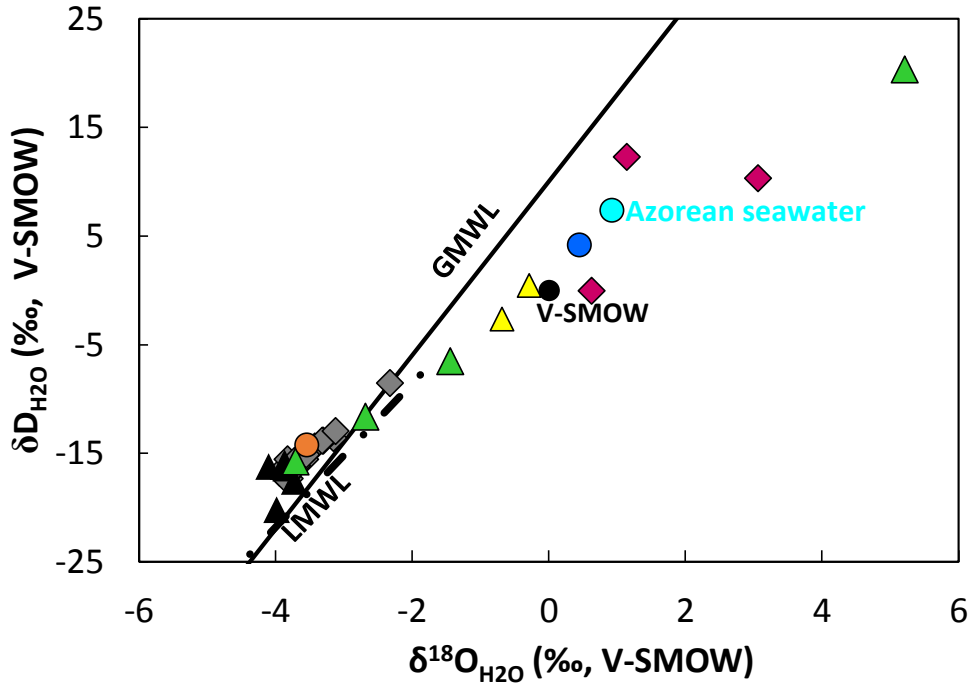

Figure 23 $\delta^{18}O$ vs. δD plot of sampled natural waters from São Miguel for instance thermal, mineral, cold, sea, lake as well as tap water (vs. SMOW standard). The majority of samples plot close to the GMWL (black line: GMWL, black line: LMWL; ◇ : Furnas springs, ◇ : Furnas boiling pools, ▲: Fogo springs, △: Fogo boiling pools, △ : Sete Cidades lake samples, ● : Ferraria sample, ● : Azorean seawater, ● : seawater, ● : drinking water taken in São Miguel).

SO_4^{2-} concentrations show a wide variation from 0.04 to 32.9 mmol L^{-1} in São Miguel and especially samples from Furnas and Fogo. Also the $\delta^{34}S$ of SO_4^{2-} shows a wide range between -1 and +21 ‰ (CDT). The lowest $\delta^{34}S$ values can be found in Furnas village with -4 ‰ (Figure 24). All samples can be roughly divided into 2 groups based on their $\delta^{34}S$ values, one group at about 21 ‰ and the other between -5 and +5 ‰. The $\delta^{18}O$ values of dissolved sulphate range between 0.5 and 10.5 ‰ (V-SMOW) (Figure 25).

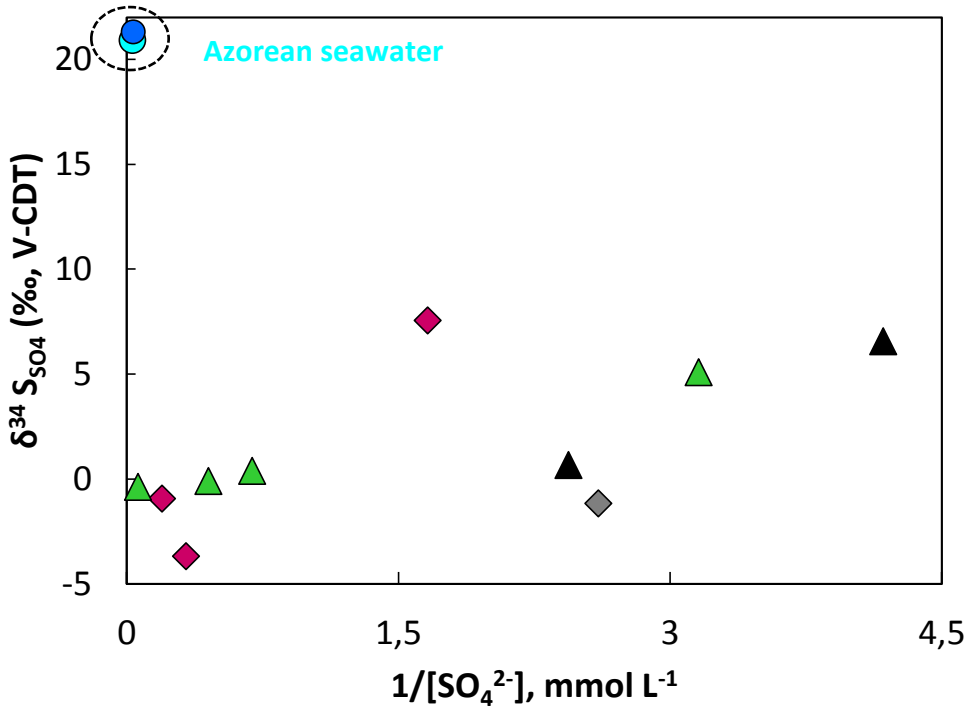

Figure 24 $\delta^{34}S_{SO4}$ vs. $1/[SO_4^{2-}]$ plot shows an increase of SO_4^{2-} concentration leads to a decrease of $\delta^{34}S$. (Fogo: ▲: discharges, △: boiling pools, Furnas : ◇: discharges, ◆: boiling pools, ●: seawater, ●:Ferraria).

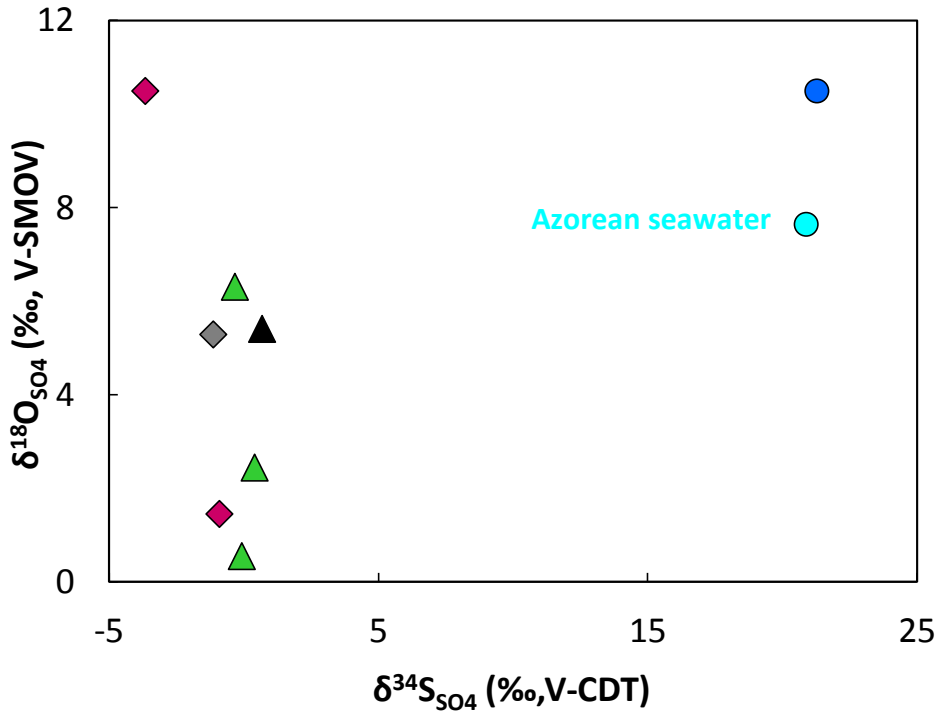

Figure 25 $\delta^{18}O_{SO4}$ vs $\delta^{34}S_{SO4}$ diagram shows an independently increase of $\delta^{18}O_{SO4}$ values while most $\delta^{34}S_{SO4}$ values are around -1.5 ± 2.5‰. (Fogo: ▲: discharges, △: boiling pools, Furnas : ◇: discharges, ◆: boiling pools, ●: seawater, ●: Ferraria).

There is a narrow range of $\delta^{13}C_{DIC}$ for all samples between -8 and -1 ‰ (V-PDB). The lowest $\delta^{13}C_{DIC}$ value can be found in Fogo village with -8 ‰ and the highest belongs to Azorean sea water with 0.9 ‰ (Figure 26). The measured

seawater had a $\delta^{13}C_{DIC}$ signature of 0.9 ‰. At pH above 5 a significant increase in $\delta^{13}C$ values are remarkable, up to 1 ‰ (V-PDB).

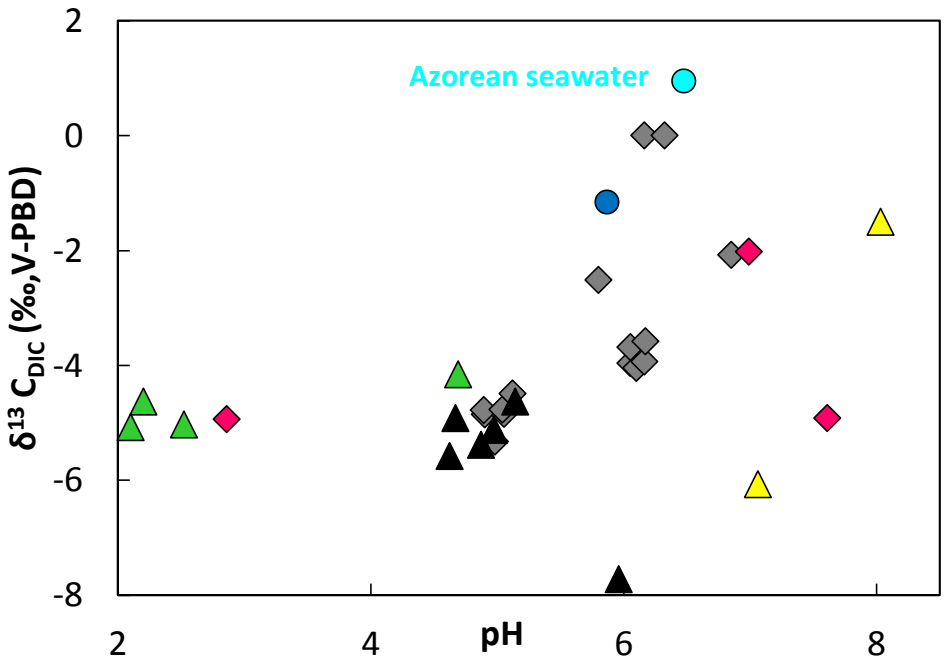

Figure 26 $\delta^{13}C$ values of dissolved inorganic carbon is increasing as a function of increasing pH. (Fogo: ▲: Fogo discharges, ▲: boiling pools, Furnas : ◆: discharges, ◆: boiling pools, ●: seawater, ●: Ferraria, △: lakes).

6. Discussion

6.1 Solids

6.1.1 Volcanic rocks

The microstructure of sample *SW* could be identified as microcrystalline porphyric. Most of the minerals are alkali feldspars, pyroxene, and amphibole. Moreover, opaque and iron rich phases occur (Figure 27). Sandine appears with a euhedral grain shape as Carlsbad twins or fine-grained in the matrix. The pyroxenes are even visible with the naked eye and their sizes ranged between 5 and 7 mm, as well as several opaque phases. A sign for alteration is the development of a goethite crust around the pyroxene, same to amphiboles (Appendix: Figure B 1). Due to the IR vibrations the mineral hornblende could be identified (Appendix: Figure C 2).

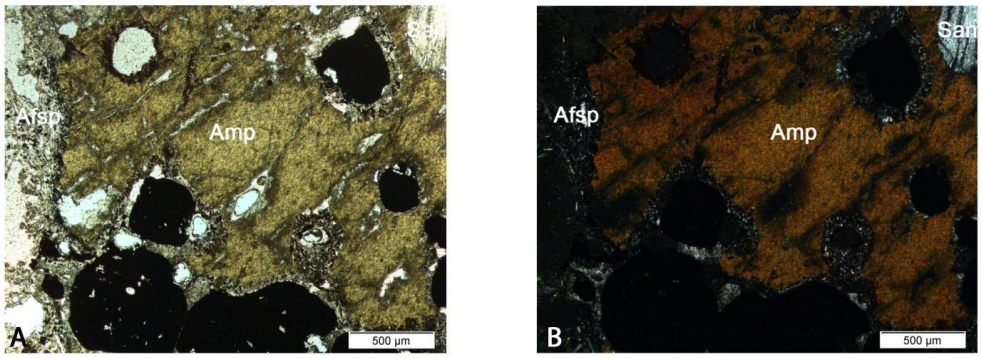

Figure 27 Optical microscopy images of the thin section of sample *SW* which was taken close to the Atlantic Ocean. Images were taken with transmitted light (A) and with crossed nicols (B) Alteration process of the amphibole has already started, recognized by fissures of the minerals and the development of a goethite curst. Alkali feldspar= Afsp, Amphibole= Amp, Sanidine= San

Majority of all minerals, in the *Fo9* sample, are alkali feldspar, amphibole and iron rich phases, like goethite. Also opaque phases appeared. Additionally, the formation of a goethite crust was visible in the thin section, with a mean thickness of 350 µm, named unconformity (Figure 28). Moreover, this unconformity consisted of six different layers and the formation of these thick Fe oxide/hydroxide layers may had its origin in rapid dissolution of volcanic rock caused by thermal spring. Besides the crust, also goethite oncoids formation developed (Figure 29). Furthermore, the appearance of small green pieces of amphibole (20- 80 µm) is associated with the goethite crust. Several sanidine inclusions were visible. Sanidine shows alteration if located next to the goethite crust.

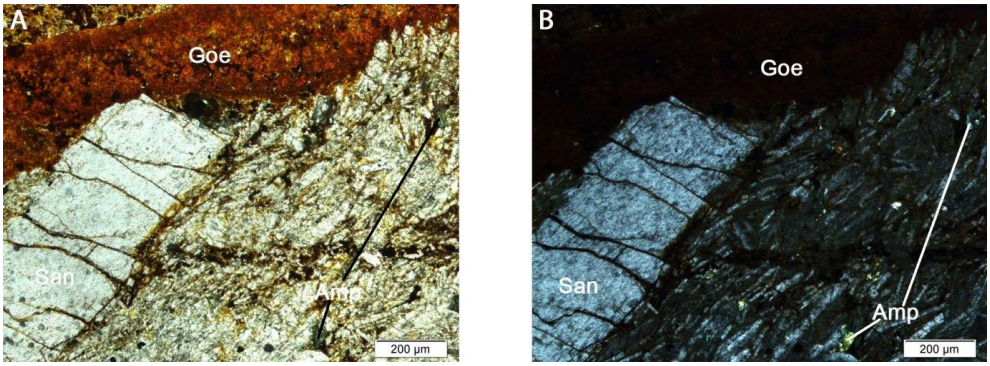

Figure 28 Optical microscopy images of the thin section *Fo9* shows one taken transmitted light (A) and one image with crossed nicols (B). In the microcrystalline matrix appears a euhedral sanidine with several fissure tracks. The goethite crust has a strong influence on minerals which appear close to it. Amphiboles are hard to identify because of their size and flaky form. Amphibole= Amp, Sanidine= San, Goe= Goethite

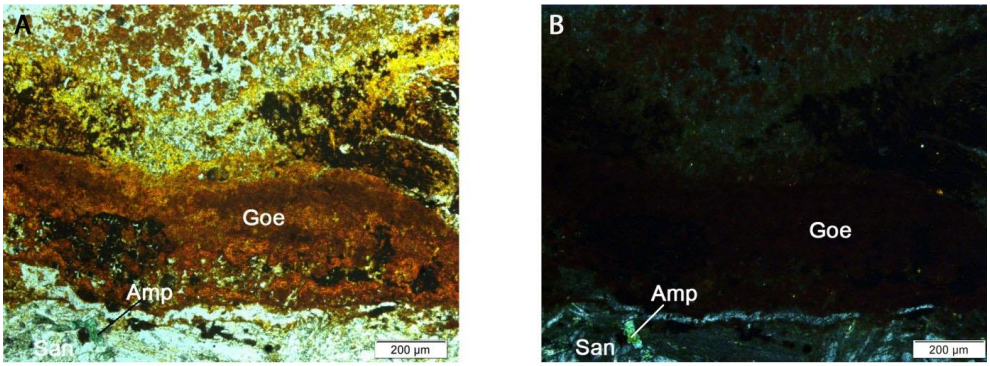

Figure 29 Images of the thin section *Fo9*. Image was taken with transmitted light (A) and with crossed nicols (B). In the middle of the image an oncoid structure is identified. Above this structure the alteration is stronger than below. The alteration is clearly visible because of different reddish to yellowish colours and because of the appearance of mineral flakes. Amphibole= Amp, Sanidine= San, Goe= Goethite

Volcanic rocks of *Fo9* and *Fo10* differ in their grain size despite their small distance between each other. The grain size of *Fo10* is smaller (Figure 30) and it has a higher content of volcanic glass, less iron and opaque components compared to *Fo9*. Another difference is the stronger alteration as result of a higher volcanic activity by gaseous emission above the boiling pool. Furthermore, the main mineralogical component of *Fo10* is potassium feldspar (Appendix: Figure C 3) as phenocrystal sanidine inclusion in a fine grained matrix.

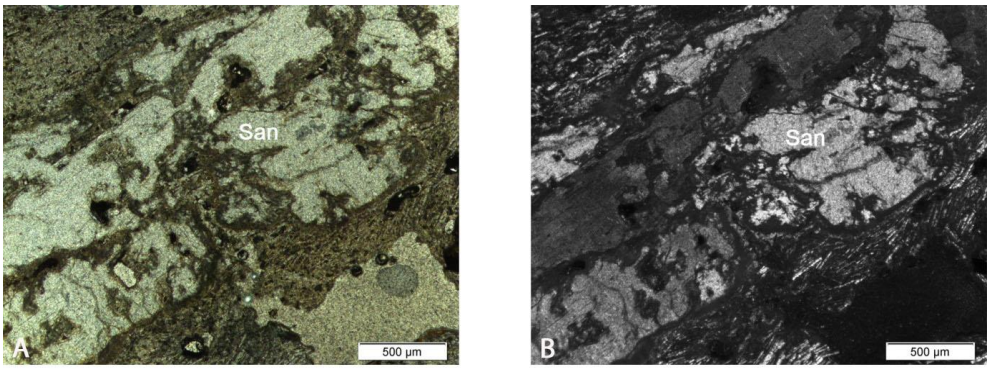

Figure 30 Both optical microscopy images taken with transmitted light (A) as well as with crossed nicols (B). In the center of the image a strong altered sanidine crystal is visible. This alteration is recognisable by the destroyed sanidine and the occurrence of the fine grained mass inside it. Despite the alteration, Carlsbad twins are still identifiable crossed nicols. San= sanidine

6.1.2 Precipitates

Sample *Fu9*, which was taken at the hot spring named ‘’Caldeira Grande’’, shows alternating red and white layers which could be the result of environmental changes during precipitations. Supposed parameters for such alternating layers are composition of hydrothermal water, its temperature as well as changes in the gaseous emissions; the water level of the boiling pool could play a role too. However, these red and white layers are barely visible through the crossed nicols (Figure 31). Red layers consist mainly of iron rich hydroxides like goethite and opaque phases compared to the

mineralogical components of the white layers. They are quite difficult to identify with microscope, because of the permanent alteration through the contact with boiling thermal water. Another point to be made is that the groundmass of *Fu9* has a vitrophyric microstructure of volcanic glass and new minerals were formed like opal and alunite (Appendix, Figure B 4). Furthermore, alunite is a typical alteration product, identified by XRF pattern and IR vibrations pattern (Appendix, Figure C 4). Apart from that, sanidine inclusions (Carlsbad twins) occur as relicts of the former parent rock. Another sign for alteration are fissure tracks filled with opaque minerals and deteriorated preexisting minerals (Figure 32). To sum up, sampling side of *Fu9* is supposed to be a classic acid sulphate geothermal field with intense leaching. Its porous and powdery appearance is a result of intense rock leaching.

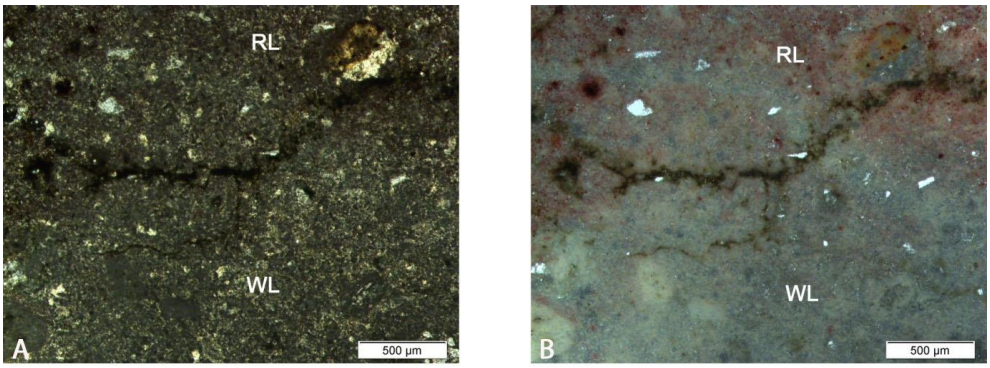

Figure 31 Both optical microscopy images of thin section show lamination of sample *Fu9*. The differences between A and B is that one was taken with transmitted light (A), but the layers are not visible and for the other crossed nicols had been used (B). Besides the appearance of alunite also fissure tracks indicate alteration processes RL= red layer, WL= white layer.

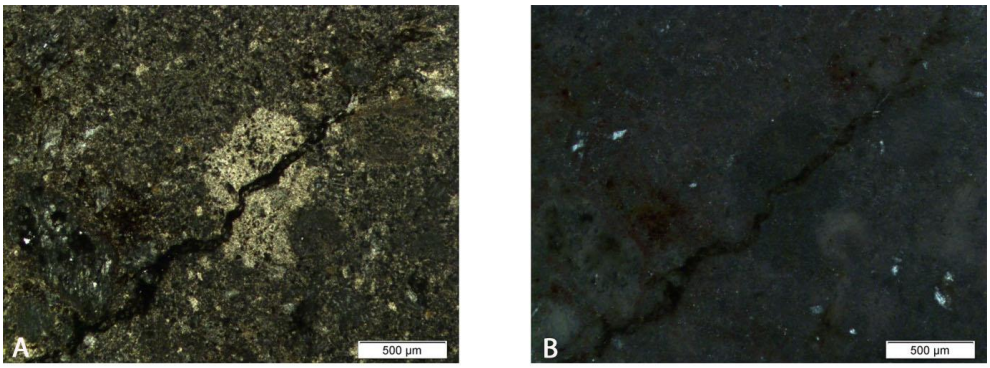

Figure 32 For the optical image transmitted light (A) and crossed nicols (B) had been used. In both types of pictures a fissure track in is destroying a feldspar crystal which implicates alteration.

Sample *Fu10* mainly consisted of opal, sanidine and pyroxene. Sandine and pyroxene appeared as phenocrystals compared to cryptocrystalline quartz. Both samples showed silicifications and alterations (Figures 33 and 34). The degree of silicification is in *Fu10_1* higher compared to *Fu10_2* as a result of the development of stromatolite-like structures and related unconformities. Three unconformities occurred, which differ in colour and thickness. These unconformities represent the substrate which is one of

the prerequisite for stromatolites and their development (Hofmann, 1973). Stromatolites are referred to different bacterial taxa, which have the ability to precipitate e.g. silica including their loss of details of their cytoplasm and cell wall structure, (Krumbein and Werner, 1983; Guidry and Chafetz, 2003, Birnbaum and Wireman, 1984, Fernandez-Turiel et al., 2005). Two different stromatolite structures occurred, a laminar and a dome-shaped structure (Figure 35). In addition to this, typical structures of stromatolite showed laminations (laminae) of alternating black- brown and white layers (Chapter 2.2.2). The white one consists of chert and the darker layers are supposed to have a higher content of organic material. In general, the origin of unconformities could be inorganically or organically induced. Inorganic processes like thermal water rock interaction would lead to dissolution and leached layers. However, organic precipitation is induced by microorganisms, which are colonised at the surface of the host rock as a bio-film.

Fu10 is also a possible example for active high-sulfidication epithermal system in the first stage.

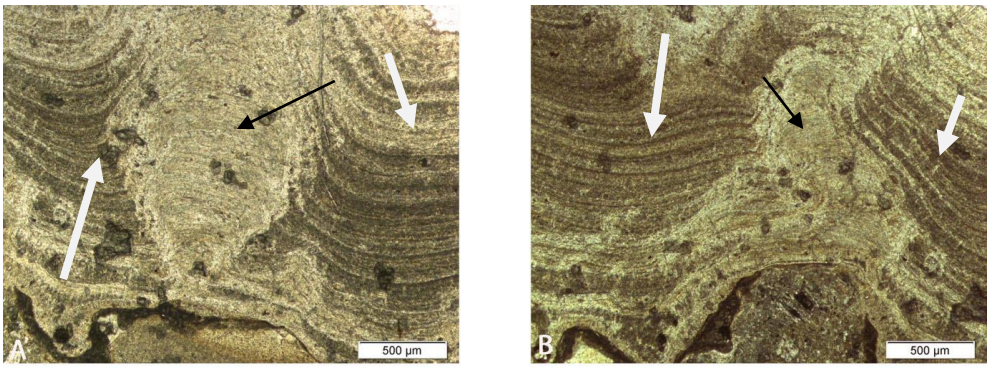

Figure 33 Both images (A,B) of the thin section *Fu10_1* show stromatolitic structures (black arrows) and the development of opal-A cementation (white arrows).

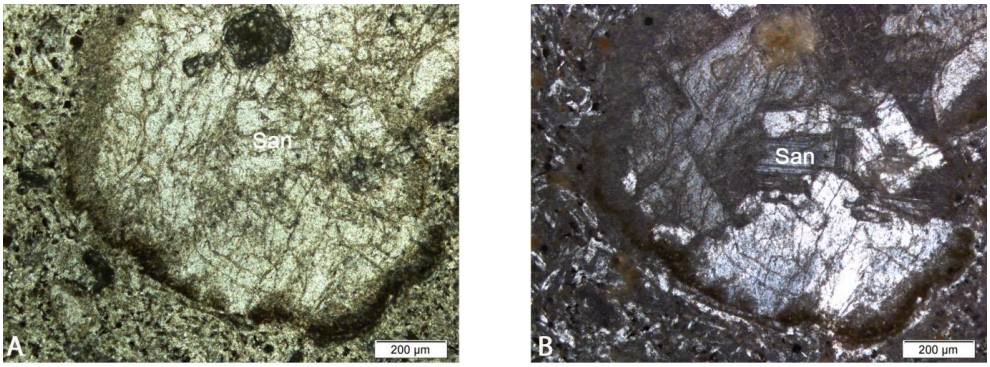

Figure 34 Thin section of *Fu10_2*. Optical images were taken with transmitted light (A) and with crossed nicols (B). Sanidine has an alteration crust because of the interaction with thermal fluids and volcanic emissions. Sanidine is bounded by a fine matrix of opal and sanidine minerals. San= sanidine

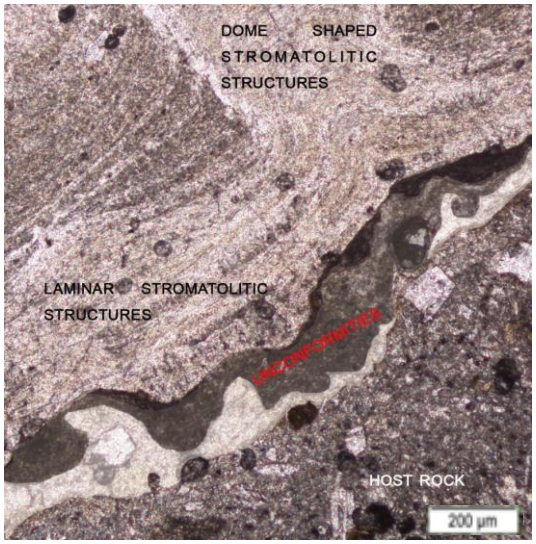

Figure 35 Several layers of different thickness and colours build up the unconformity. It appears just between host rock and the stromatolitic structures. Furthermore, two different kinds of stromatolitic structures are visible. Dome-shaped and laminar stromatolictic structures. The reason for the two different shapes could have their origin in two different kinds of microbes.

Remarkable for the thin section of *Fu17_1* is that not the whole rock is alterated (Figure 36). Furthermore, on the top of the sample a crust is visible. In addition, the size of the inclusions varies from 250 to 2500 µm and the major (mass related component) is opal, but also pyroxene and sanidine appear. However, *Fu17_2* (Figures 37 and 38) is compared to *Fu17_1* full of organic structures and the minerals are not recognisable anymore. The organic structures could be divided into stromatolitic and peloidal microstructures, whereby the stromatolitic content is higher. Alternating brown and white layers are better visible compared to thin section *Fu10_1* (Figures 33 and 35). Also stromatolitic structures are more dominant in Furnas village (*Fu10_2*) compared to Lagoa das Furnas (*Fu17*). For this reason, probably different organism species exists in Lagoa das Furnas and Furnas village.

The complete thin section *Fu17_2* is silicificated. In the XRF pattern a high background is visible, due to the formations of silicificated (chert) structures (Appendix, Figure B 8). IR vibration pattern correlates with the XRF of *Fu17_1* due to the existence of alunite (Appendix, Figure B7) and of *Fu17_2* with the appearance of anorthite (Appendix, Figure C 8).

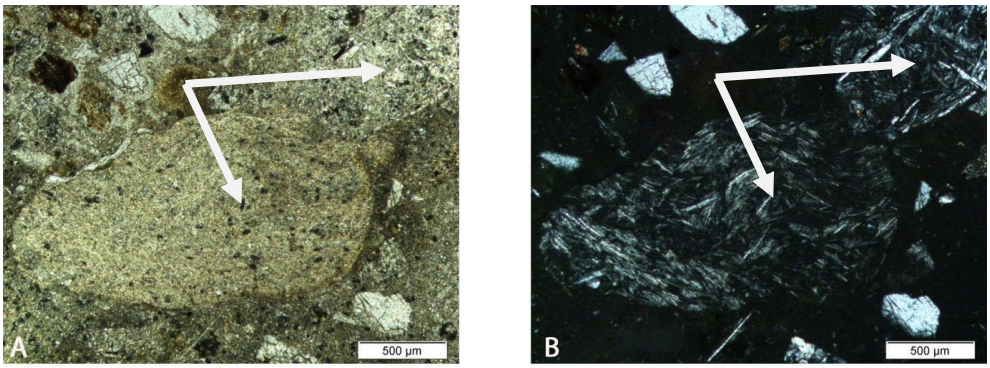

Figure 36 Thin section of sample *Fu17_1* One was taken with transmitted light (A) and the other one with crossed nicols (B). White arrows show the unaltered parts. These structures occur all over the thin section and could be a sign that the alteration has not finished yet.

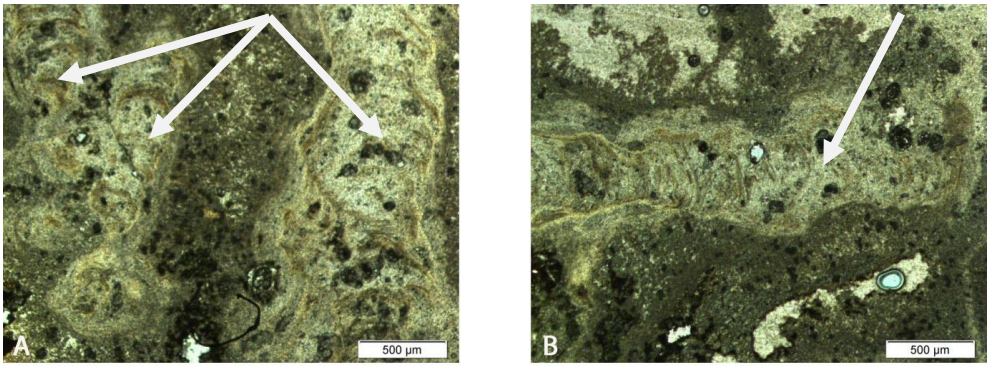

Figure 37 Optical microscopy images of the thin section *Fu17_2*. In both images stromatolitic microstructures are visible (white arrows) also known as spiculae Geyserites.

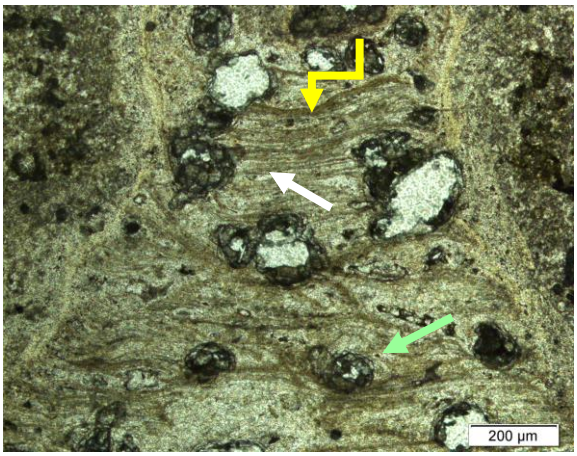

Figure 38 Image of stromatolitic and peloidal microstructure of *Fu17_2* with transmitted light. White arrow shows the white layers, yellow one pointed out the back-brown alternating layers and light green arrow indicates a peloidal microstructure.

6.1.3 Geometry of the siliceous sinters of São Miguel

It is the first characterisation of siliceous sinters of São Miguel with distinct analogues to those observed in Yellowstone (e.g.Guidry and Chafetz, 2003). The main geometry is called domal mound which indicates a subareas siliceous sinter structure. Typical for this structure is that the pool rim is covered by stromatolites (Figures 39-41). These stromatolites form an overhanging edge as well as shrubby siliceous precipitates. These precipitations are the result of the boiling water spray and its emergence and gaseous emissions. Therefore, two types of sinter precipitations in a domal mound after Guidry and Chafetz (2003) exists:

- upper one: grey indurated sinter with stromatolites
- lower one: powdery sinter with stromatolites

Both formations are visible in Furnas (Figure 41), whereas in Fogo and Ferraria had been no biotic influence.

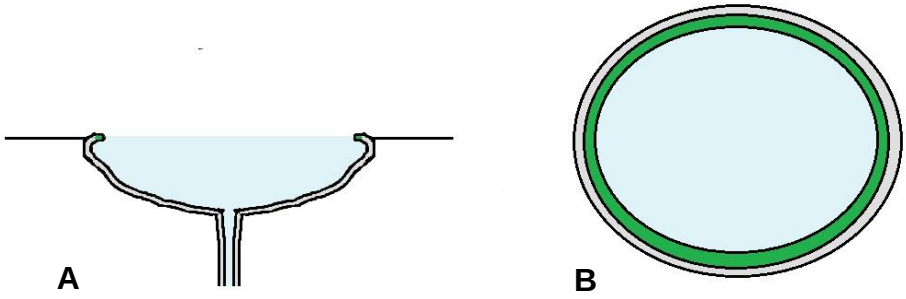

Figure 39 Schematic sketch of a domal mound of its cross cut (A) and over view of it (B). The blue colour indicates the hot spring, the green colour stands for the formation of stromatolites and the light grey colour shows the silicification.

Figure 40 Caldeira do Asmodeu with its domal mound structure. In the right picture zooming a part of the overhanging ledge formed through the activity of organisms, probably stromatolites.

It seems that there had been a water level change in the past because of the development of two stages in the case of Caldeira Grande. Such a change could be a result of earthquake activity, because it has an impact of the subterranean water flow (Xiaotong and Jones, 2012). The thick crust of the powdery sinter could be an indicator for organisms.

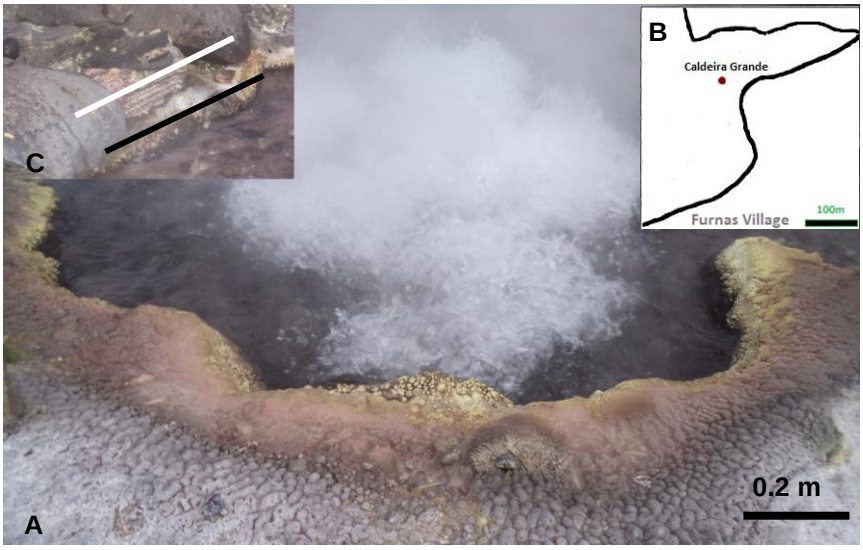

Figure 41 Picture of Caldeira Grande (A) located in Furnas village (B). Here are both stages developed, including the lower stage with the formation of the powdery sinter (white line: upper stage; black line: lower stage) (C).

6.2 Solutions

As in most geothermal active regions the chemistry of thermal waters could reach high contents of dissolved CO_2. In general, the CO_2 content of thermal waters of São Miguel decreases at higher temperature (Figure 42). Therefore, cold springs have the highest CO_2 contents (dissolution of gaseous CO_2 in aqueous solution is negative related to temperature), besides Fo6 as one exception (boiling pool of Fogo). However, the amount of CO_2 had a direct influence on the pH-value, for instance Fo6 had the highest CO_2 and SO_4 concentration as well as the highest evaporation degree and the lowest pH-value.

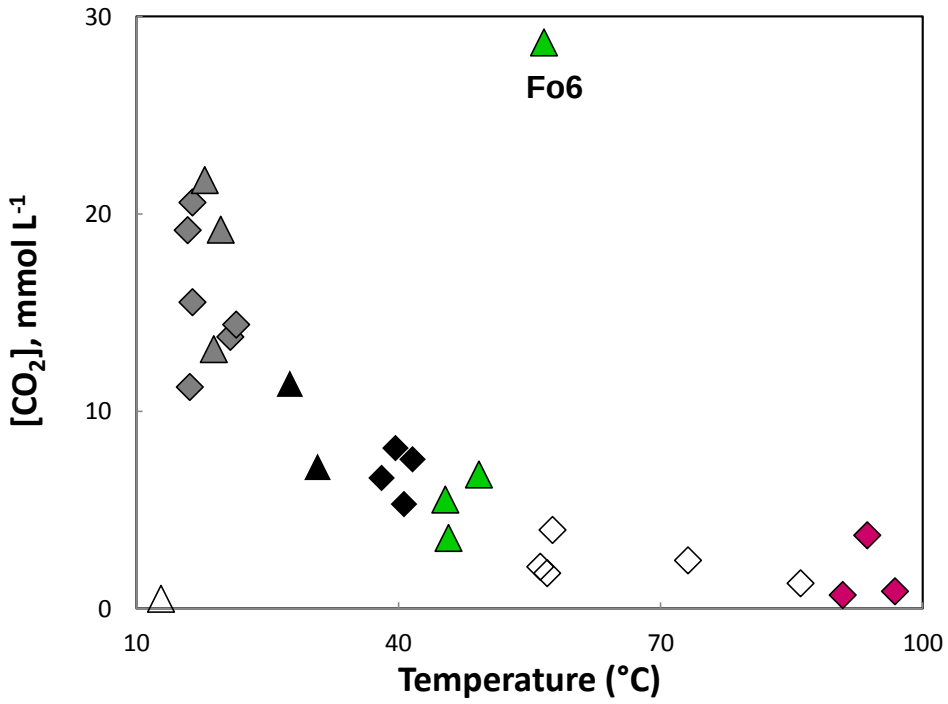

Figure 42 Plot of CO_2 concentration in mmol L^{-1} as a function of temperature for all samples of Furnas and Fogo volcano. At higher temperatures the CO_2 content is decreasing. The decreasing behaviour of CO_2 could have its origin in leaching rocks and/or magnitude of uptake of CO_2. Samples discharging at lower temperatures have the highest CO_2 contents, besides the exception sample Fo6 of a boiling pool of Fogo volcano. Cold CO_2 rich springs (<20 °C): ▲ (Fogo) ◆ (Furnas) cold CO_2 poor spring (<20 °C): △ ,warm thermal discharges (20-40 °C): ▲ (Fogo) ◆ (Furnas) , mesothermal water (40-75 °C): ▲(Fogo) ◇(Furnas) : hypothermal type (>75 °C): ◇ ◆ (Furnas).

Mineral and thermal water chemistry of São Miguel can be divided into groups based on their major ionic composition. Grouping makes it easier to identify chemical processes and their influence on the water composition. In general, the composition can be also influenced by the mixture with meteoric and/or seawater as well as magmatic gases and rock leaching. A rough classification into 3 groups by chemical composition is given in the following.

Na-SO_4 type

A high SO_4^{2-} content suggested that the water chemistry is controlled by a shallow steam heating process (if mixing with sea water can be ruled out). Volcanic gases like SO_2 and H_2S interact with shallow aquifer (meteoric water). The oxidation of H_2S by atmospheric O_2 and bacterial activity can explain elevated SO_4^{2-} content in modern volcanic settings. As a result the SO_4^{2-} content increases and the pH-value decreases in the surface water (Szynkiewicz et al., 2012). A low pH-value has also a positive effect on the rock leaching.

Na-HCO_3 type

This kind of water belongs to springs which are usually discharging in the vicinity of geothermal surface manifestations like fumarolic grounds or cold mineral waters. Apart from that, this type is the most common in the whole Azores archipelago (see also Cruz and França, 2006). The HCO_3^- enrichment is a result of the capture of CO_2 - rich gas emission and also indicates an early stage of rock and meteoric water interaction. HCO_3^- content has also a close relation to TDS (total dissolved solids) value.

Na-Cl type

This type discharges from a basal aquifer and shows clearly the influence of seawater. The mineralization increases independently of the HCO_3^- content in contrast to Na-HCO_3 and Na-SO_4 type (Figure 43). The marine components are mainly e.g. Na^+, Cl^- and K^+. However, chloride and other dissolved salts in thermal waters can be also the result of rock leaching (Ellis an Mahon, 1964; Saki and Matsubaya, 1977). Another model for the explanation for elevated content of chloride is that the steam from the magma chamber contains quantities of hydrogen chloride which will be neutralised due to the reactions with rocks (Saki and Matsubaya, 1977). However, in the present case seawater is the source for both Na^+ and Cl^-.

Figure 44 shows silicate weathering reaction. During the weathering process H^+ atoms (or any kind of acids) were consumed, which resulted in rising pH- values.

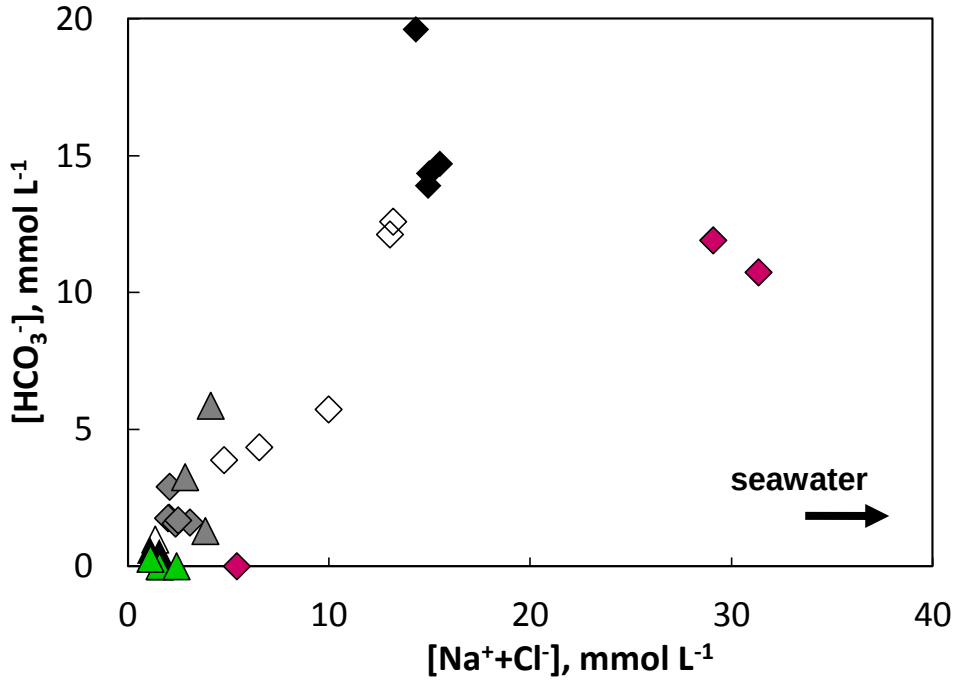

Figure 43 Plot of HCO_3^- versus $Na^+ + Cl^-$ concentrations showing a positive trend. This distribution is influenced by the result of water- rock interaction as a neutralisation processes. Furthermore, it is obvious that samples of Furnas (◇:cold and CO_2 rich water, ◆: warm water, ◇: mesothermal water, ◆: boiling pools) tend to have higher concentrations compared to samples of Fogo area (△: cold and CO_2 rich water, △:cold and enriched in CO_2, ▲: warm water and ▲ : boiling pools). Boiling pools show a different trend in both areas (◆: Furnas boiling pools, ▲ : Fogo boiling pool). Black arrow indicates seawater.

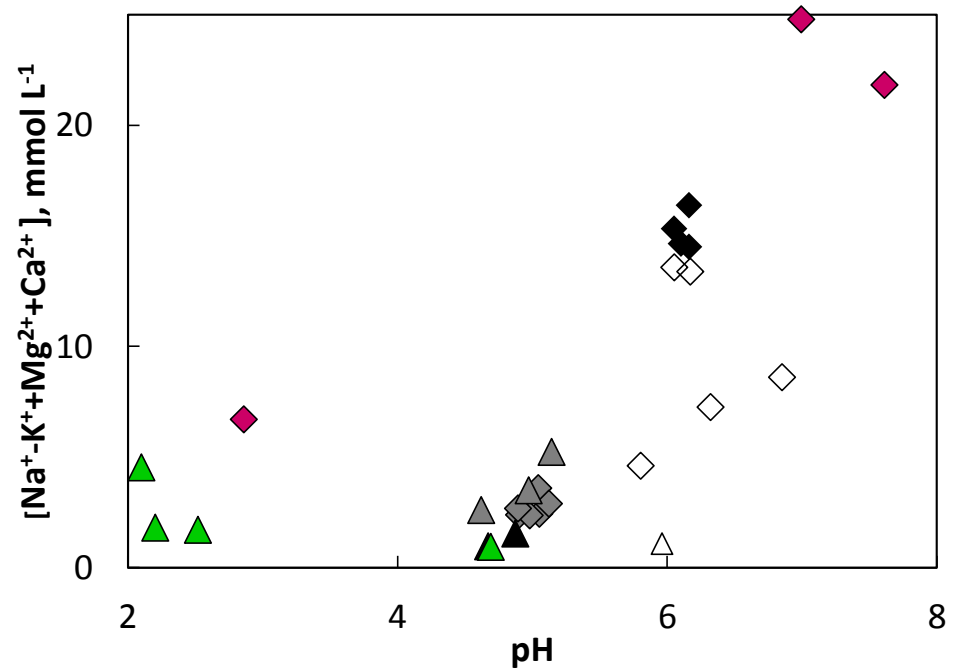

Figure 44 Plot of rising pH-values as function of $Na^+ + K^+ + Mg^{2+} + Ca^{2+}$ concentration which is a hint for water-rock interaction. The boiling pools from Fogo- Ribeira Quente as well as the sample of the boiling pool of Furnas lake with the highest SO_4^{2-} contents have the lowest pH-values (Furnas samples: ◇: cold and CO_2 rich water, ◆: warm water; ◇: mesothermal water, ◆ : boiling pools; Fogo: △ : cold and CO_2 rich water, △ : cold and enriched in CO_2, ▲ : warm water and ▲ : boiling pools).

Another reason for the pH value distribution could be the influence of seawater or magmatic activity in form of CO_2. The $\delta^{13}C$ values can be used to distinguish if the carbon species have their origin in magmatic processes or not (see section 2.4.3).

Figure 45 shows that the increase of silica content depends on temperature. At higher temperature the leaching of silicates from the host rocks is enhanced. There are just two exceptions: Fo10 and Fu3. $Si(OH)_4$ concentration as a function of temperature divided Furnas springs in three groups of surface discharges. These three groups matched together with the sampling site. Besides samples of boiling pools also Fu6 and Fu3 were exceptions. Fu3 and Fu6 have higher temperatures compared to the other springs, but the $Si(OH)_4$ content is low. Boiling pools show a different behaviour compared to springs, because the $Si(OH)_4$ content decreases with increasing temperature. One possibility of the behaviour of Fu3 and Fu6 could be that their discharges are strongly influenced by boiling pools. Furthermore, also the pH-value has an impact on the distribution of $Si(OH)_4$. At $3 < pH$ and $pH > 9$ the silicate weathering generally increases strongly (Figure 44). Another point to be made is, that sampling sites Furnas and Fogo show a completely different silicate weathering trend as function of the CO_2 content. For instance, in Furnas the $Si(OH)_4$ content is increasing at lower CO_2 content compared to Fogo with increasing $Si(OH)_4$ content at higher CO_2 amount (Figure 42). The strong impact of CO_2 on the silica content can be explained by the pH value distribution as a function of CO_2. The higher the CO_2 content the lower the pH value. Therefore, the silica weathering at Fogo Volcano is rather independent on temperature, but depends strongly on pH.

The total amount of aluminium in solution is related to the dissolution of silicates as a function of pH-value (Figure 46). Therefore, Fo6 has the highest concentrations and Fo3 the lowest. Fu6 showed similar behaviour like the boiling pools in Furnas village.

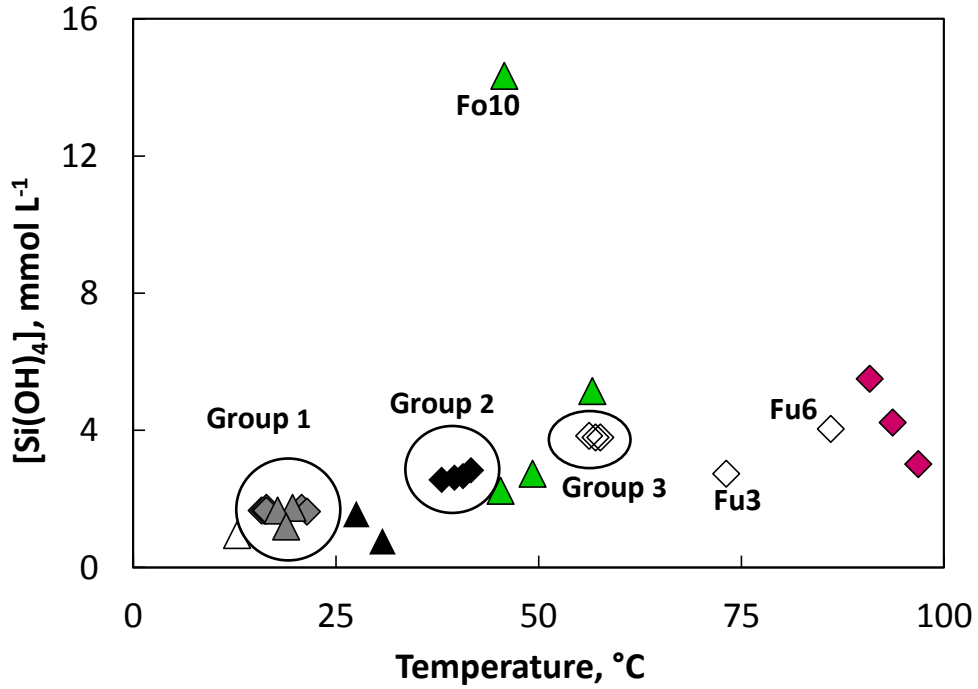

Figure 45 Plot of temperature as a function of $Si(OH)_4$ concentrations. At higher temperatures the silica concentration is increasing in all spring samples (Furnas: ◇: cold and CO_2 rich water, ◆: warm water; ◇ : mesothermal water; Fogo: ▲ : cold and CO_2 rich water, △: cold and enriched in CO_2, ▲ : warm water). There are just few exceptions like boiling pools of Furnas Fu9, Fu10 and Fu17 (◆) as well as boiling pools of Fogo (▲), especially Fo10 with the highest $Si(OH)_4$content of all samples Furthermore, three spring groups are easy to distinguish and also occur in Furnas next to each other ; Group 1 stands for cold and CO_2 rich water types with a $Si(OH)_4$ content between 1,5 and 2 mmol L^{-1} (◇), Group 2 implies warm water samples with $Si(OH)_4$ concentration between 2.5 and 3 mmol L^{-1}(◆) and Group 3 stands for mesothermal type with $Si(OH)_4$ content of 3.5-4 mmol L^{-1} (◇).

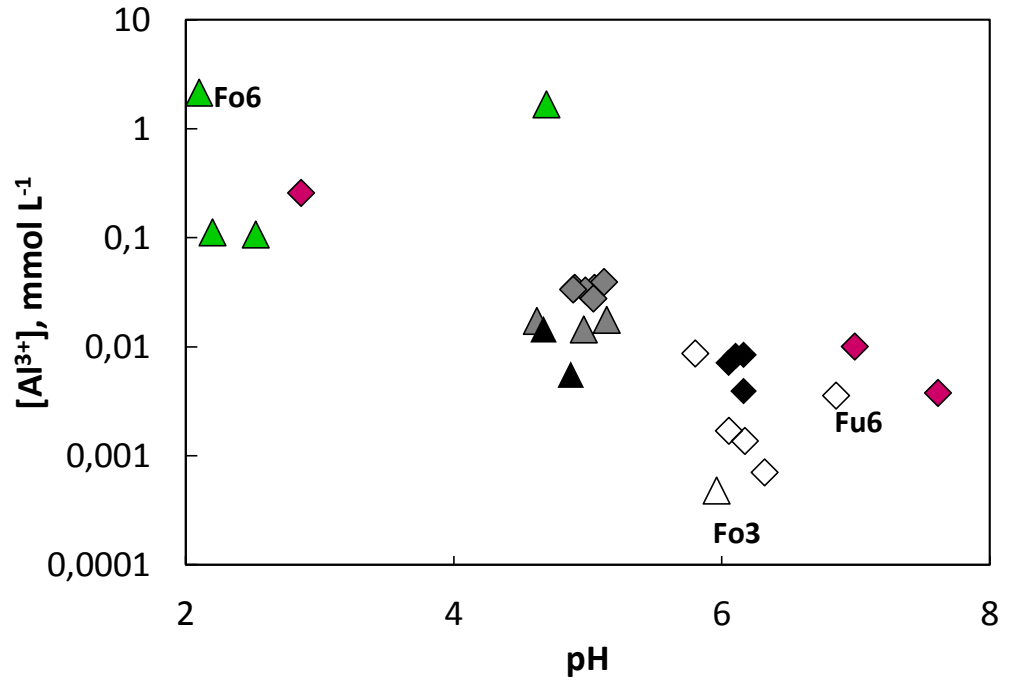

Figure 46 Relation between pH value and Al^{3+} concentration. Plot shows that with increasing pH-value, the Al^{3+} content in the samples is reduced. Boiling pools have the highest concentrations in Al^{3+}. (Furnas samples: ◇: cold and CO_2 rich water, ◆: warm water; ◇: mesothermal water, ◆: boiling pools; Fogo: ▲: cold and CO_2 rich water, △ : cold and enriched in CO_2, ▲: warm water and ▲ : boiling pools).

Compared to the results of the average composition of ocean island basalts in São Miguel (Dasgupta et al., 2010) and average values of 1558 analysed basalts (Hess, 1967) the Ca^{2+}/Mg^{2+} content of São Miguel basalt samples with 0.78 fitted with the average value of the Ca^{2+}/Mg^{2+} content of all liquid samples with 0.77. (Figure 47). Therefore, the Mg^{2+} and Ca^{2+} concentration originated from basalt weathering processes and had less been influenced by the potential admixing of seawater.

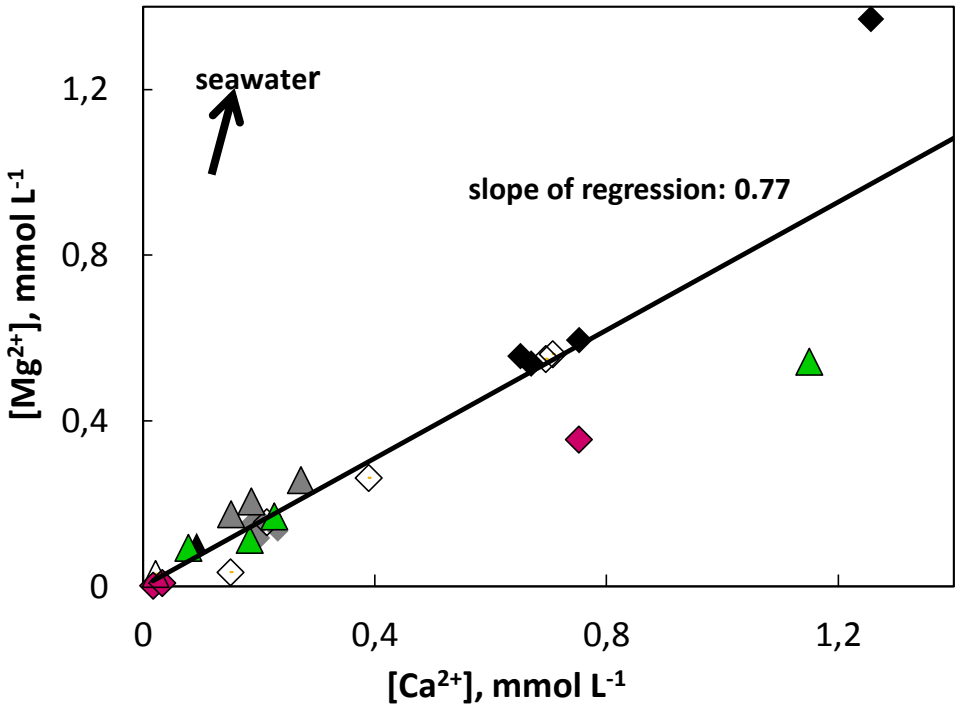

Figure 47 Plot of Ca^{2+} and Mg^{2+} concentrations. The slope of regression line varied from the seawater mixing trend (black arrow; Mg:Ca ratio of Azorean Sea Water is about 4.6). (Furnas samples: ◇ : cold and CO_2 rich water, ◆ : warm water, ◇: mesothermal water, ◆: boiling pools; Fogo: △: cold and CO_2 rich water, △: cold and enriched in CO_2, ▲: warm water and ▲: boiling pools).

The measured molar ratio of Sr^{2+} and Ca^{2+} concentration for the Atlantic ocean water, which was sampled in Ferraria, is 0.0069 and samples taken in 1999 (de Villiers) in the vicinity of Azores (coordinates: 40°N/20°W) were similar with a ratio of 0.0085. Nevertheless, all the other samples of São Miguel had lower ratio of Sr^{2+}/Ca^{2+} ratios compared to the Atlantic Ocean (Figure 48). Only the sample of Ferraria had a Sr^{2+}/Ca^{2+} ratio of 0.0075 close to seawater with a ratio of 0.0069. A hint for proceeding water-rock interaction is the increasing content of Sr^{2+} as a function of increasing temperature. Differences in the Ca^{2+} concentration of both boiling pool and springs are mostly in relation with the results of Ca^{2+} wt.% in rock samples (Appendix, Table C 1). For instance, in Furnas village the Ca^{2+} content in rocks is 12- times higher compared to Furnas Lake. However, samples from Fogo volcano had lower Ca^{2+} concentrations but all their boiling pools were enriched in Sr^{2+}.

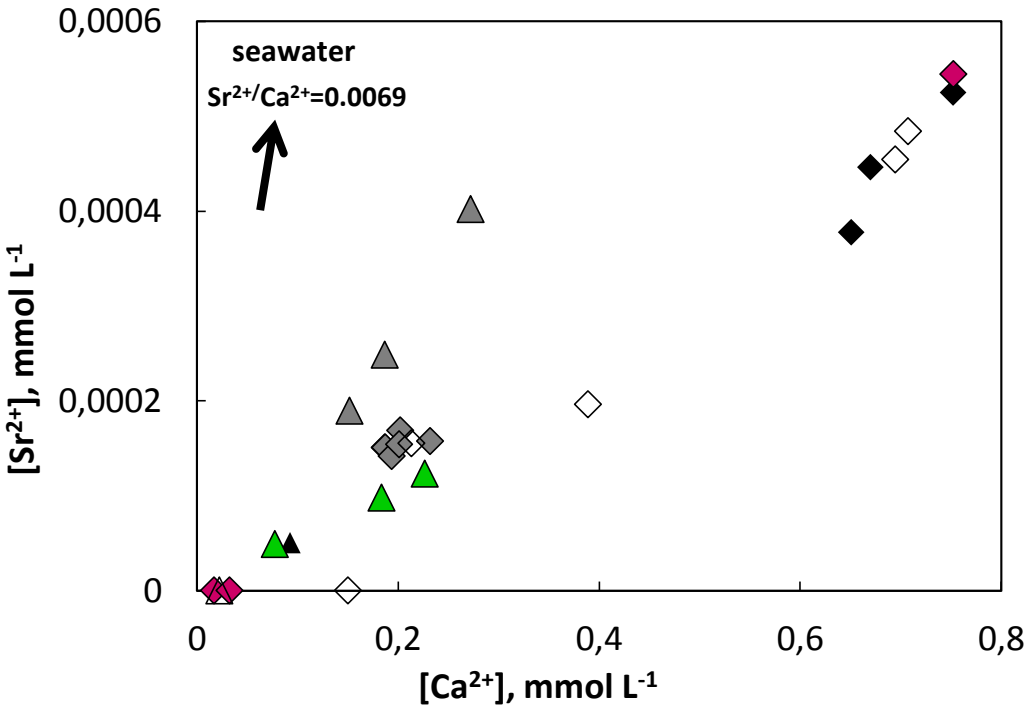

Figure 48 Plot of Ca^{2+} versus Sr^{2+} concentrations shows a positive trend for an increase ot he amount of both Sr^{2+} and Ca^{2+} Furnas springs (◈: cold and CO_2 rich water, ◆: warm water; ◇ : mesothermal water,) as well as for Fogo springs (△: cold and CO_2 rich water,△: cold and enriched in CO_2,▲: warm water). However, the behaviour of both elements are not related to the influence of sea water (black arrow). As a result, the trend can be explained by the water-rock interaction. Especially in Furnas the Sr^{2+} concentration is increasing with temperature, besides for the boiling pools in Furnas village, which could have volcanogenic origin (Furnas boiling pools: ◈; Fogo boiling pools: ▲) .

Saturation index

Saturation index diagram shows that all samples are undersaturated with respect to amorphous silica and albite (Figure 49). Exceptions are boiling pools Fo10 and Fu17, which is a clear hint for water interaction with igneous rocks at elevated temperature (Armienta et al., 2008). Moreover, all samples are undersaturated with respect to anhydrite and calcite. Thus e.g. precipitation of calcite from the analysed solutions at the time of sampling can be ruled out.

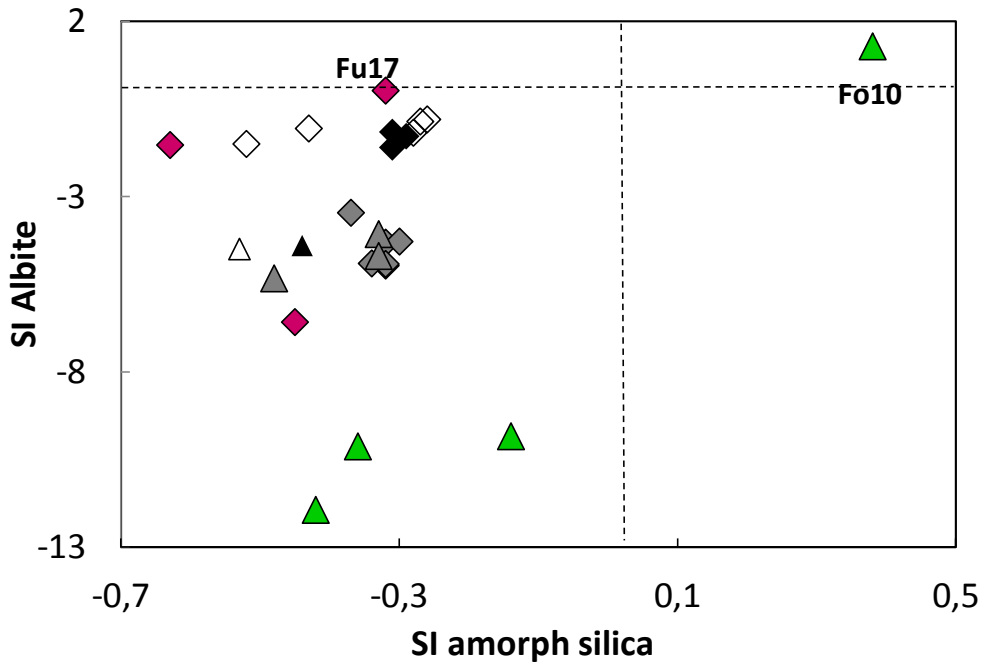

Figure 49 Saturation index diagram of amorphous silica and albite. The only solution with is supersaturated with respect to amorphous quartz is sample Fo10 (▲). Samples are undersaturated in albite, besides boiling pool samples Fo10 and Fu17. Lowest albite saturation indices observed in boiling pools of Ribeira Grande (▲). Also springs sample of Furnas (Fu1, Fu2, Fu4, Fu5, Fu7, Fu8) have similar saturation indices such as Fogo springs. Solutions of Fu3 and Fo6 plot in the vicinity of the boiling pools of Furnas city). (Furnas samples: ◆: cold and CO_2 rich water, ◆: warm water; ◇: mesothermal water, ▲: boiling pools; Fogo: ◆: cold and CO_2 rich water, ▲: cold and enriched in CO_2, △: warm water and: ▲ boiling pools).

Furnas

There is a weak relation between $Si(OH)_4$ and other elements like K^+, Na^+, Ca^{2+} and Mg^{2+}. An increase of K^+ due to the increasing of $Si(OH)_4$ is however visible in springs but not in boiling pools. Eq (6) suggests the release of K^+ as a result of the incongruent solution of potash feldspar to kaolinite, hence in sample Fu9 should be an increase of K^+ concentration in water but alunite is also formed and therefore there is no increase in K^+ in the respective sample. According to chemical analyses of natural rock samples, Fu9 and Fu10 solutions have the highest amounts of K^+ (Appendix, Table C 1).

Figure 50 shows an opposite behaviour of Al^{3+} and $Si(OH)_4$ concentrations. For instance the solubility of aluminium hydroxide can explain the evolution of dissolved Al^{3+} as a function of pH. Below pH 4.5 and above pH 7 the total solubility of Al^{3+} increases (Apello and Postma, 2005). In the present case at acid conditions the solubility and dissolution kinetics of silicates are enhanced. The lowest Al^{3+} can be found in the group of springs with the highest temperatures and pH-values between 5.8 and 6.8 (pH is limiting the Al content).

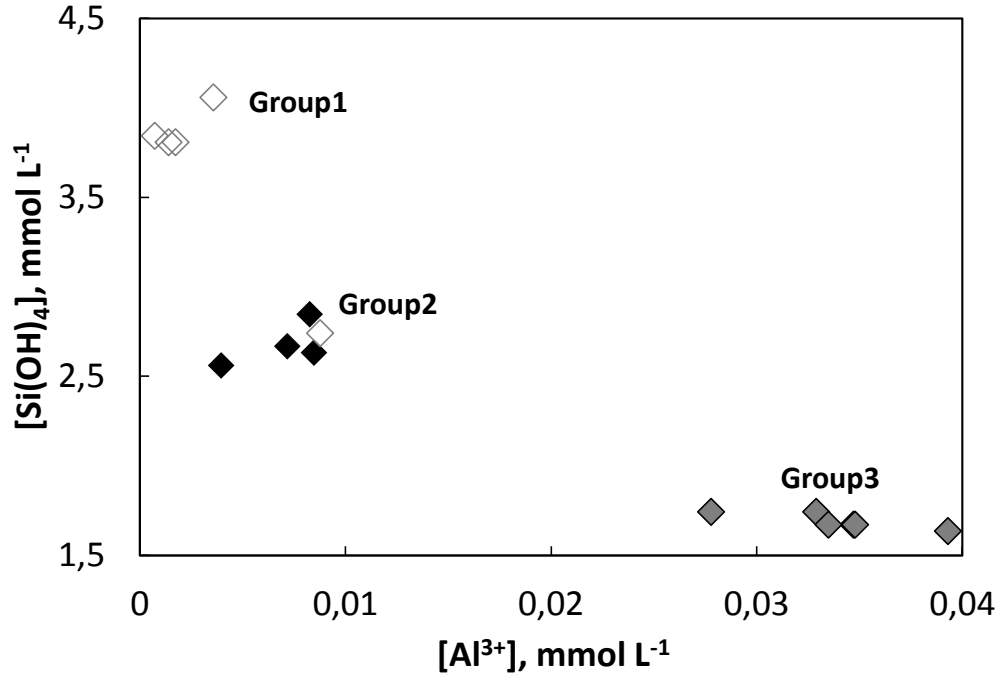

Figure 50 Diagram of Al^{3+} and $Si(OH)_4$ content distribution in different Furnas springs. With increasing $Si(OH)_4$ concentration Al^{3+} is decreasing for all samples. A clear grouping of spring groups is obvious: Group1 indicates mesothermal samples Fu11, Fu12, Fu16 with Fu6 in their vicinity (◇), Group 2 are a mixture of warm water with Fu13, Fu14 and Fu18 nearby (◆) and mesothermal sample Fu3 (◈), Group 3 stands for cold and CO_2 rich samples like: Fu2, Fu7, Fu8 with Fu4 and Fu5 close to them (◇).

The content of SO_4^{2-} and Al^{3+} concentrations could have their origin in uptake of sulphur gases and rock-water interaction which strongly depends e.g. on temperature conditions (Figure 51). As mentioned in Chapter 2.3 the pH-value is influenced by volcanic gases and rock- water interaction (and in principle also seawater contamination). It is clearly visible that the amount of sulphate in the boiling pools influenced the pH-value. The higher the sulphate content, the lower the pH-value due to the formation of sulphuric acid (H_2SO_4). Alunite and kaolinite can be formed in such a sulphur-aluminium and silica rich environment. Fu16 solution had the lowest Al^{3+} contents and Fu6 shows again a similar behaviour such as boiling pools from Furnas village.

Figure 52 shows the concentration of Na^+ as a function of Br^- content. The Na^+ content is increasing at higher Br^- concentrations, but the direction of this trend differs from the Meteoric-Azorean Seawater Mixing Line. Therefore, the Na^+ content is suggested to be a result of rock-water interaction.

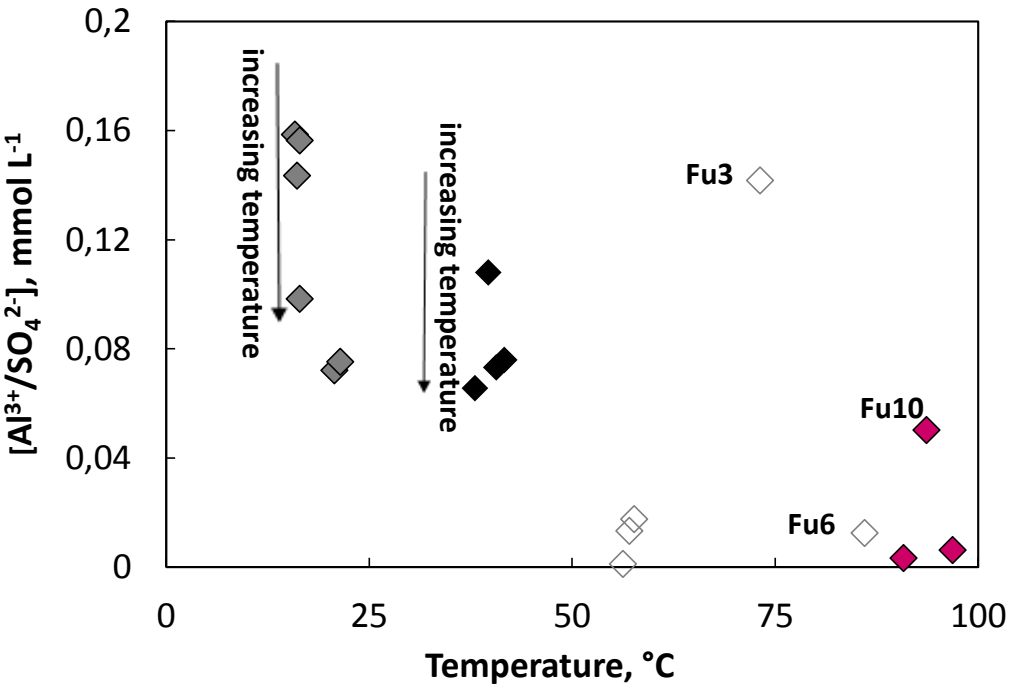

Figure 51 Al^{3+}/SO_4^{2-} content distribution depends on temperature. In general, the higher the temperature the higher the SO_4^{2-} vs. Al^{3+} content. In contrast, at lower temperatures the Al^{3+} concentration increases relative to SO_4^{2-}. Also the internal distribution of cold and CO_2 rich water types (◈), warm water (◆) and mesothermal samples (◇) depends on temperature. Therefore, with decreasing Al_3^+/SO_4^{2-} ratio temperature increases. Fu3, Fu10 as well as Fu16 differ in their behaviour. (◈: boiling pools).

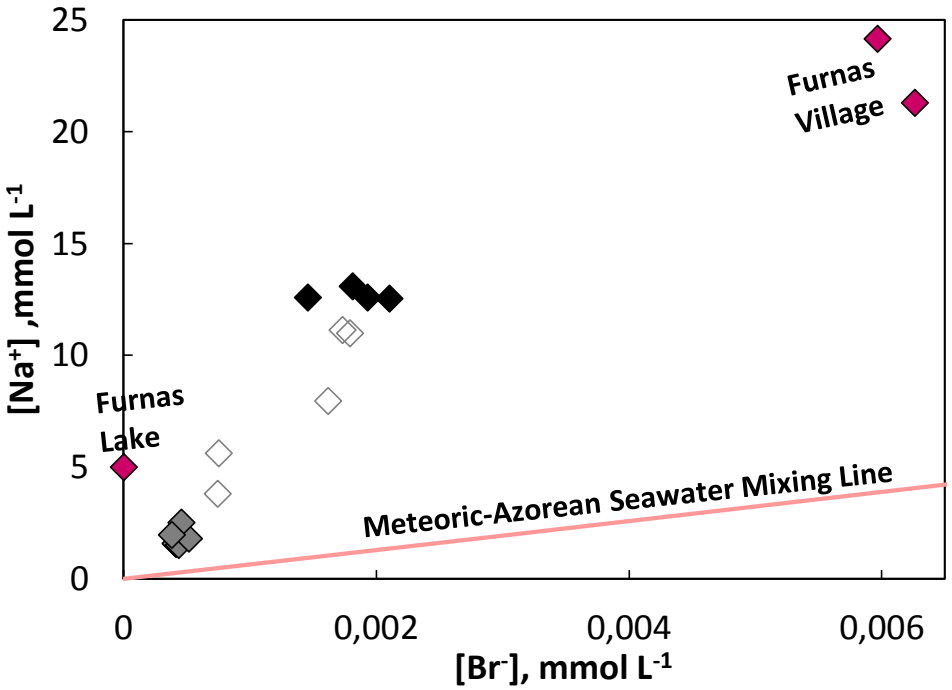

Figure 52 Correlation of Na^+ and Br^- concentration. All samples appear above the Meteoric-Azorean Seawater Mixing Line (rose line) and indicate therefore that the Na^+ content is rather due to water-rock interaction depending on the solubility of sodium containing silicates and temperature of water than on mixing with sw. Therefore, all Furnas spring samples show the same trend (◈: cold and CO_2 rich, ◆ : warm water , ◇ : mesothermal type), compared to Furnas boiling pools (◈). It is obvious that especially samples of boiling pools from Furnas village and Furnas Lake differ in their behaviour.

Figure 53 shows the relative stability of minerals during water rock interaction for all Furnas samples in the log[Al^{3+}] + 3pH vs. log[H_4SiO_4] plot at 25 °C. Stability lines indicated a solubility control of $Si(OH)_4$ in thermal discharges in Furnas by amorphous silica precipitation at 25 °C. There was just one exception, the sample from Furnas Lake with a solubility control by kaolinite.

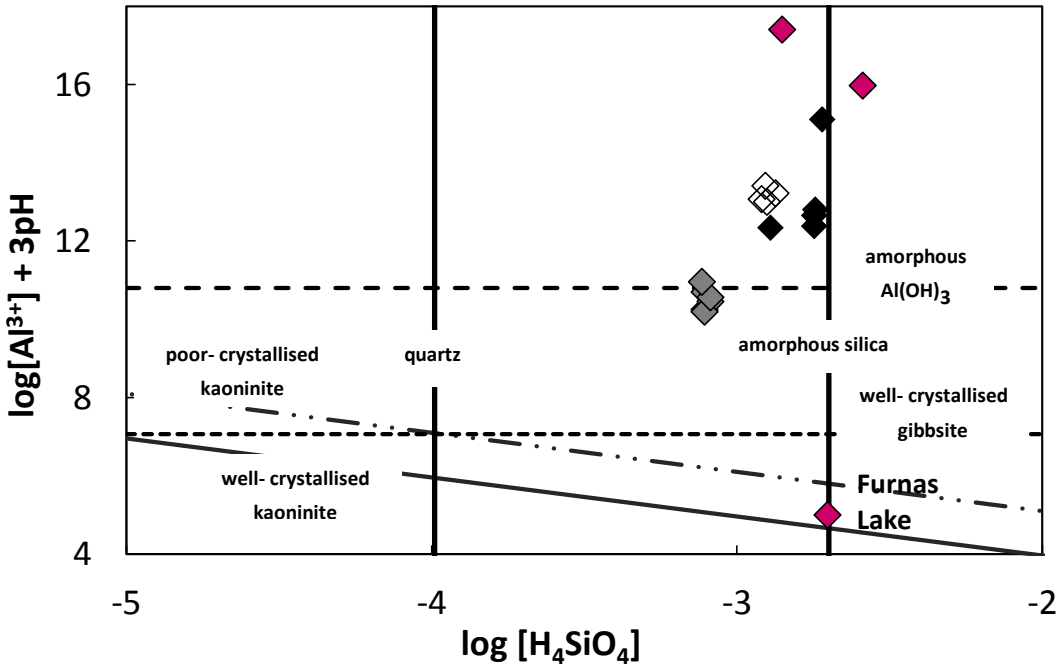

Figure 53 Log activities of Al^{3+},H^+ and H_4SiO_4 in a mineral stability diagram of the Al_2O_3-SiO_2-H_2O system (25°C). (◈: cold and CO_2 rich water, ◆: warm water, ◇: mesothermal type) and Furnas boiling pools (◈) had been modeled for 25°C. Solubility control in most of the samples is given by amorphous silica. Thermodynamic data for mineral stabilities are from Gerard et al., (2001) and Appelo and Postma (2005).

6.2.1 Water geothermometers and saturation indices evolution

Temperatures estimated from water hydrochemistry (e.g. Na-K, Na-K-Ca cationic geothermometers) let assume that the solutions of Furnas with discharging temperatures between 32 and 74°C were close to “equilibrium” with respect to local rocks. Various geothermometers had been used (Appendix.Eq1-Eq8.) especially Na-K, Na-K-Ca and Li-Mg ratios shows comparable temperatures between 200 and 300 °C. In contrast, Si-thermometer reveals lower temperatures around 150 °C (Table1). According to Fournier (1977) quartz geothermometry works best at temperatures between 150 and 225 °C and at lower discharging temperatures amorphous silica chalcedony or cristobalite control silica dissolution. Thus, geothermeters by using elemental concentrations cannot be reasonably apply in the above rather simple approaches to the given solutions.

Table 1 Calculated temperatures (in °C obtained by the use of liquid cationic geothermometers (see Appendix Eq1-Eq9 and Table A6; T&F=Truesdell and Fournier, 1975; T= Tonani, 1980; A= Arnorsson et al., 1983; F= Fournier, 1979; N&N= Nieva and Nieva, 1987; G= Giggenbach, 1981; K&M= Kharaka and Mariner, 1988; F= Fournier, 1977))

Samples	Na- K (T&F)	Na-K (T)	Na-K (A)	Na-K (F)	Na-K (N&N)	Na-K (G)	Li-Mg (K&M)	SiO_2 (F)
Grutinha I	248	240	241	229	216	244	254	146
Quentura I	317	305	229	273	258	283	269	166
Água do Torno	234	228	298	220	207	236	255	145

Saturation indices for various minerals calculated at different temperatures under oxidising conditions are shown in SI vs. T plots (Figure 54-58) for Furnas area. The green line indicates the in-situ measured value. Main differences between boiling pools in Furnas village (Fu9, Figure 54) and lake (Fu10, Figure 55) are increasing saturation indices as a function of increasing temperature for the lake area.

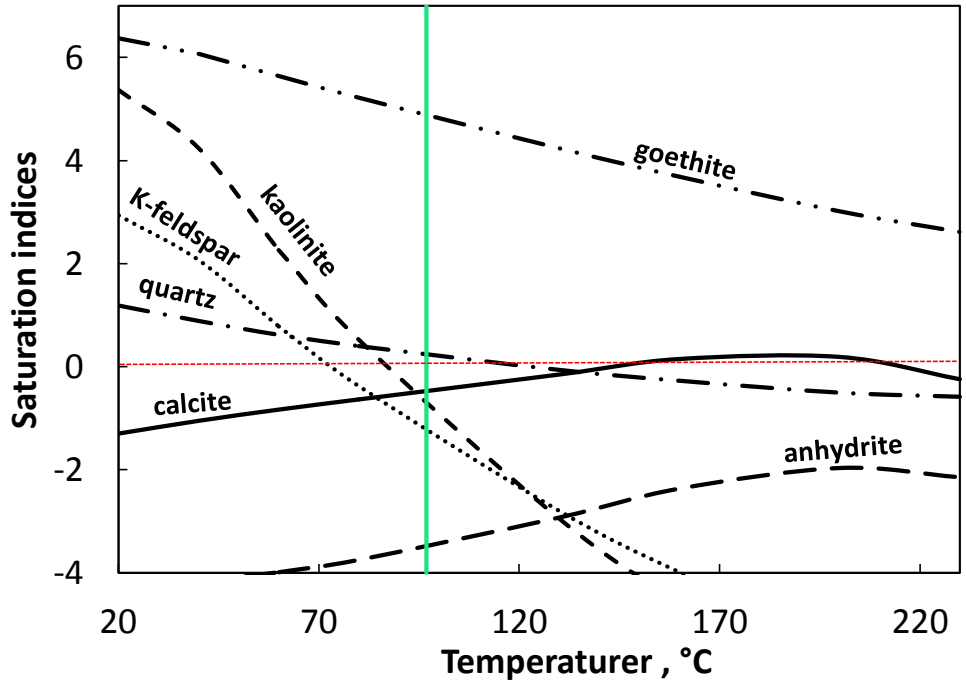

Figure 54 Saturation indices for goethite, kaolinite, k-feldspar, quartz, calcite and anhydrite at temperatures from 20 to 230 °C for sample Fu9. Equilibrium conditions at discharging temperature (96.8 °C) are shown by the green line.

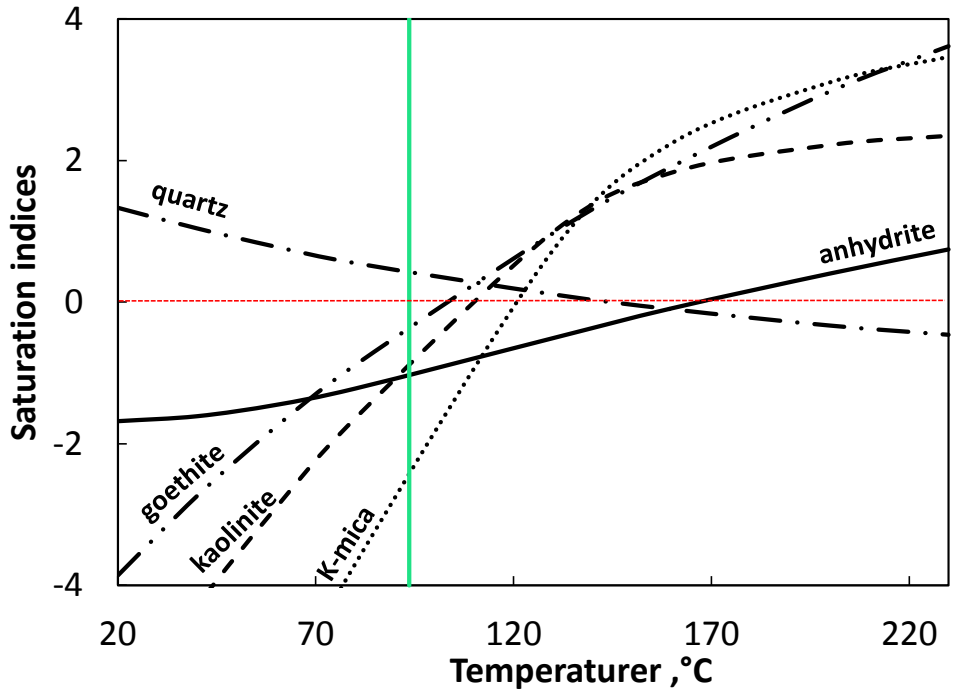

Figure 55 Saturation indices for goethite, kaolinite, k-feldspar, quartz, K-mica and anhydrite at temperatures from 20 to 230 °C for sample Fu10. Equilibrium conditions at discharging temperature (93.6 °C) are shown by the green line.

6.2.1 Isotopic composition

Water samples have their overall origin in meteoric water by the fact that they lie close to the global meteoric water line (GMWL) line with $\delta^{18}O$ between -4 and -2 ‰ (V-SMOW) and δD values range from -20 to -6 ‰ (V-SMOW) (Figure 56). Magmatic water has $\delta^{18}O$ values ranging from 0 to 10 ‰ and δD values which range from -80 to -40 ‰ (Yardley and Bodnar. 2014; Sheppard, 1986). It is obvious that none of the waters have primary magmatic H_2O origin, so they are not juvenile waters. Thus, meteoric water penetrates into the crust to generate a ''magmatic fluid''. In general, the trend shows a deviation from the GMWL-line. Reasons for the deviation could be differences in the humidity above the oceans (Merlivat and Jouzel, 1979; Gerardo et al., 1993), or effects of ocean vapour and terrestrial vapour produced by evaporation and transpiration (Ingraham and Matthews, 1990; Gerardo et al., 1993) or from an ^{18}O exchange with meteoric water at the surface (Delalande et al., 2011). Furthermore, steam heated water has even a lighter signature because of steam as heat source and surface evaporation. Figure 56 compares annual regional meteoric water measurements with global meteoric water line as well as with samples taken in the Azores 2006 (Cruz and França, 2006) and 2013 (this study). Most of the regional values are plotting close to the GMWL. Boiling pools differ in general, caused by the degree of evaporation shifting from GMWL. Also remarkable is that most of the spring samples are depleted in ^{18}O and in D compared to the GMWL. This is explained by the isotopic composition of Azorean rain, because also LMWL (local meteoric waterline)

shows a slightly depletion in isotopes. The LMWL resulted from the average mean of the isotopic composition of meteoric water (from 2009 to 1962, measured by IAEA) (Appendix: Table A4). Also isotopic measurements by Cruz (Cruz and França, 2006) showed the same trend for analysed samples in São Miguel. Moreover, variations in $\delta^{18}O$ could be attributed to exchange reactions with silicates and thermal water at elevated temperature during leaching (Pasvanoğlu et al., 2006).
According to Figure 56 Ferraria is a mixture between seawater and meteoric water and consists of 88.5% of seawater. Also both lake samples and one boiling pool of Fogo (Fo4) could have their origin in seawater admixture. Due to their isotopic $\delta^{18}O$ and δD signature they plot on the Meteoric-Azorean Seawater Mixing Line. According to hydrochemical analyses, of these 3 samples, they are not influenced by seawater. For instance, both lake samples (AS and AS23) are too low in ion content for a significant seawater admixture. Low Br^- concentrations (0.004 mmol L^{-1}), Ca:Mg ratio (Figure 47) and Ca:Sr ratio (Figure 48) of sample Fo4 indicated that mixture between seawater and meteoric water can be ruled out. The $\delta^{18}O$ and δD evolution below the GMWL and LMWL has their cause in water-rock interactions at elevated temperatures and/or evaporation processes, as seawater admixture can be excluded (see also Cruz and França, 2006).

In Figure 57 $\delta^{18}O$ and Cl^- content indicates two different trends for the evolution of natural discharges: evolved and shallow steam heating processes. Both processes are a function of discharges' distance to the magmatic source, for instance, gases like SO_2 and H_2S exsolve from the magmatic source in very shallow levels. Evolved effects imply a larger distance to the magmatic with CO_2 rich liquids and thereby elevated rock leaching.

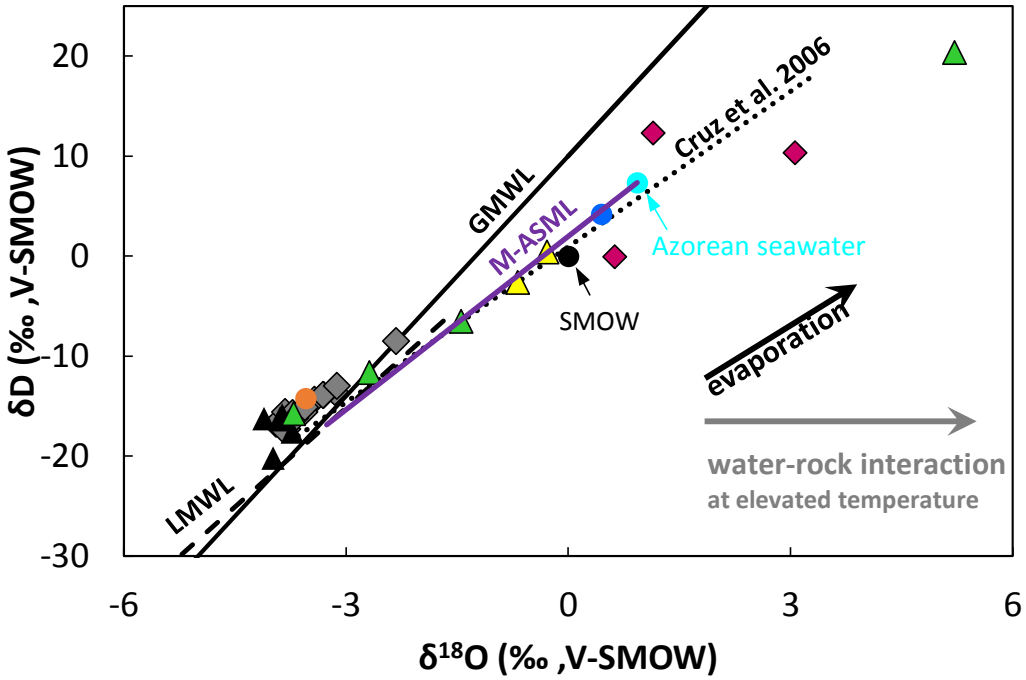

Figure 56 Plot of the isotopic composition of sampled natural waters from São Miguel. The black arrow shows the evaporation effect and the grey arrow the increasing of $\delta^{18}O$ caused by increasing of water-rock interaction. (black line: GMWL and black dashed line: LMWL (2009-1962), black dotted line: Cruz and França (2006). The violet line, implies the mixture line of water which was calculated by the average mean of the isotopic meteoric composition of the Azores and the seawater sample which was taken in Ferraria (Meteoric- Azorean Seawater Mixing Line; M-ASML).Due to hydrochemical analyses it is clear that just Ferraria sample is the product of meteoric- sea water mixing.◇: Furnas springs; ◆: Furnas boiling pools; ▲ : Fogo springs; ▲: Fogo boiling pools; △: Sete Cidades lake samples; ●: Ferraria sample, ● : Azorean seawater, ●: sea water, ●: drinking water taken in São Miguel).

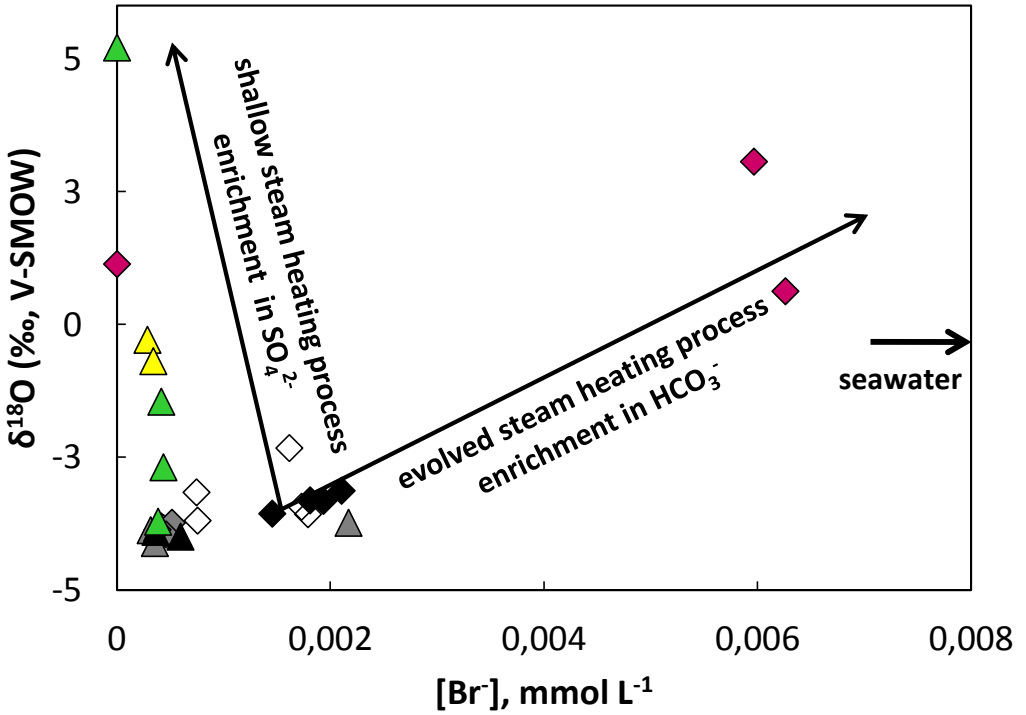

Figure 57 Plot $\delta^{18}O$ vs. Br^- concentration. Two different trends are visible: evolved steam heating process : salinity of waters increases linearly with the increasing of $\delta^{18}O$ values and shallow steam heating process: salinity of samples decrease as a function of increasing $\delta^{18}O$ values ((Furnas:◇ : cold and CO_2 rich, ◆ : warm type, ◇ : mesothermal, ◆ : boiling pools ; Fogo:▲:cold and CO_2 rich ,△:cold and CO_2 poor ▲: warm type, ▲ : boiling pool , △: caldera sample, black arrow shows the sea water direction to Azorean sea water composition).

The $\delta^{34}S$ values of dissolved sulphate show a wide range between -3.7 and 21.3 ‰ and the $\delta^{18}O$ values of sulphate vary between 0.5 and 10.5 ‰ (Appendix, Table. A. 3). According to Valentino (1999) $\delta^{34}S$ values for dissolved sulphate of about 1-2 ‰ are similar to the total sulphate/sulphide in deep-seated magmas and values between -1 and 0 ‰ may suggest a supergenetic oxidation of H_2S of volcanic/magmatic origin. The lowest $\delta^{34}S_{SO4}$ values can be found in Furnas village with -3.7 ‰ which fit with the observation of stromatolite structures in the thin sections (Figure 58). Negative $\delta^{34}S$ values could be caused by the overlapping of magmatic origin and biological processes. The high $\delta^{18}O_{SO4}$ value with 10.5 ‰ of Fu17 supports the overlapping hypothesis because of its influence of bacterial sulphate reduction.

In addition, all springs of Furnas are strongly influenced by igneous processes which controlled the isotope fractionation. Also, the SO_4^{2-} content in the boiling pools of Fogo is a result of magmatic phase separation (shallow steam heating process). Their $\delta^{34}S$ values range between 0.4 and 5 ‰. Oxygen isotope values of dissolved sulphate of the above boiling pools also indicate that the sulphate derived from the oxidation of reduced inorganic sulphur ($\delta^{18}O_{SO4}$ ranges between 0.4 and 2.5 ‰). Positive $\delta^{34}S$ values up to 7 ‰ could also originate from the weathering of basaltic rocks or oxidation of magmatic gases and overlapping of biological processes. The typical pattern for modern hydrothermal active areas can be seen in $1/[SO_4^{2-}]$ vs. $\delta^{34}S_{SO4}$ plot (Figure 58) which indicates a mixture between the two endmembers of sulphate (magmatic source and rainwater). Samples from the Atlantic Ocean (SW) and the thermal water of Ferraria (Fe) have the typical seawater signature of 21± 0.2 ‰ but for all other samples the influence of seawater can be ruled out. Also Figure 59 shows the effect of seawater in the Ferraria sample which caused in an elevation of sulphate. Higher $\delta^{34}S_{SO4}$ and $\delta^{18}O_{SO4}$ of Ferraria compared to seawater is a hint for bacterial sulphate reduction. To sum up, sulphur derived from 3 different sources: magmatic and biologically modified sources as well as seawater admixture. The SO_4^{2-} content is mainly controlled by the oxidation of magmatic sulphur except from bacterial reduction. Furthermore, magmatic processes can be divided into (weathering of) basaltic rocks and rising of magmatic gases.

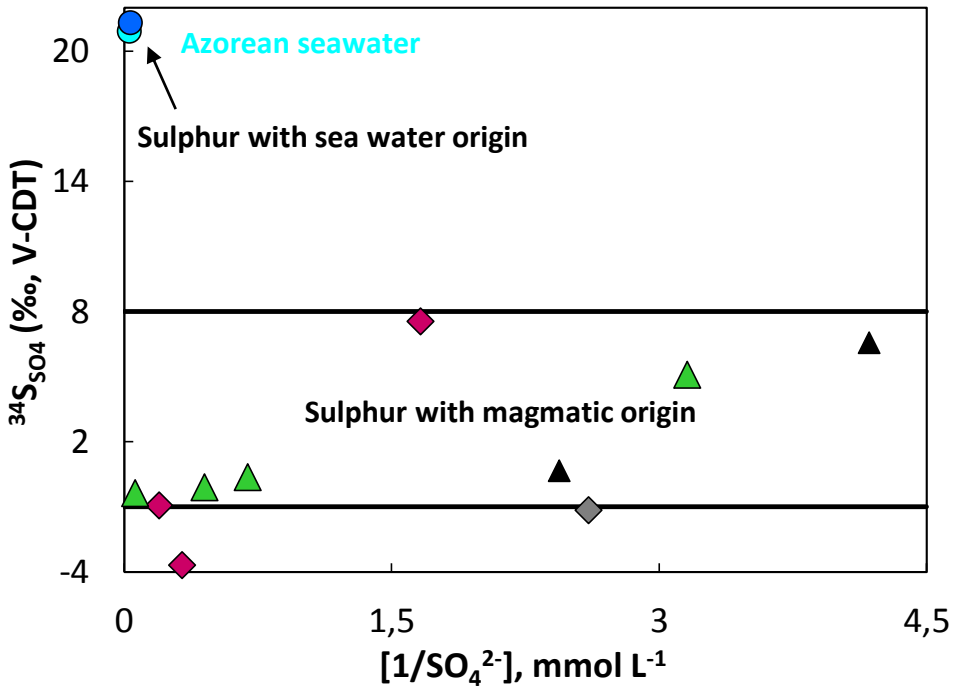

Figure 58 $\delta^{34}S$ vs. 1/[SO_4^{2-}] plot shows an increase of SO_4^{2-} concentration leads to a generally decrease of $\delta^{34}S$ (Funas: ◆ :boiling pools; ◆: warm springs;Fogo: ▲: boiling pools, ▲:cold and CO_2 rich type; ● seawater , ●:Ferraria). Mantle signature $\delta^{34}S$ = 0‰ (Prianjo, 2009).

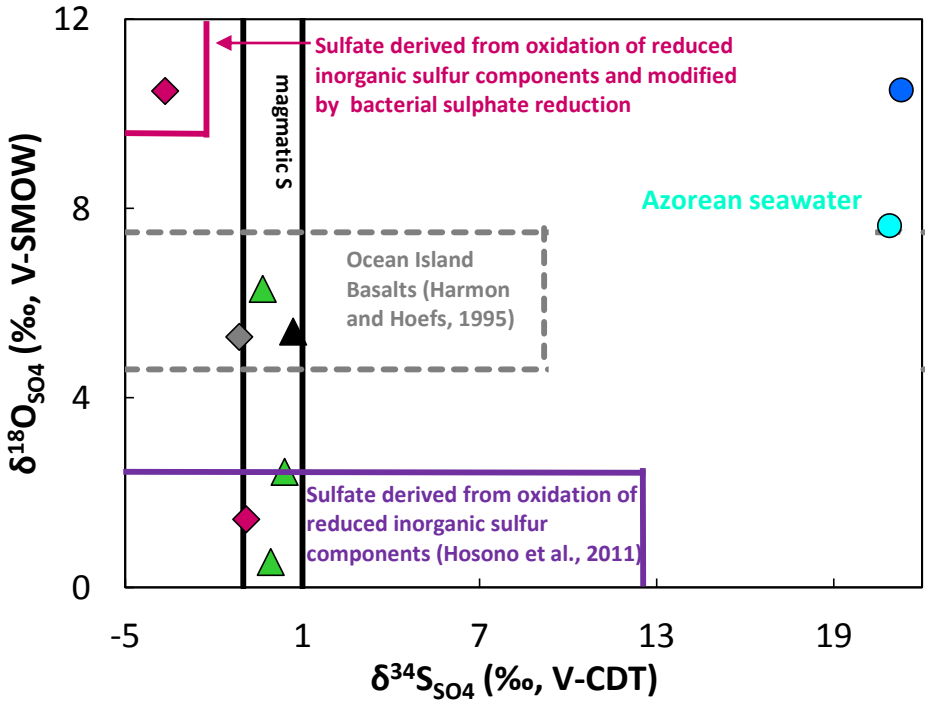

Figure 59 $\delta^{18}O_{SO4}$ vs. $\delta^{34}S_{SO4}$ diagram for water samples collected in São Miguel island. Isotopic composition reveals different origin for the sulphate in hydrothermal fluids. (Furnas: ◆: boiling pools; ◆: warm springs; Fogo: ▲ :boiling pools, ▲:cold and CO_2 rich type; ● seawater, ●:Ferraria).

Due to equations 10 and 11 fractionation factors of different carbonate species at different temperatures had been calculated to determine the origin of the carbonate (Appendix, Table A 5). As a result $\delta^{13}C_{GAS}$ values of the CO_2 suggesting isotopic equilibrium with respect to DIC species, range between -3 and -7 ‰ (V-PDB). These values give clear evidence for mantle CO_2 (Figure 60). Moreover volcanic CO_2 from different locations had similar isotopic composition, like the Kilauea volcano in Hawaii. Typical volcanic gases consider a $\delta^{13}C$ value of about -3.4 ‰ (Hoefs, 2009; Gerlach and Taylor, 1990). A degassing model can explain this range: the first step includes the ascent and pressure equilibrium and the second one decompression of shallow magma and eruption.

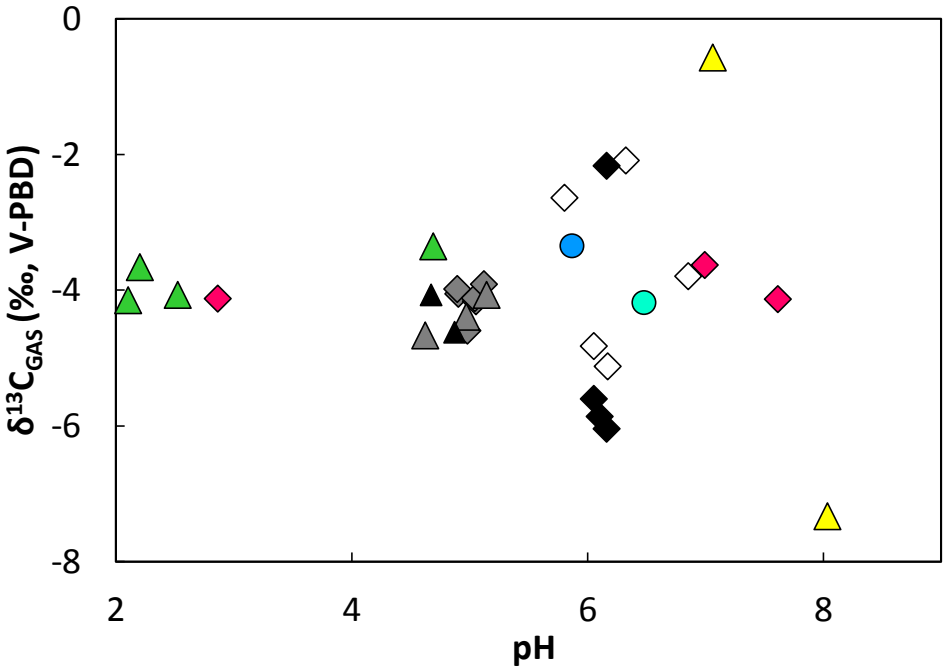

Figure 60 Calculated $\delta^{13}C_{GAS}$ vs. pH plot (Furnas: ◇ : cold and CO_2 rich, ◆ : warm type, ◇ : mesothermal, ◆ : boiling pools ; Fogo: △ cold and CO_2 rich , △ cold and CO_2 poor, ▲ : warm type, ▲ : boiling pool, △ : caldera sample, ● : seawater , ●:Ferraria).

7. Summary and conclusion

The Azores Archipelago is located in the North Atlantic Ocean, astride the Mid-Atlantic Ridge, with a distance to the Portuguese mainland of about 1500 km. Isolated from continental impacts in the Atlantic Ocean and composed of young volcanic rocks with still pronounced volcanic activities São Miguel, as one of nine islands of the Azores, was an excellent case to study the development of a locally restricted thermal system and related geochemical cycles. Therefore, in the present study 33 natural solutions and 8 local volcanic rocks and precipitates were sampled in São Miguel, belonging to three different and still active volcanoes, named Furnas, Fogo and Sete Cidades

(Furnas area) volcano, for mineralogical, geochemical, isotopic, and microstructural analyses. Sampled volcanic rocks mainly consisted of alkali feldspars, pyroxene, amphibole, opaque and iron rich phases. Several rocks developed a formation of thick Fe oxide/hydroxide layers which may have its origin in rapid dissolution of volcanic rock caused by thermal spring. In contrast, collected precipitates in the vicinity of boiling pools vary in their mineral compositions and structure (Appendix, Figure B 1-C 12) and resulted from the hydrothermal water- influence. In the boiling pools, rock alteration results in alunite formation, crust of fe-oxides/hydroxides, fissure tracks filled with opaque minerals and silicifications. All boiling pools in the Furnas caldera are supposed to be an example for active high-sulphidication epithermal system in the first stage. The silicification is associated with microorganisms suggested from stomatolitic textures. Stromatolites are referred to various bacterial taxa. Two different stromatolite structures, a laminar structure and a dome-shaped one could be found in the present case.

According to their origin, analysed water samples can be divided into 3 groups: Na-HCO_3, Na-SO_4 and Na-Cl type (Appendix, Table A 2). The Na-HCO_3 water type is predominant in Furnas village. These springs discharged in the vicinity of geothermal surface manifestations like fumarolic grounds. The HCO_3^- content can be explained by rock water interaction as a neutralisation process and evolved CO_2 outgassing processes. Thus HCO_3^- content is positively related to TDS. The origin of Na^+ and Cl^- is not related to seawater admixtures, as all samples appeared above the Meteoric-Azorean Seawater Mixing Line with the exception of Ferraria. Hence, water-rock interaction was assumed to be the origin. At higher temperature, the concentrations of $Si(OH)_4$, K^+ and Sr^{2+} increased through intensive alteration of basaltic rocks, whereas in contrast Al^{3+} and $\sum$Fe concentrations decreased by precipitation of e.g. alunite. High SO_4^{2-} concentration related to shallow outgassing processes which controlled mainly the water chemistry of boiling pools of Fogo volcano and Furnas Lake. Gases like SO_2 and H_2S exsolve from the magmatic source in very shallow levels, which may imply that the magma chamber of Furnas and Fogo occurs in different depths and also that the distance of discharges to the magmatic source has a huge impact on the water chemistry (for instance: hydrochemical differences in boiling pools of Furnas Lake and village). Sulphur derived from 3 different sources, magmatic and organic as well as seawater admixture. However, the SO_4^{2-} content is mainly controlled by the oxidation of magmatic sulphur. Also the oxygen isotopes of sulphate favour this hypothesis of organic origin of SO_4^{2-}. The lowest $\delta^{34}S$ values with -3.7 ‰ were in accordance with the occurrence of stromatolites observed in the thin section. Bacterial sulfate reduction normally resulted in heavier sulphur isotopic signature in the remaining sulfate, but the observed negative values in dissolved sulphate may be caused by the overlapping magmatic and biogenic signatures. Elevated $\delta^{34}S_{SO4}$ values are due to weathering of basaltic rocks (up to 7 ‰). At Fogos' higher altitude in particular CO_2 rich water at

T ≈ 20 °C occurs. In this case, the extent of basaltic rock leaching rather depends on uptake of volcanic CO_2 than on temperature. $\delta^{13}C_{GAS}$ values (CO_2), calculated by the measured $\delta^{13}C_{DIC}$ values, range between -3 and -7 ‰ which clearly reveals magmatic origin. In Ferraria, water is discharging from a basal aquifer and belongs to the Na-Cl type, where stable hydrogen and oxygen isotopes reveal mixing of meteoric and seawater. Thus, the mineralisation correlated not with the HCO_3^- content in contrast to Na-HCO_3 and Na-SO_4 type. The $\delta^{18}O$ and δD values for thermal water indicated their origin from meteoric water, according to the LMWL by infiltration in the ground, with the exception of Ferraria. Evaporation of boiling pools and potential rock leaching were indicted by a shift of $\delta^{18}O$ and δD. In accordance, $\delta^{18}O$ and δD of Ferraria had a similar isotopic composition to seawater.

To sum up, in Figure 61 a conceptual model for a hydrogeothermal system in the evolving basaltic ocean island of São Miguel is developed. The geochemical and isotopic evolution of the thermal waters of São Miguel clearly reveals that different solutions have their primary origin in meteoric water by the fact that they lie close to the local (LMWL) and global meteoric water line (GMWL) line. All samples chemically evolved by the uptake of volcanic gas, leaching of local basaltic rocks/precipitates and in some cases the admixture of sea water. Furthermore, shallow and evolved processes can be distinguished. Following the individual concentrations supports this theory. HCO_3^- concentration and its isotopic composition ($\delta^{13}C_{DIC}$ = -5 ± 3 ‰ V-PDB) reflect evolved CO_2 uptake and subsequent leaching progress. High SO_4^{2-} concentration of up to 16.5 mmol L^{-1} with $\delta^{34}S_{SO4}$ = 0.35 ± 0.3 ‰ (V-CDT) reflected magmatic origin which mainly controls water chemistry of boiling pools of both Fogo and Furnas Lake. The molar Mg/Ca ratio (0.77) of all thermal discharges reflects leaching of analysed local basalt (Mg/Ca ≈ 0.78). Changes in water chemistry could be used as an indicator for the volcanic activity.

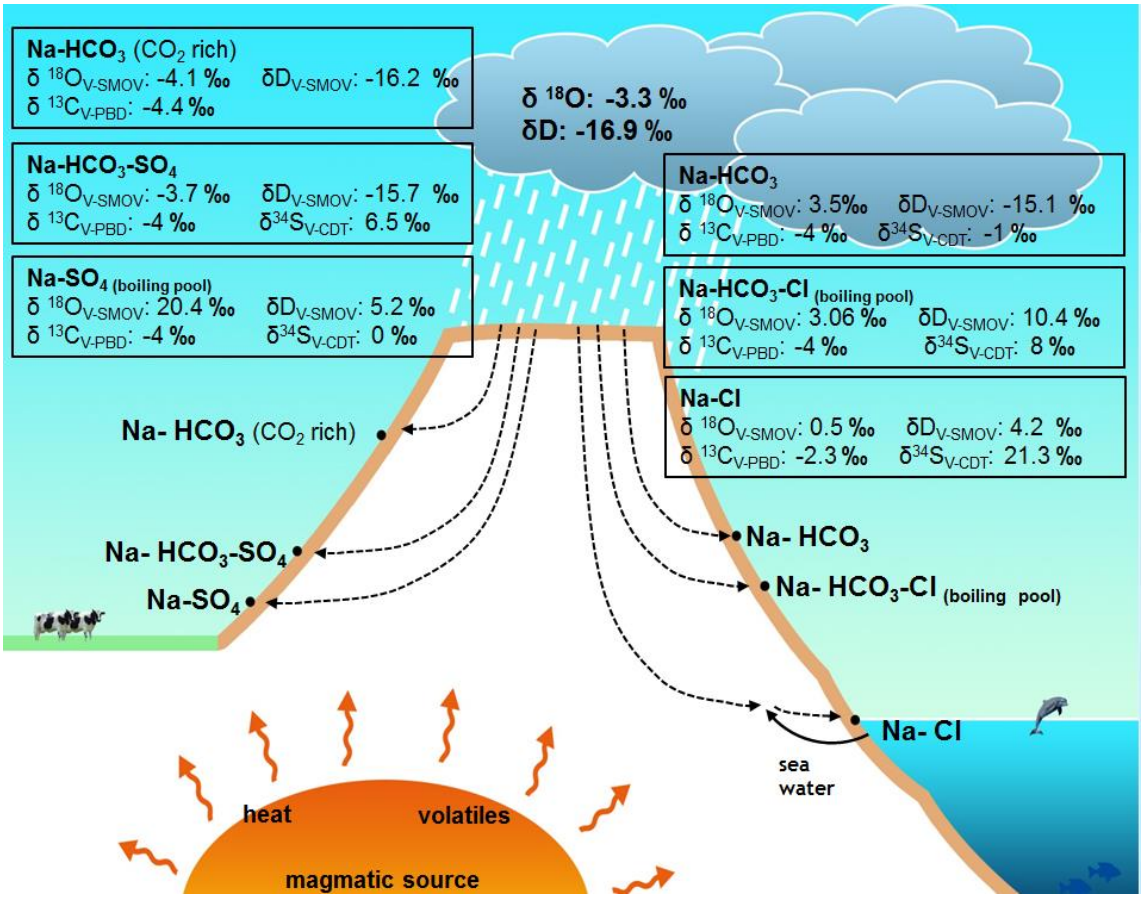

Figure 61 Schematic model for the evolution of the hydrothermal system of São Miguel (Azores) with different thermal water types and their varying isotopic composition.

8. References

Aguilera, E., Cioni, R., Gerhardi, F., Magro, G., Marini, L., Pang, Z., 2005. *Chemical and isotope characteristics of the Chachimbiro geothermal fluids (Ecuador).* Geothermics 34, **495-517**

Appelo, C.A.J., Postma,D., 2005. *Geochemistry, groundwater and pollution*. 2nd Edition. A.A. Balkema Publishers, Leiden, The Netherlands a member of Taylor & Francis Group plc, **pp 649**

Armienta, M.A., Vilaclara, G., De la Cruz- Reyna, S., Ramos, S., Ceniceros, N., Cruz, Olivia, Aguayo, A., Arcega- Cabera, F., 2008. *Water chemistriy of lakes related to active and inactive Mexican volcanoes.* Journal of Volcanology and Geothermal Research 178, **249-258**

Beier,C., Haase, K.M., Turner, S.P., 2012. *Conditions of melting beneath the Azores*. Lithos 144- 145, **1-11**

Berg, A., Banwart, S, A., 2000. *Carbon dioxide mediated dissolution of Ca-feldspar: implications for silicate weathering.* Chemical Geology 163, **25-42**

Birnbaum, S.J., Wireman, J.W., 1984. *Bacterial sulfate reduction and pH: implications for early diagenesis.* Chemical Geology 43, **143-149**

Boyce, A.J., Fulignati, P., Sbrana, A., Fallick, A.E., 2007. *Fluids in early stage hydrothermal alteration of high- sulfidation epithermal systems: A view from the Volcano active hydrothermal system (Aeolian Island, Italy).* Journal of Volcanology and Geothermal Research 166, **76-90**

Booth, B., Croasdale, R., Walker, G.P.L., 1978. *A quantitative study of five thousand years volcanism on São Miguel, Azores.* Philosophical Transactions of the Royal Society of London 288, **271-319**

Bourdon, B., Turner, S.P., Ribe, N.M, 2005. *Partial melting and upwelling rates beneath the Azores from a U- series isotopes perspective.* Earth and Planetary Science Letters 239, **42- 56**

Brand, W. A., Geilmann, H., Crosson, E.R., 2009. *Cavitiy ring-down spectroscopy versus high temperature conversation isotope ratio mass spectrometry: a case study on δ^2H and $\delta^{18}O$ of pure water samples and alcohol/water mixtures*. *Rapid Communications* in *Mass Spectrometry*. Volume *23*, **1879-1884**

Brantley, S,L., 2008. *Kinetics of mineral dissolution*. Kinetics of Water-Rock Interaction, Springer Verlag Berlin- Heidelberg **151-210**

Buforn, E., Udìas, A., Comombás, M.A., 1988*. Seismicity, source mechanisms and tectonics of the Azores – Gibraltar plate boundary*. Tectophysics 152, **89-118**

Cannat, M,. Escartin, J., Georgen, J., Lin, J., Mercouriev, S., Meyzen, C., Muller, M., Pouliquen, G., Rabain, A., da Silva, P.,1999. *Mid-Atlantic Ridge-Azores hotspot interactions: along-axis of a hotspot-derived event of enhanced magmatism 10 to 4 Ma ago*. Earth and Planetary Science Letters 173, **257-269**

Chorover, J., Brusseau, M,L., 2008. *Kinetics of Sorption- Desorption. Kinetics of Water-Rock Interaction*, Springer Verlag Berlin- Heidelberg, **109-149**

Cioni, R., Fanelli, G., Guidi, M., Kinyrario, J.K., Marini, L.,1992. *Lake Bogoria hot springs (Kenya): geochemical features and geothermal implications*. Journal of Volcanology and Geothermal Research 150, **231-246**

Colaço, A., Bustamante, P., Fouquet, Y., Sarradin, P.M., Serrão- Santos, R., 2006. *Bioaccumulation of Hg, Cu and Zn in the Azores triple junction hydrothermal vent fields food web*. Chemosphere 65, **2260-2267**

Cruz,J., Coutinho R.M., Carvalho M.R., Oskarsson, N., Gislason, S.R., 1999. *Chemistry of waters from Furnas volcano, São Miguel, Azores: fluxes of volcanic carbon dioxide and leached material*. Journal of Volcanology and Geothermal Research 92, **151- 167**

Cruz,J., 2003. *Groundwater and volcanoes:examples from the Azores archipelago*. Environmental Geology 44, **343- 355**

Cruz,J., França,Z., 2006. *Hydrogeochemestry of thermal and mineral water springs of the Azores archipelago (Portugal)*. Journal of Volcanology and Geothermal Research 151, **382-389**

Cruz,J., Freire P., Costa A., 2010. *Mineral waters characterization in the Azores archipelago (Portugal)*. Journal of Volcanology and Geothermal Research 190, **335-364**

Dasgupta, R., Jackson, M. G., Lee, C.A., 2010. *Major element chemistry of ocean island basalts-Conditions of mantle melting and heterogeneity of mantle source.* Earth and Planetary Science Letters 289, **377-392**

De Villiers, S. 1999. *Seawater strontium and Sr/Ca variability in the Atlantic and Pacific oceans.* Earth and Planetary Science Letters 171, **623-634**

Deines, P., Gold, D.P., 1973. *The isotopoc composition of carbonatite and kimberlite carbonates and their bearing on the isotopic composition of deep-seated carbon.* Geochimica et Cosmochimica Acta 37, **1709-1733**

Delalande, M., Bergonzini, L., Gherardi, F., Guidi, M., Andre, L., Abdallah, I., Williamson, D., 2011. *Fuild geochemistry of natural manifestions from the Sothern Poroto- Rungwe hydrothermal system (Tanzania): Preliminary conceptional model.* Journal of Volcanology and Geotherm Research 199, **127-141**

Desbruyères, D., Biscoito, M., Caprais, J.-C., Colaço, A., Comet,T., Crassous, P., Fouquet, Y., Khripounoff, A., Le Bris, N., Olu,K., Riso, R., Sarradin, P.-M., Segonzac, M., Vangriesheim, A., 2001. *Variations in deep- sea hydrothermal vent communities on the Mid- Atlantic Ridge near the Azores plateau.* Deep Sea Research I 48, **1325-1346**

Di Liberto, V., Nuccio, P,M., Paonita, A., 2002. *Genesis of chlorine and sulphur in fumarolic emissions at Vulcano Island (Italy): assessment of pH and redox conditions in the hydrothermal system*. Journal of Volcanology and Geothermal Research 116, **137-150**

Dietzel, M., SS 2004. *Aquatic Geochemistry (Low Temperature Environments)*

Dietzel, M., Schwecke, A., Hirschfeld, A., Röhring, A., Böttcher, M,E.,1997. *Geochemical and $^{13}C/^{12}C$-isotopical investigation of Minerl Waters in Northern Hessia (Germany) and the Origin of their CO_2 content.* Acta hydrochimica et hydrobiologica 25, **191-201**

DROTRH- INAG (2001) *Plano regional da água*. Relatório téctonico. Versão para consulta pública. DROTH-INAG, Ponta Delgada

Edmonds, M., Pyle, D., Oppenheimer, C., 2001. *A model for degassing at the Soulfrière Volcano, Montserrat, West Indies, based on geochemical data*. Earth and Planetary Science Letters 186, **159-173**

Ellis, A.J., Mahon, W.A., 1964. *Natural hydrothermal systems and experimental hot-water/- rock interactions.* Geochimica et Cosmochimica Acta 28, **1322-1357**

Fernandez- Turiel, J.L., Gracia-Valles, M., Gimeno- Torrente, D., Saavedra- Alonso, J., Martinez-Manet, S., 2005. *The hot spring and geyser sinters of El Tatio, Northern Chile.* Sedimentary Geology 180, **125-147**

Ferreira, D.B., 1980. *Contribution á l'étude des ventes et de l'humidité dans les îles centrales de l'archipel des Açores*. Centro Estudos Geográficos, Lisboa

Ferreira,T., 1994. *Contribução para o estudo das emanações gasosas associadas a processos de vulcanismo no arquipélago dos Açores*. Unpuplished MSc Thesis, University of the Azores, Ponta Delgada, 183pp

Ferreira,T., Oskarsson, N., 1999. *Chemistry and isotopic composition of fumaroles discharges of Furnas caldera* . Journal of Volcanology and Geothermal Research 92, **169- 179**

Forjaz, V.H., 1988. *Azores study tour. Field trip guide: Seminar on the prediction of earthquakes*. Econ. Comm. For Europe-UN, Lisbon, 26pp

Forjaz, V.H., 1986. Ilha *de S. Migues (Açores) – Carta tectónica na escala 1:50000*. Doc Int CV/INIC 09/86, Dept Geociências, Universtiy of Azores, Ponta Delgada

Fournier, R.O., 1977. Chemical geothermometers and mix mixing models for geothermal systems. Geothermics 5, **41-50**

Gérard, F., Boudot, J-P., Ranger, J.,2001. *Consideration on the occurrence of the Al_{13} polycation in natural soil solutions and surface waters*. Applied Geochemistry 16, **513-529**

Gerardo, J.Y., Nuti, S., D'Amore, F., Seastres JR, J.S., Gonfiantini, R., 1993. *Isotopic evidence for magmatic and meteoric water recharge and the processes affecting reservoir fluids in the Palinpinon geothermal system, Philippines*. Geothermics 22, **521-533**

Gerlach, T. M., Taylor, B.E., 1990. *Carbon isotope constraints on degassing of carbon dioxide from Kilauea volcano.* Geochimica et Cosmochimica Acta 54, **2051-5058**

German, C.R., Parson, L.M., HEAT Scientific Team, 1996. *Hydrothermal exploration near the Azores Triple Junction: tectonic control of venting at slow- spreading ridges?.* Earth and Planetary Science Letters 138, **93-104**

Georgen, J.E., Sankar, R.D., 2010. *Effects of ridge geometry on mantle dynamics in an ocean triple junction region: Implications for Azores Plateau*. Earth and Planetary Letters 298, **23-32**

Gente, P., Dyment, J., Maia M., Goslin, J., 2003. *Interaction between the Mid- Atlantoc Ridge and the Azores hot spot during the las 85 Myr: Emplacement and rifting of the hot spot- derived plateaus*. Geochemistry, Geophysics, Geosystems 4, **1-23**

Grand,S.P., 1994. *Mantle shear structure beneath the Americans and surroundings.* Journal of Geophysical Journal 99, **591-621**

Gripp, A.E., Gordon, R.G., 2002. *Young tracks of hotspots and current plate velocities*. Geophysical Journal International 150, **321-398**

Google Inc. (2015). *Google Earth*, 1600 Amphitheatre Parkway Mountain View, CA 94043 USA

Guest,J., Gaspar,J., Cole, P., Queiroz,G., Duncan,A., Wallenstein, N., Ferreira,T., Pacheco J., 1999. *Volcanic geology of Furnas volcano, São Miguel*, Azores. Journal of Volcanology and Geothermal Research 92, **1-29**

Guidry,S. A., Chafetz, H.S., 2003. *Anatomy of siliceous hot springs: examples from Yellowstone National Park, Wyoming, USA.* Sedimental Geology 157, **71-106**

Guidry,S. A., Chafetz, H.S., 2003. *Siliceos shrubs in hot spring from Yellowstone National Park, Wyoming, USA.* Canadian Journal of Earth Sciences 40, **1571-1583**

Harmon, R.S., Hoefs, J., 1995. *Oxygen isotope heterogeneity of the mantle deduced from global 18O systematics of basalts from different geotectonic settings*. Contribution to Mineralogy and Petrology 120, **95-114**

Herzberg,C., Asimow,P.D., 2008. *Petrology of some oceanic island basalts: PRI-MELT2.XLS software for primary calculations*. Geochemistry, Geophysic, Geosystem 9, **1-25**

Hess, H.H., 1967. *Basalts: The Poldervaart Treatise on Rocks of Basaltic Compostion,Volume 1* , John Wiley& Sons ,Inc, **pp 512**

Hoefs, J., 2009. Stable Isotope Geochemestry. 6th Edition. Springer- Verlag Berlin Heidelberg, **pp 285**

Hofmann,J.H., 1973. *Stromatolites: Characteristics and Utility.* Earth Science Reviews 9, **339-373**

Horita, J., Wesolowski, D, J., 1994. *Liquid- vapor fractionation of oxygen and hydrogen isotopes of water from the freezing to the critical temperature.* Geochimica et Cosmochima Acta 58, **2797-2817**

Hosono, T., Delinom, R., Nakano, T., Kagabu, M., Shimada, J., 2011. *Evolution model of $\delta^{34}S$ and $\delta^{18}O$ in dissolved sulfate in volcanic fan aquifers from recharge to coastal zone through the Jakarta urban area, Indonesia*. Science of the Total Evnironment 409, **2541-2554**

IAEA, Water Resource Programme 2014. *Measurements of the isotopic composition of meteoric water of São Miguel, Azores from 1962 till 2009.* http://www.univie.ac.at/cartography/project/wiser/gui/gnip_all_index.php?wmo_region=6

Ingraham, N., Matthews, R., 1990. *Stable isotope study f fog: the Point Reyes Peninsula, California. U.S.A.* Chemical Geology (Isotope Geoscience Section) 60, **281-290**

Inguaggiato, S., Martin-Del Pozzo, A.L., Aguayo, A., Capasso, G., Favara, R.,2005. *Isotopic, chemical and dissolved gas constraints on spring water from Popcatepelt volcano (Mexico): evidence of gas-water interaction between magmatic component and shallow fluids.* Journal of Volcanology and Geothermal Research 141, **91-108**

Inguaggiato, S., Pecoraino, G., Amore F,D., 2000. *Chemical and isotopical characterization of fluid manifestations of Ischia Island (Italy)*. Journal of Volcanology and Geothermal Research 99, **151-178**

Jones, B., Renaut, R.W., 2003. *Hot springs and geyser sinters: the integrated product of precipitation, replacement, and deposition.* Canadian Journals of Earth Science 40, **1549-1569**

Konhauser, K.O., Jones, B., Rysenbach, A., Renout, R.W., 2003. *Hot spring sinters: key to understanding Earth'a earlist life forms.* Canadian Journal of Earth Science 40, **1713-1724**

Krumbein, W.E., Werner, D., 1983. *The microbial silica cycle*. In Micobial geochemetry. Eddited by W.E. Krumbein. Blackwell Scientific Publications, Oxford U.K., **125-157**

Kyser, T.K., 1986. *Stable isotope variations in the mantle.* In Valley, J.W., Taylor Jr., H.P., O'Neil, J.R. (Eds.), *Stable Isotopes in High Temperature Geological Processes*, Reviews in Mineralogy 16, **141-164**

Lüttge, A., Arvidson, R.S., 2008. *The Mineral- Water Interface*. Kinetics of Water-Rock Interaction, Springer Verlag Berlin- Heidelberg ,**73-107**

Luis, J.F., Miranda, J.M., Galdeano, A., Patriat, P., Rossignol, J.C., Mendes Victor, L.A., 1994. *The Azores triple junction evolution since 10 Ma from an aerogmagnetic survey of Mid-Atlantic Ridge.* Earth and Planetary Science Letters 125, **439-459**

Luis, J.F., Neves, M.C., 2006. *The isostatic compensation of the Azores Plateau: A 3D admittance and coherence analysis.* Journal of Volcanology and Geothermal Research 156, **10- 22**

Madeira, J., Ribeira A., 1990. *Geodynamic models for the Azores triple junction: a contribution from tectonics*. Tectophysics 184, **405-415**

Madureira P., Moreira,M., Mata, J., Allégre C.J., 2005. *Primitive neon isotopes in Terceira Island (Azores archipelago)*. Earth and Planetary Science Letters 233, **429-440**

Marques, F.O., Catalão, J.C., DeMets, C., Costa, A.C.G., Hildenbrand, A., 2013. *GPS and tectonic evidence for a diffuse plate boundary at the Azores Triple Junction*. Earth and Planetary Science Letters 381, **177- 187**

Martin-Del Pozzo, A,L., Aceves a F., Espinasa a R., Aguayoa A., Inguaggiato S., Morales P., Cienfuegos E., 2002. *Influence of volcanic activity on spring water chemistry at Popocatepetl Volcano*, Mexico. Chemical Geology 190, **207–229**

Merlivat, L., Jouzel, J., 1979. Global climatic interpretation of the deuterium- oxygen 18 relationship for precipitation. Journal of Geophysics Research 84, **5029-5033**

Montagner,J.-P., 2001. *Interactions between ridges and plumes*. Science 294, **1472-1473**

Misra, K, C., 2000. *Understanding mineral deposits*. Kluwer Academic Publications, Dordrecht, p**p 759**

Moreira, M., Doucelance R., Kurz. M.D., Dupré, B., Allègre, C.J.,1999. *Helium and lead isotopes geochemistry of the Azores Archipelago*, Earth and Planetary Science Letters 169, **189-205**

Moore, R.B., 1991. *Geology of three quaternary stratovolcanoes on São Miguel, Azores*, US Geological Survey Bulletin 1900,**pp 46**

Neves, M.C., Miranda, J.M., Luis, J.F.,2013. *The role of the lithospheric processes on the development of linear volcanic ridges in the Azores.* Tectonophysics 608, **378- 388**

Parkhurst, D,L., Appelo, C,A,J., *1999. User's Guide to PHREEQC (version2)- A Computer Program for Speciation, Batch- reaction, One- dimensional Transport, and Inverse Geochemical Calculations*. U.S Geological Survey, **pp 4259**

Pasvanoğlu, D., Chandrasekharam, D., 2011. *Hydrogeochemical and isotopic study of thermal and mineralized waters from the Nevşehir (Kozakli) area, Central Turkey.* Journal of Volcanology and Geothermal Research 202, **241-250**

Phoenix, V.R., Adams, D.G., Konhauser, K.O., 2000. *Cyanobacertial viability during hydrothermal biomineralisation*. Chemical Geology 169, **329-338**

Piranjo, F., 2009. *Hydrothermal Processes and Mineral Systems.* Geological Survey of Western Australia, Perth, Springer Science and Business Media B.V. **pp 1250**

Rossmann, J.R., Taylor, P.D., 1998. *Isotopic composition of the elements (technical report): commission on atomic weights and isotopic abundances*. Pure and Applied Chemistry 70, **217-235**

Sakai, H., Matsubaya, A., 1977. *Stable isotopic study studies of Japanese geothermal systems*. Geothermics 5, **97-124**

Schilling, J., 1991. *Fluxes and excess temperatures of mantle plumes inferred from their interaction with migrating mid- ocean ridges.* Nature 352, **397- 403**

Schlummberger Water Service, 2007. *AquaChem v.5.1 User's Manual: Water Quality Date Analysis, Plottting and Modelling*. Canada, **pp 404**

Sheppard, S.M.F.,1986. *Characterization and isotopic variations in natural waters.* Reviews in Mineralogy and Geochemestry 16, **165-183**

Sigg, L., Stumm, W., 2011. *Aquatische Chemie- Einführung in die Chemie natürlicher Gewässer*. Hochschulverlag AG an der ETH Zürich. **pp 522**

Silveira,S., Strutzmann, E., Davaille, A., Montagner, J., Mendes- Victor, L., Sebai, A., 2006. *Mantle Azores hot spot signature in the upper mantle.* Journal of Volcanology and Geothermal Research 156, **23-34**

Spötl, C., 2005. A *robust and fast method of sampling and analysis of ı13C of dissolved inorganic carbon in ground waters*. Isotopes in Environmental and Health Studies 41, **217–221**

Szynkiewicz, A., Johnson, A.P., Pratt, L.M., 2012. *Sulfur species and biosignatures in Sulphur Springs, Valles Caldera, New Mexico- Implications for Mars astrobiology.* Earth and Planetary Science Letters 321-322, **1-13**

Trota, A., SS 2013. *Mineralogia e Geologia*. Universidade dos A*çores*

Valentino, G.M., Cortecci, G., Franco,E., Stanzione, D., 1999. *Chemical and isotopic composition of mineral and waters from Campi Flegrei volcanic system, Naples,Italy.* Journal of Volcanology and Geothermal Research 91, **329-344**

Wallenstein, N., Duncan, A., 1998. The *geology of Fogo volcano, S. Miguel island*. Gaspar JL (ed) Abstr. Vol Advanced Study Course Volcanic Harzard Assessment, Monitoring and Risk Mitigation, Ponta Delgada

Walter, M.R., 1976. *Stromatolithes.: Development in Sedimentology*. Volume.20 Elsevier Science, Amsterdam , **193-249**

Weston, F.S., 1963/1964. *List of recorded volcanic eruptions in the Azores with brief reports*. Bol.Mus.Lab.Min.Geol.Fac.Ciên. Lisboa, 10 (1): **3-18**

White, M., Schilling, J.-E, Hart, S., 1976. *Evidence for the Azores mantle plume from strontium isotope geochemistry of the central north Atlantic*. Nature 263, **659–663**

Widom,E,. Shirey S.B., 1996. *Os isotopes systematic in the Azores: implication for mantle plume sources*. Earth and Planetary Science Letters 142, **451-465**

Wogelius R,A., Walther, J, V., 1991. *Olivine dissolution at 25°C: Effects of pH, CO_2, and organic acids.* Geochimica and Cosmichimica Acta Vol. 55, **943-954**

Xiaotong, P., Jones, B., 2012. *Rapid precipitation of silica (opal- A) disguises evidence of biogenicity in high- temperature geothermal deposits: Case study from Dagunguo hot spring, China.* Sedimentary Geology 275-260, **45-62**

Yang, T., Shen, Y., Van der Lee, S., Solomon,S.C., Hung, S.H., 2006. *Upper mantle structure beneath the Azores hotspot from finite- frequency seismic tomography*. Earth and Planetary Science Letters 250, **11-26**

Yardley, B, W, D., Bodnar, R,J., 2014. *Fluids in the Continental Crust*. Geochemical Perspectives, 3,1. **pp 127**

Zbyszewski, G., 1963. *Les phénoménes volcaniques moderns das l'archipel des Açores*. *Comunicaooes* dos *Services* Geologicos.47, **pp 230**

9. Appendix

Table A 1 Abbreviation for all samples

Fu1	Água Azeda de Rebentão	AS	Sete Cidades Azul- surface
Fu2	Dr. Dinis	AS23	Sete Cidades Azul- 23m deepth
Fu3	Caldeirão	Fo1	Lombadas Furo II
Fu4	Água Dr. Miguel Henrique	Fo2	Lombadas
Fu5	Água Prata	Fo3	Lombadas doce
Fu6	Água Santa	Fo4	Caldeira Grande da Ribeira Grande
Fu7	Água Azeda	Fo5	Caldeira Pequena da Ribeira Grande
Fu8	Água do Rego	Fo6	Fumarol Ribeira Grande
Fu9	Caldeira Grande	Fo7	Pocinha
Fu10	Caldeira da Lagoa Furnas	Fo8	Magarça
Fu11	Quenturas I	Fo9	Caldeira Velha spring
Fu12	Quenturas III	Fo10	Caldeira Velha fumarol
Fu13	Grutinha I	Fe	Ferraria
Fu14	Grutinha II	SW	Seawater
Fu15	Água do Torno	DW	Drinking water
Fu16	Padre José	spr	spring
Fu17	Caldeira do Asmodeu	bpool	boiling pool
Fu18	Banhos Férreos	tap	tap water

Table A 2 Chemical composition of all 33 water samples of São Miguel (T: temperature in °C, M and P: Coordinates UTM WGS 84 System, SpC in (µS/cm), A: Alkalinity in mmol/L, all other elements are given in mmol/L). Abbreviations are given in Table A1

References	M	P	type	T	ph	SpC	Alkalinity	CO2	Li^{+}	Na^{+}	K^{+}	Mg^{2+}	Ca^{2+}	Sr^{2+}	F^{-}	Cl^{-}	Br^{-}	SO_4^{2-}	Al^{3+}	Σ Fe	Mn^{2+}	Si^{+4}	As^{3+}
Fu1	649418	4182035	spr	15.8	4.90	312	1.78	19.2	0.000000706	1.56	0.499	0.155	0.186	0.000151	0.0784	0.469	0.000414	0.219	0.0347	0.109	0.0105	1.67	0.0000910
Fu2	649415	4182031	spr	16.1	5.05	313	2.91	11.2	0.000000764	1.59	0.506	0.148	0.187	0.000151	0.0775	0.472	0.000412	0.242	0.0348	0.0969	0.0105	1.67	0.0000182
Fu3	649410	4182025	spr	73.1	5.80	496	3.88	2.46	0.00000522	3.80	0.437	0.155	0.213	0.000155	0.1209	0.964	0.000745	0.062	0.00875	0.0182	0.0182	2.74	0.0007645
Fu4	649362	4182018	spr	20.7	5.04	441	1.61	13.8	0.00000173	2.52	0.712	0.134	0.232	0.000157	0.0914	0.550	0.000458	0.384	0.0278	0.100	0.0155	1.74	b.d.l
Fu5	649365	4182020	spr	21.4	5.12	368	1.68	14.4	0.000000922	1.97	0.604	0.117	0.201	0.000154	0.0795	0.525	0.000380	0.522	0.0393	0.0681	0.00987	1.64	0.000127
Fu6	649417	4182022	spr	86.0	6.85	835	5.73	1.27	0.0000113	7.96	0.476	0.033	0.150	b.d.l	0.289	2.00	0.00162	0.284	0.00356	0.000448	0.00222	4.06	0.00342
Fu7	649452	4182034	spr	16.4	4.98	307	1.76	20.6	0.000000620	1.51	0.504	0.164	0.202	0.000169	0.0675	0.480	0.000437	0.210	0.0329	0.103	0.0112	1.74	0.0000546
Fu8	649487	4182046	spr	16.4	4.89	325	1.57	15.5	0.000000648	1.81	0.532	0.136	0.193	0.000142	0.0759	0.559	0.000514	0.340	0.0335	0.0127	0.0126	1.67	0.0000182
Fu9	649349	4181933	bpool	96.8	7.61	2080	11.9	0.879	0.0000380	21.3	0.506	0.001	0.017	b.d.l	1.06	7.80	0.00626	0.602	0.00378	0.0000895	0.000218	3.03	0.0168
Fu10	646908	4181504	bpool	93.6	2.86	1087	0.00	3.73	0.0000227	4.99	0.611	0.355	0.752	0.000544	0.102	0.427	0.000000	5.17	0.2598	0.154	0.0213	4.24	0.0001092
Fu11	649307	4181753	spr	57.6	6.05	1366	12.6	3.99	0.0000204	11.1	1.17	0.561	0.707	0.000484	0.198	2.05	0.001730	0.097	0.00170	0.0372	0.00783	3.81	0.0003094
Fu12	649307	4181752	spr	57.0	6.17	1349	12.1	1.81	0.0000200	11.0	1.16	0.549	0.694	0.000454	0.197	2.04	0.00179	0.104	0.00137	0.0364	0.00784	3.81	0.0004004
Fu13	649255	4181710	spr	40.6	6.05	1518	14.7	5.29	0.0000278	13.1	0.884	0.595	0.752	0.000525	0.249	2.41	0.00181	0.098	0.00715	0.0994	0.0136	2.67	0.0011831
Fu14	649247	4181706	spr	41.6	6.10	1486	13.9	7.57	0.0000261	12.6	0.871	0.538	0.670	0.000446	0.258	2.33	0.00193	0.108	0.00823	0.123	0.0167	2.85	0.00116
Fu15	649238	4181701	spr	39.6	6.16	1473	14.4	8.13	0.0000264	12.5	0.767	0.556	0.651	0.000378	0.253	2.41	0.00210	0.078	0.00845	0.126	0.0172	2.63	0.00115
Fu16	649344	4181882	spr	56.2	6.32	781	4.35	2.11	0.00000752	5.62	0.991	0.262	0.389	0.000196	0.132	0.909	0.000753	0.563	0.000704	0.0777	0.0302	3.84	b.d.l
Fu17	649383	4181951	bpool	90.8	6.99	2420	10.7	0.688	0.0000431	24.2	0.592	0.008	0.032	b.d.l	0.969	7.18	0.00596	3.084	0.0101	0.000215	0.000546	5.52	0.0262
Fu18	648697	4181939	3spr	38.0	6.16	1702	19.6	6.62	0.0000210	12.6	1.17	1.37	1.26	0.000653	0.135	1.71	0.00146	0.060	0.00393	0.0657	0.00945	2.56	0.0003094
As	608188	4192423	lake	19.6	8.03	112	0.810	0.200	0.0000000288	0.71	0.069	0.048	0.035	0.000051	0.0365	0.404	0.000285	0.022	0.000519	0.000215	0.0000182	b.d.l	b.d.l
A23	608185	4192423	lake	16.7	7.06	111	0.690	0.234	0.0000000288	0.69	0.074	0.060	0.050	0.000074	0.0301	0.393	0.000340	0.016	0.000259	0.010	0.00661	b.d.l	b.d.l
Fo1	635564	4182177	spr	19.6	5.14	554	5.87	19.2	0.00000458	3.71	0.987	0.257	0.272	0.000402	0.0538	0.395	0.000353	0.025	0.0178	0.000179	0.0361	1.74	0.0000910
Fo2	635560	4182116	spr	17.8	4.97	385	3.27	21.7	0.00000146	2.49	0.618	0.205	0.186	0.000249	0.0380	0.359	0.000313	0.019	0.0145	0.000859	0.0325	1.67	b.d.l
Fo3	635579	4182124	spr	12.8	5.96	113	0.980	0.495	0.000000231	0.90	0.131	0.030	0.022	b.d.l	0.0313	0.446	0.000353	0.027	0.000482	0.000304	0.0000182	0.961	0.0000182
Fo4	633200	4184460	bpool	45.3	2.20	937	0.00	5.53	0.000000475	1.10	0.310	0.169	0.226	0.000123	0.0377	0.499	0.000414	2.228	0.1128	0.0950	0.00244	2.24	0.0000364
Fo5	633186	4184464	bpool	49.2	2.52	546	0.00	6.80	0.000000317	1.07	0.335	0.113	0.183	0.000098	0.0120	0.480	0.000437	1.45	0.1069	0.0859	0.00391	2.74	0.0000000
Fo6	633213	4184476	bpool	56.6	2.10	4370	0.00	28.7	0.00000228	2.05	0.792	0.543	1.15	0.000655	0.0623	0.377	b.d.l	16.5	2.1419	0.645	0.0327	5.16	0.000419
Fo7	632950	4184670	spr	27.5	4.87	230	0.52	11.4	0.000000648	0.99	0.363	0.104	0.092	0.0000502	0.00896	0.570	0.000594	0.410	0.00556	0.0617	0.00750	1.57	0.0000364
Fo8	632181	4184467	spr	18.8	4.62	344	1.29	13.2	0.000000504	1.98	0.298	0.175	0.151	0.000189	0.0258	1.86	0.00217	0.112	0.0173	0.000233	0.00557	1.21	b.d.l
Fo9	632123	4182543	spr	30.7	4.67	156	0.580	7.19	0.000000403	0.68	0.109	0.095	0.079	0.0000457	0.0160	0.427	0.000358	0.239	0.0145	0.0660	0.00653	0.783	b.d.l
Fo10	632051	4182678	bpool	45.7	4.69	148	0.280	3.58	0.000000375	0.67	0.106	0.093	0.077	0.0000491	0.0153	0.431	0.000385	0.317	1.6714	8.05	2.17	14.3	0.0000182
Fe	600927	4190708	spr	31.1	5.87	49200	5.42	2.49	0.0000521	434.9	10.7	46.2	10.1	0.0753	b.d.l	502	0.708	27.9	0.0373	0.00421	0.00930	1.03	0.0000000
Sw			sea	19.2	6.48	53400	3.44	0.831	0.0000178	482.6	10.6	54.5	10.3	0.0714	b.d.l	565	0.824	32.9	0.0268	0.00184	0.000692	0.107	0.00135
Dw			tap	21.6	7.66	126	0.520	0.0	0.000000288	0.87	0.097	0.036	0.046	0.0000354	0.0477	0.432	0.000473	0.041	0.00126	0.00111	0.0000182	0.712	0.0000182

Table A 3 Isotopic vales of sampled solutions given in respect to their specific standard and in ‰ (δD(H2O) (V-SMOW) ,$\delta^{18}O(H2O)$(V-SMOW), $\delta^{18}O(SO_4)$(V-SMOW), $\delta^{13}C$ (DIC) , $\delta^{34}S(SO_4)$ (V-CDT))

References	$\delta D(H_2O)$	$\delta\ ^{18}O(H_2O)$	$\delta\ 18O(SO_4)$	$\delta^{34}S\ (SO_4)$	$\delta\ ^{13}C$ (DIC)
Fu1	-17.3	-3.80			-4.85
Fu2	-17.1	-3.83			-4.84
Fu3	-13.5	-3.16			-2.51
Fu4	-16.7	-3.95	5.28	-1.14	-4.77
Fu5	-17.3	-3.86			-4.49
Fu6	-8.49	-2.33			-2.08
Fu7	-15.5	-3.83			-5.33
Fu8	-15.7	-3.73			-4.78
Fu11	-14.4	-3.43			-3.68
Fu12	-15.6	-3.57			-3.58
Fu13	-13.8	-3.31			-3.96
Fu14	-13.8	-3.32			-4.05
Fu15	-12.9	-3.13			-3.93
Fu16	-16.1	-3.69			
Fu18	-15.1	-3.56			
Fu9	-0.03	0.62	4.22	7.56	-2.47
Fu10	12.3	1.14	1.44	-0.917	-4.94
Fu17	10.4	3.06		-3.66	-2.02
Fo1	-16.2	-4.11			-4.63
Fo2	-15.9	-3.87			-5.12
Fo3	-16.3	-3.86			-7.72
Fo7	-20.2	-3.99	5.39	0.676	-5.38
Fo8	-17.6	-3.73			-5.58
Fo9	-16.2	-3.90		6.58	-4.92
Fo4	-6.48	-1.45	0.54	0.083	-4.63
Fo5	-11.6	-2.69	2.44	0.39	-5.03
Fo6	20.4	5.21	6.29	-0.349	-5.08
Fo10	-15.7	-3.71		5.109	-4.16
AS	0.46	-0.29			-1.5
AS23	-2.6	-0.69			-6.07
Fe	4.18	0.45	10.50	21.3	-1.17
SW	7.38	0.93	7.62	20.9	0.940
DW	-14.3	-3.54		1.87	

Table A 4 Isotopic composition of meteoric water of São Miguel, Azores from 1962 to 2009. All isotopic values are given in respect to their specific standard and in ‰ (IEA, 2014)

Year	$\delta^{18}O$	δD
2009	-2.55	-10.8
2008	-2.62	-10.7
2007		
2006	-3.70	-19.4
2005	-3.59	-18.0
2004	-2.71	-12.6
2003	-3.39	-17.0
2002	-3.37	-17.0
2001	-3.31	-17.6
2000	-3.83	-18.5
1998	-6.57	-41.2
1997	-3.73	-19.0
1996	-3.60	-18.9
1995	-3.17	-15.4
1994	-2.66	-11.9
1993	-1.63	-10.1
1990	-3.93	-22.0
1989	-3.18	-17.7
1988	-2.42	-14.3
1975	-3.34	-17.6
1974	-2.00	-7.4
1973		
1972		
1971		
1970		
1969		-28.8
1968		
1967		
1966	-4.09	-18.4
1965	-3.68	-17.4
1964	-4.03	-17.3
1963	-4.01	-17.7

Table A 5 Calculations of $\delta^{13}C_{GAS}$ of the CO_2 gas in equilibrium to DIC from $\delta\ ^{13}C$ of dissolved inorganic carbon. (H^+, H_2CO_3, HCO_3^- and CO_3^{2-}stands for the activity- calculated by PHREEQC; K values shows the equilibrium between H_2CO_3, HCO_3^- and CO_3^{2-} (first and second dissociation constant); x: mol fraction for sub-pools; alpha: ratios of C12 and C13 - comparison with other samples, instead of standard; α: fractionation coefficient for delta ^{13}C of different phases; f, b and c correspond to carbonate species .Equations 17 and 18 were used for the calculations. (Logarithmic values are given for H^+, H_2CO_3, HCO_3^-,CO_3^{2-}, x_{H2CO3}, $_{HCO3-}$ and x_{CO32})

References	H^+	H_2CO_3	HCO_3^-	CO_3^{-2}	K1	K2	x_{H2CO3*}	x_{HCO3-}	x_{CO32-}	α_{H2CO3*}	α_{HCO3-}	α_{CO32-}	αDIC	$deltaC_{GAS}$
Fu1	-4.9	-1.18	-2.69	-8.21	-8.21	-10.4	-0.0131	-1.53	-7.05	0.999	1.01	1.01	0.999	-4.05
Fu2	-5.05	-1.12	-2.48	-7.85	-7.85	-10.4	-0.0185	-1.38	-6.75	0.999	1.01	1.01	0.999	-4.16
Fu3	-5.8	-1.85	-2.37	-6.69	-6.69	-10.1	-0.115	-0.632	-4.96	0.999	1.00	1.00	1.00	-2.64
Fu4	-5.04	-1.40	-2.74	-8.07	-8.07	-10.4	-0.0195	-1.36	-6.69	0.999	1.01	1.01	0.999	-4.11
Fu5	-5.12	-1.47	-2.72	-7.96	-7.96	-10.4	0.0236	-1.28	-6.52	0.999	1.01	1.01	0.999	-3.91
Fu6	-6.85	-2.70	-2.21	-5.49	-5.49	-10.1	-0.611	-0.122	-3.4	0.999	1.00	1.00	1.00	-3.80
Fu7	-4.98	-1.27	-2.7	-8.13	-8.13	-10.4	-0.0159	-1.44	-6.88	0.999	1.01	1.01	0.999	-4.60
Fu8	-4.89	-1.23	-2.74	-8.27	-8.27	-10.4	-0.013	-1.53	-7.05	0.999	1.01	1.01	0.999	-3.98
Fu9	-7.61	-3.13	-1.93	-4.47	-4.47	-10.1	-1.23	-0.0278	-2.57	0.999	1.00	1.00	1.00	-4.13
Fu10	-2.86						1.00	0	0	0.999	1.00	1.00	0.999	-4.12
Fu11	-6.05	-1.64	-1.88	-5.98	-5.98	-10.1	-0.198	-0.436	-4.54	0.999	1.00	1.00	1.00	-4.82
Fu12	-6.17	-1.78	-1.89	-5.88	-5.88	-10.2	-0.246	-0.364	-4.35	0.999	1.00	1.00	1.00	-5.12
Fu13	-6.05	-1.57	-1.81	-5.98	-5.98	-10.2	-0.195	-0.442	-4.61	0.999	1.01	1.01	1.00	-5.60
Fu14	-6.10	-1.64	-1.84	-5.95	-5.95	-10.2	-0.215	-0.409	-4.52	0.999	1.01	1.01	1.00	-5.86
Fu15	-6.16	-1.68	-1.82	-5.89	-5.89	-10.2	-0.237	-0.376	-4.44	0.999	1.01	1.01	1.00	-6.04
Fu16	-6.32	-2.36	-2.33	-6.16	-6.16	-10.2	-0.318	-0.285	-4.12	0.999	1.00	1.00	1.00	-2.09
Fu17	-6.99	-2.58	-1.97	-5.12	-5.12	-10.1	-0.704	-0.096	-3.24	0.999	1.00	1.00	1.00	-3.63
Fu18	-6.16	-1.55	-1.69	-5.77	-5.77	-10.2	-0.236	-0.378	-4.45	0.999	1.01	1.01	1.00	-2.16
Fo1	-5.14	-0.94	-2.19	-7.42	-7.42	-10.4	-0.024	-1.27	-6.51	0.999	1.01	1.01	0.999	-4.07
Fo2	-4.97	-1.00	-2.43	-7.86	-7.86	-10.4	-0.0159	-1.44	-6.87	0.999	1.01	1.01	0.999	-4.39
Fo3	-5.96	-2.46	-2.94	-7.43	-7.43	-10.5	-0.125	-0.602	-5.1	0.999	1.01	1.01	1.00	-9.19
Fo4	-2.20						1.00	0	0	0.999	1.01	1.01	0.999	-3.66
Fo5	-2.20						1.00	0	0	0.999	1.01	1.01	0.999	-4.07
Fo6	-2.10						1.00	0	0	0.999	1.01	1.01	0.999	-4.15
Fo7	-4.87	-1.75	-3.22	-8.65	-8.65	-10.3	-0.0145	-1.48	-6.92	0.999	1.01	1.01	0.999	-4.62
Fo8	-4.62	-1.06	-2.83	-8.59	-8.59	-10.4	-0.0073	-1.78	-7.55	0.999	1.01	1.01	0.999	-4.66
Fo9	-4.67	-1.51	-3.16	-8.77	-8.77	-10.3	-0.0095	-1.67	-7.28	0.999	1.01	1.01	0.999	-4.07
Fo10	-4.69	-1.86	-3.46	-8.98	-8.98	-10.2	-0.0108	-1.61	-7.13	0.999	1.01	1.01	0.999	-3.35
Fe	-5.87	-1.98	-2.44	-6.85	-6.85	-10.3	-0.129	-0.591	-5	0.999	1.01	1.01	1.00	-2.26
AS	-8.03	-4.67	-3.03	-5.38	-5.38	-10.4	-1.66	-0.012	-2.36	0.999	1.01	1.01	1.00	-7.33
AS23	-7.06	-3.75	-3.09	-6.44	-6.44	-10.4	-0.741	-0.087	-3.44	0.999	1.01	1.01	1.00	-0.57
SW	-3.48	0.265	0.349	-3.55	-3.55	-7.38	-0.345	-0.261	-4.16	0.999	1.01	1.01	1.00	-4.18

Table A 6 -1 Temperature estimation as function of water geothermometers (Inguaggiato et al., 2000)

Na-K	t=(854/0.700 + log Na/K) – 273.15	T&F: Truesdell and Fournier, 1975	(Eq1)
Na-K	t=(883/0.780 + log Na/K) – 273.15	T: Tonani, 1980	(Eq2)
Na-K	t=(933/0.993 + log Na/K) – 273.15	A: Arnorsson et al. 1983	(Eq3)
Na-K	t=(1271/1.483 + log Na/K) – 273.15	F: Fournier, 1979	(Eq4)
Na-K	t=(1178/1.470 + log Na/K) – 273.15	N&N: Nieva & Nieva, 1987	(Eq5)
Na-K	t=(1390/1.750 + log Na/K) – 273.15	G: Giggenbach, 1981	(Eq6)
Li-Mg	t=(2200/5.470 + log Li/√Mg) – 273.15	K&M: Kharaka and Mariner, 1988	(Eq7)
SiO_2	t=(1390/5.18 + log SiO2) – 273.15	F: Fournier, 1977	(Eq8)

Table A 6 -2 Calculated temperatures for sample which are in equilibrium by using cationic geothermometers. See equations Eq1 –Eq8

Thermometer References	Na-K (T&F)	Na-K (T)	Na-K (A)	Na-K (F)	Na-K (N&N)	Na-K (G)	Li-Mg (K&M)	SiO2 (F)
Fu13	248	240	241	229	216	244	254	146
Fu14	251	244	244	231	218	246	254	150
Fu15	234	228	229	220	207	236	255	145
Fu18	296	285	280	260	246	272	295	144
Fu3	333	320	310	282	268	292	315	148
Fu6	232	225	227	219	205	234	226	171
Fu11	317	305	298	273	258	284	269	167
Fu12	317	305	298	273	258	284	270	167

Figure A 7 Saturation indices for goethite, kaolinite, quartz, K-mica, talc, calcite and Ca-montmorillonite at temperatures from 20 to 230 °C for sample Fu14. Equilibrium conditions at discharging temperature (41.6 °C) are shown by the green line.

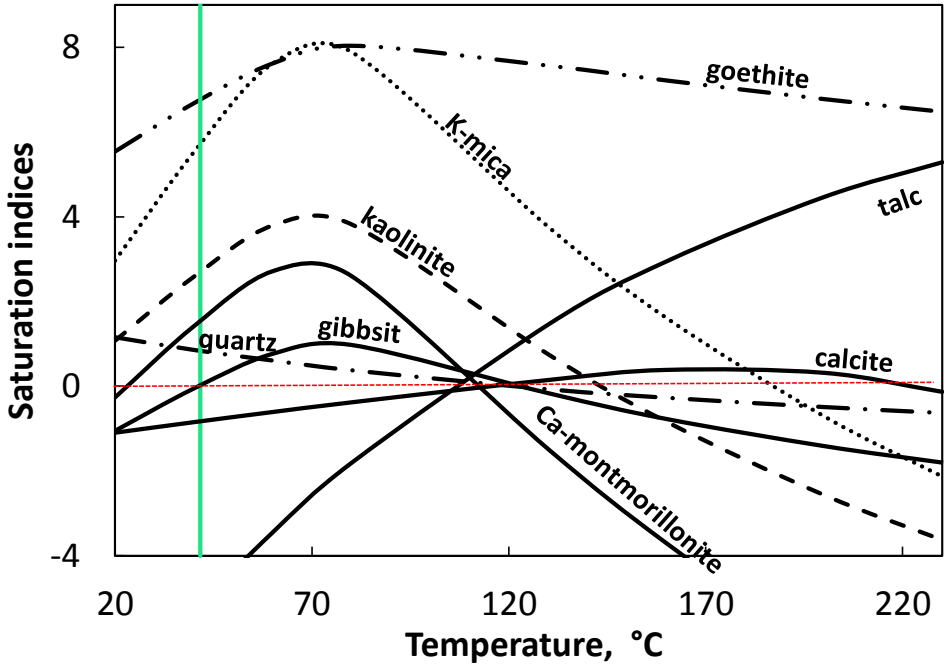

Figure A 8 Saturation indices for goethite, kaolinite, quartz, K-mica, talc, Ca-montmorillonite and gibbsite at temperatures from 20 to 230 °C for sample Fu3. Equilibrium conditions at discharging temperature (73.1 °C) are shown by the green line.

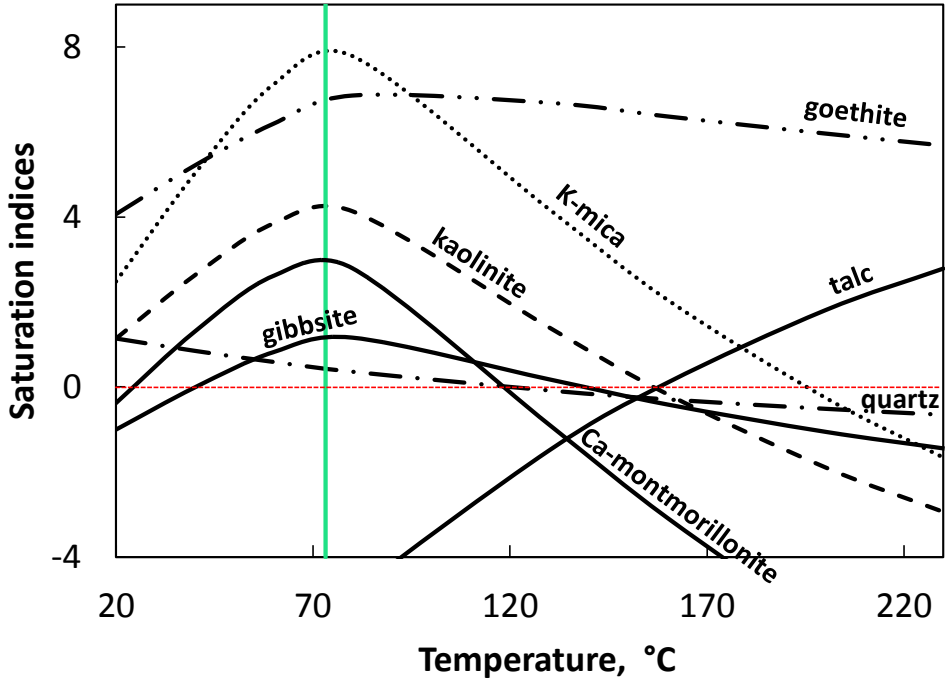

Figure A 9 Saturation indices for goethite, kaolinite, quartz, K-mica, talc, Ca-montmorillonite, gibbsite and albite at temperatures from 20 to 230 °C for sample Fu6. Equilibrium conditions at discharging temperature (86 °C) are shown by the green line.

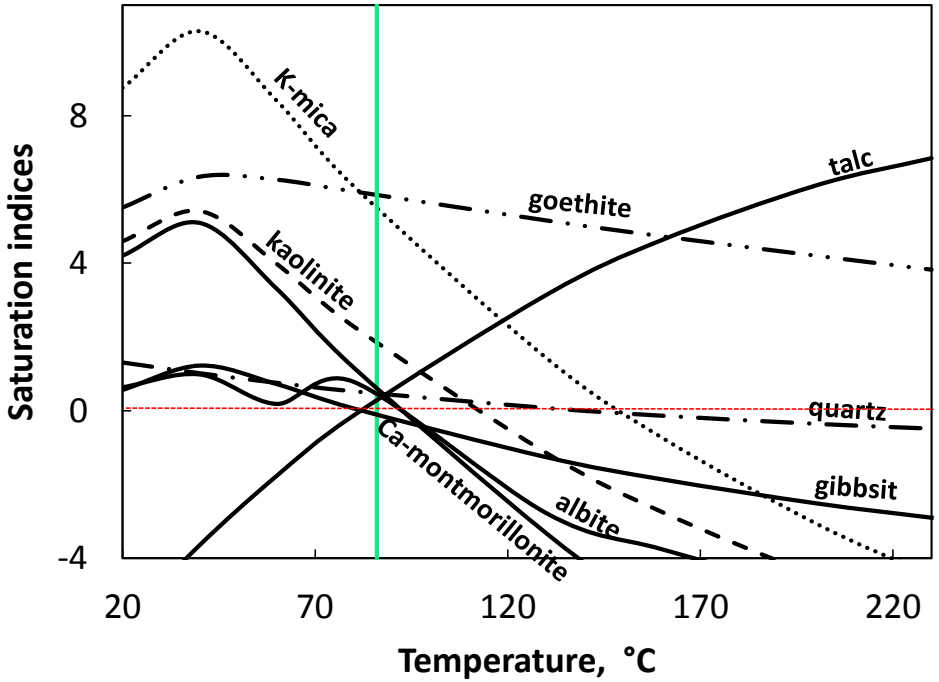

Figure B 1 Rock sample *SW* (A) and overview of thin section (B), in the green square even more detailed pictures were taken with transmitted and crossed nicols (see Figure 27)

Figure B 2 Rock sample *Fo9* (A) and overview of thin section (B), in the green square even more detailed pictures were taken with transmitted and crossed nicols (see Figures 28 and Figure 29)

Figure B 3 Overview of thin section *Fo10*, in the green square even more detailed pictures were taken with transmitted and crossed nicols (see Figure 30)

Figure B 4 Rock sample *Fu9* (A) and Overview of thin section (B), in the green square even more detailed pictures were taken with transmitted and crossed nicols (see Figures 31 and 32)

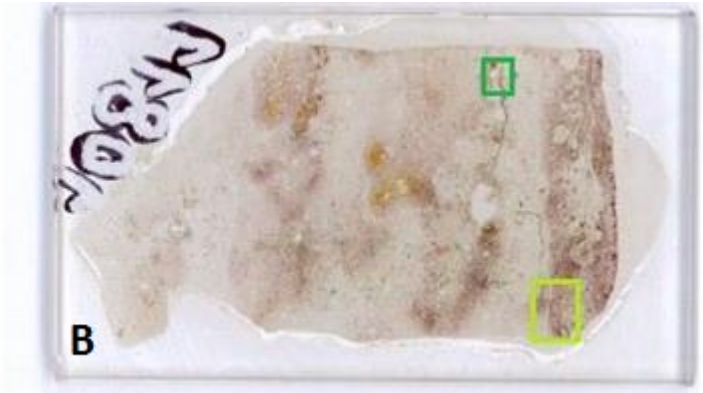

Figure B 5 Rock sample *Fu10_1* (A) and Overview of thin section (B), in the green square even more detailed pictures were taken with transmitted and crossed nicols (see Figures 33 and 35)

Figure B 6 Overview of thin section *Fu10_2*, in the green square even more detailed pictures were taken with transmitted and crossed nicols (see Figure 34)

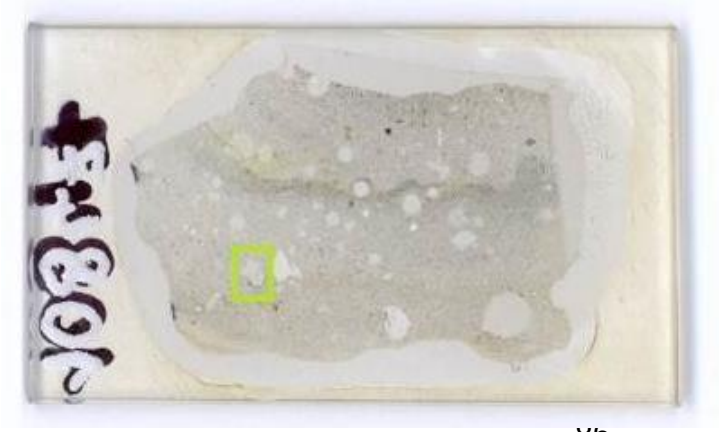

Figure B 7 Overview of thin section *Fu17_1*, in the green square even more detailed pictures were taken with transmitted and crossed nicols (see Figure 36)

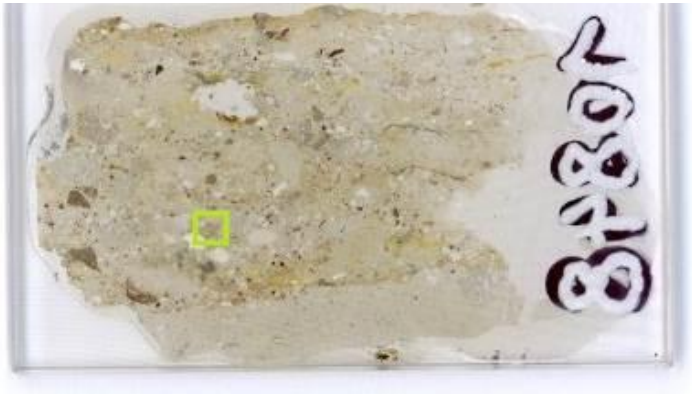

Figure B 8 Rock sample *Fu17_2* (A) and Overview of thin section (B), in the green square even more detailed pictures were taken with transmitted and crossed nicols (see Figure 37 and 38)

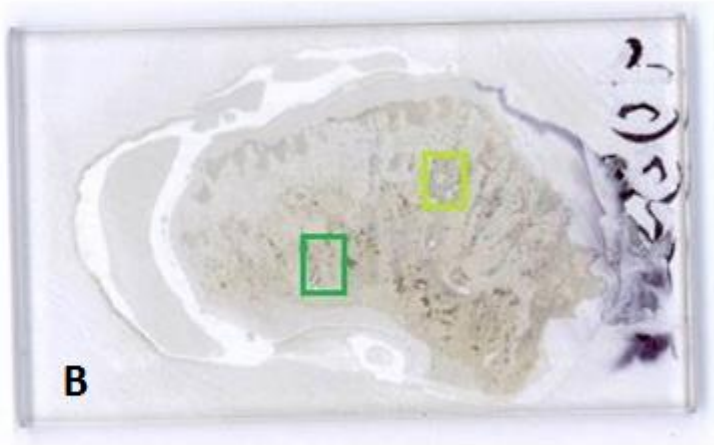

Table C 1 Chemical composition of rock and precipitate samples by X – ray fluorescence spectroscopy in weight percentage

References	Na_2O	MgO	$Al2O_3$	SiO_2	SO_3	K_2O	CaO	TiO_2	Fe_2O_3	Annealing loss	Σ
Fo9	6.27	0.39	16.5	60	0.03	4.73	0.78	0.6	8.37	1.54	99.2
Fo10	5.53	0	15.8	68.7	0.21	4.7	0.48	1.07	0.81	2.41	99.8
Fu9	0.62	0	14.7	68.2	1.57	0.78	0.12	0.6	3.19	9.99	99.7
Fu10_1	4.38	0.27	16.9	62.7	0.26	4.01	0.85	1.03	2.95	6.1	99.5
Fu10_1(inside)	4.25	0.21	17.3	62.8	0.36	4.37	0.81	1.05	2.72	5.57	99.5
Fu10_2	4.42	0	17.5	63.3	0.92	5.43	1.45	2.38	1.22	2.69	99.3
Fu17_1	1.5	0	1.81	88.1	0.2	0.48	0.21	0.05	0.15	7.43	99.9
Fu17_2	2	0	5.14	84.4	0.32	1.11	0.38	0.32	0.3	5.87	99.9

Figure C 2 X-ray diffraction of *SW* (P: potassium feldspar, G: Goethite, H: Hornblende, AG: Augite, SC: Sanidine)

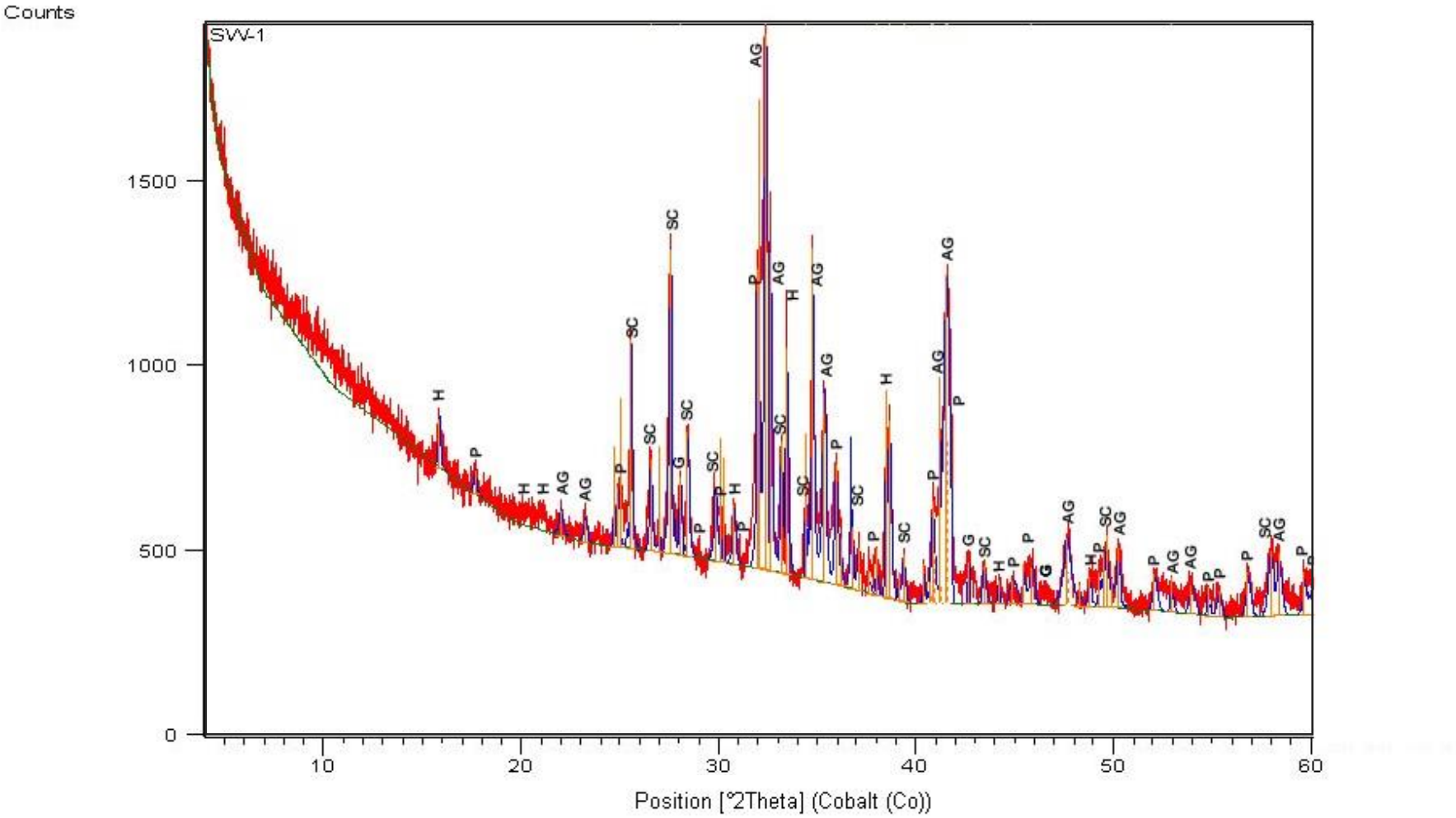

Figure C 3 X-ray diffraction of *Fo10* (P: potassium feldspar)

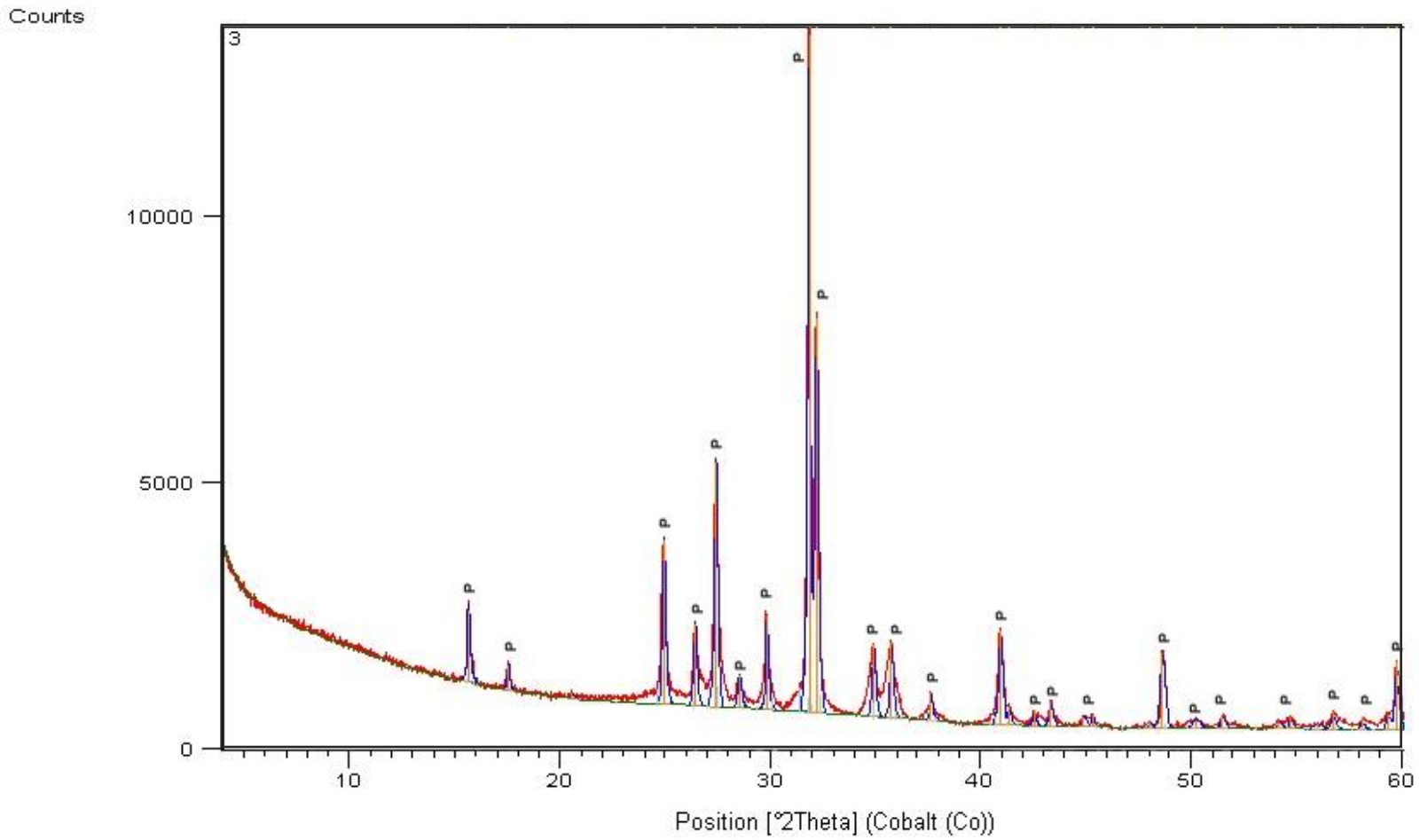

Figure C 4 X-ray diffraction of *Fu9* (K: Kaolinite, Au: Alunite; Q: Quartz, I: Ironoxide, P: potassium feldspar)

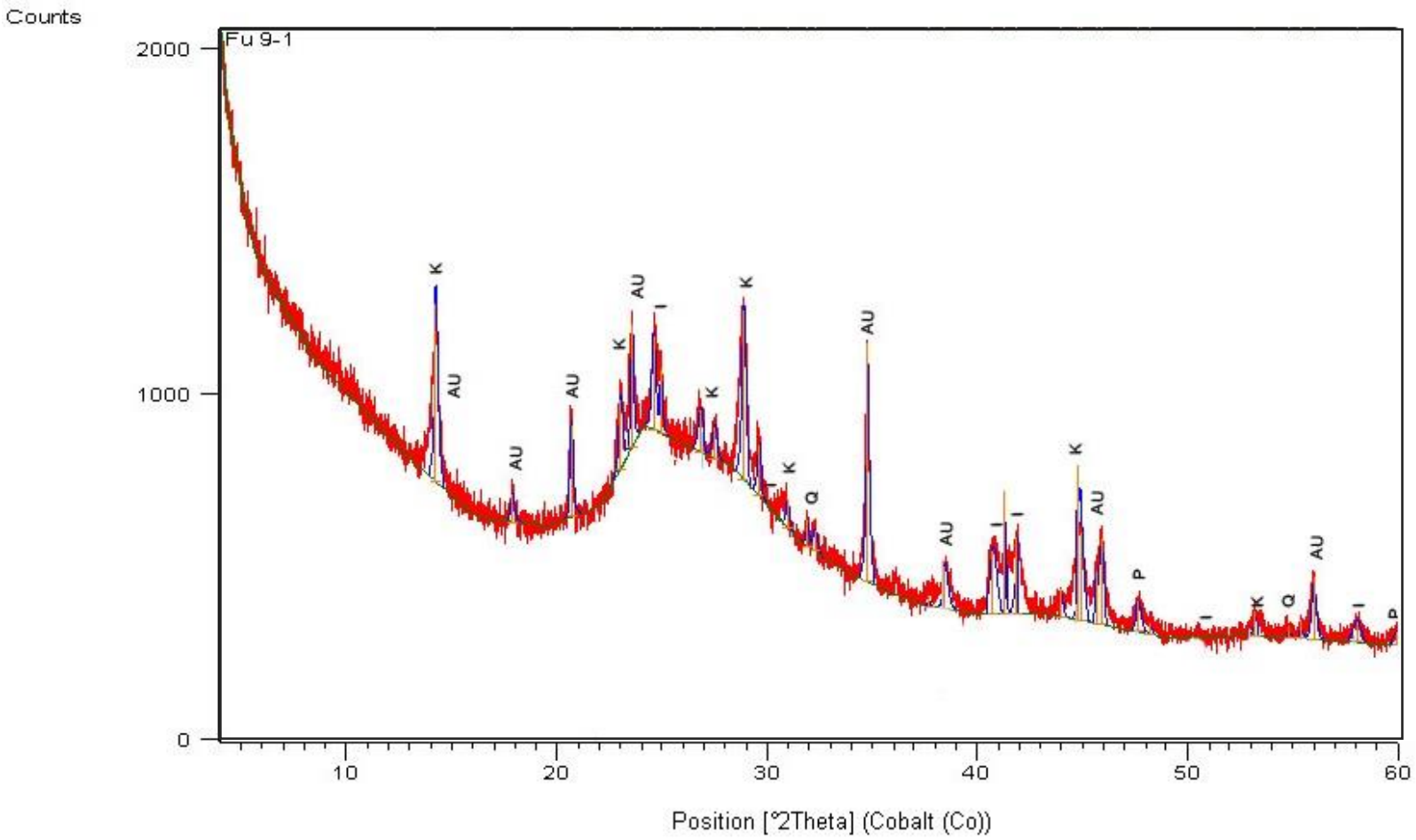

Figure C 5 X-ray diffraction of *Fu10_1* (P: potassium feldspar, AB: Albite, G: Goethite. Q: Quartz)

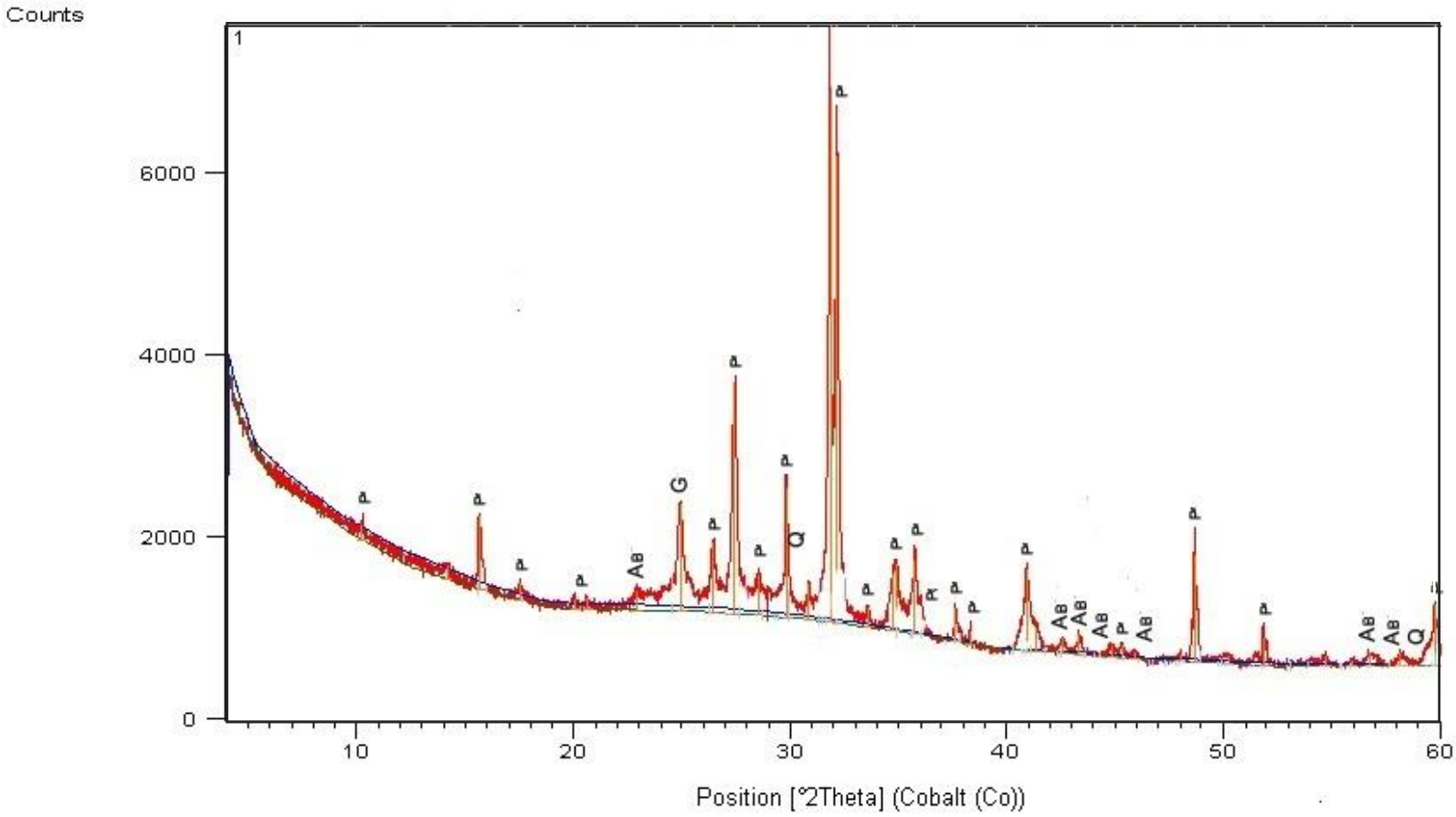

Figure C 6 X-ray diffraction of *Fu10_1* inside (P: potassium feldspar, Q: Quartz, C: Clinopyroxene)

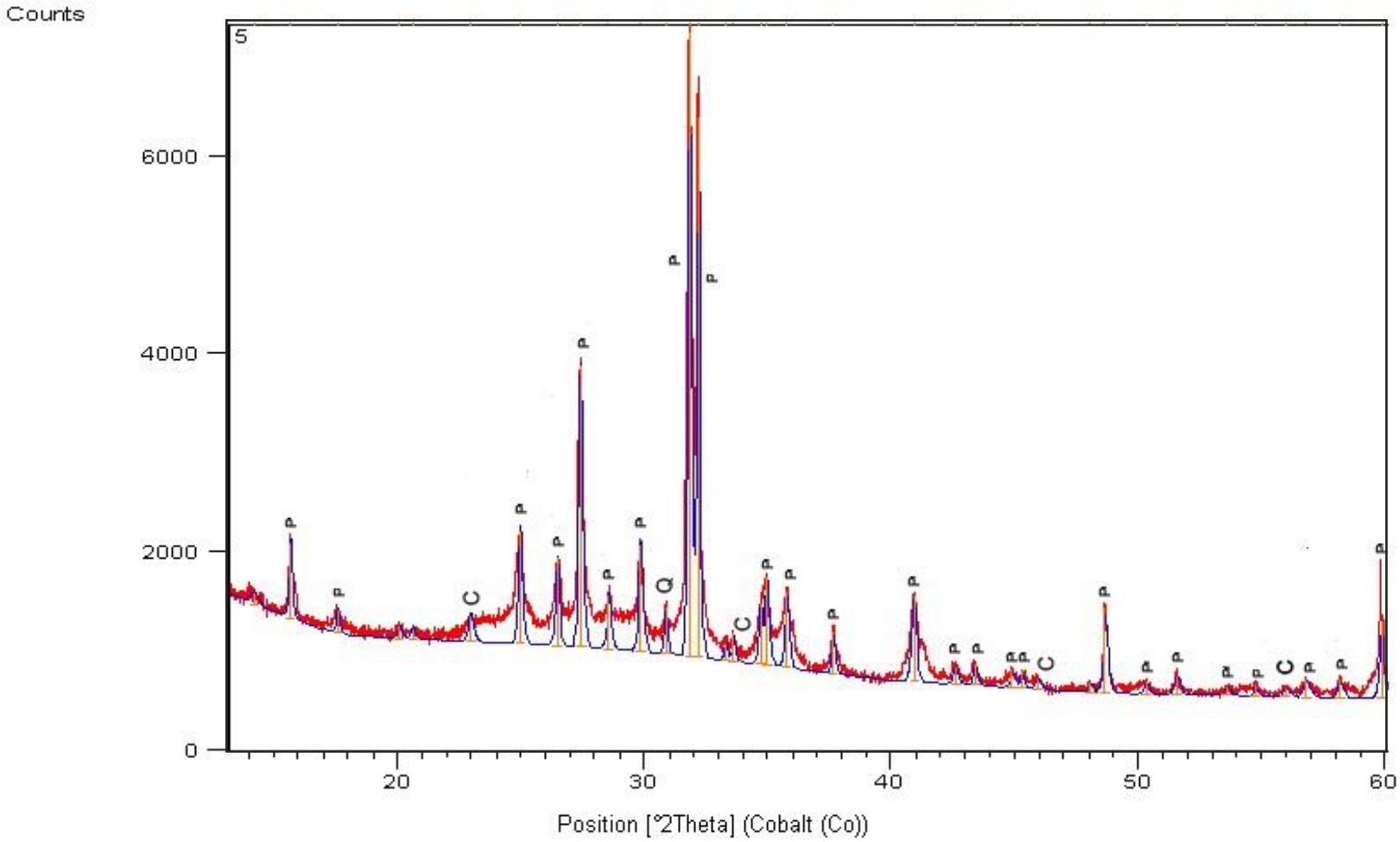

Figure C 7 X-ray diffraction of *Fu10_2* (P: potassium feldspar, AB: Albite, AU: Alunite, G: Goethite, CP: Clinopyroxene)

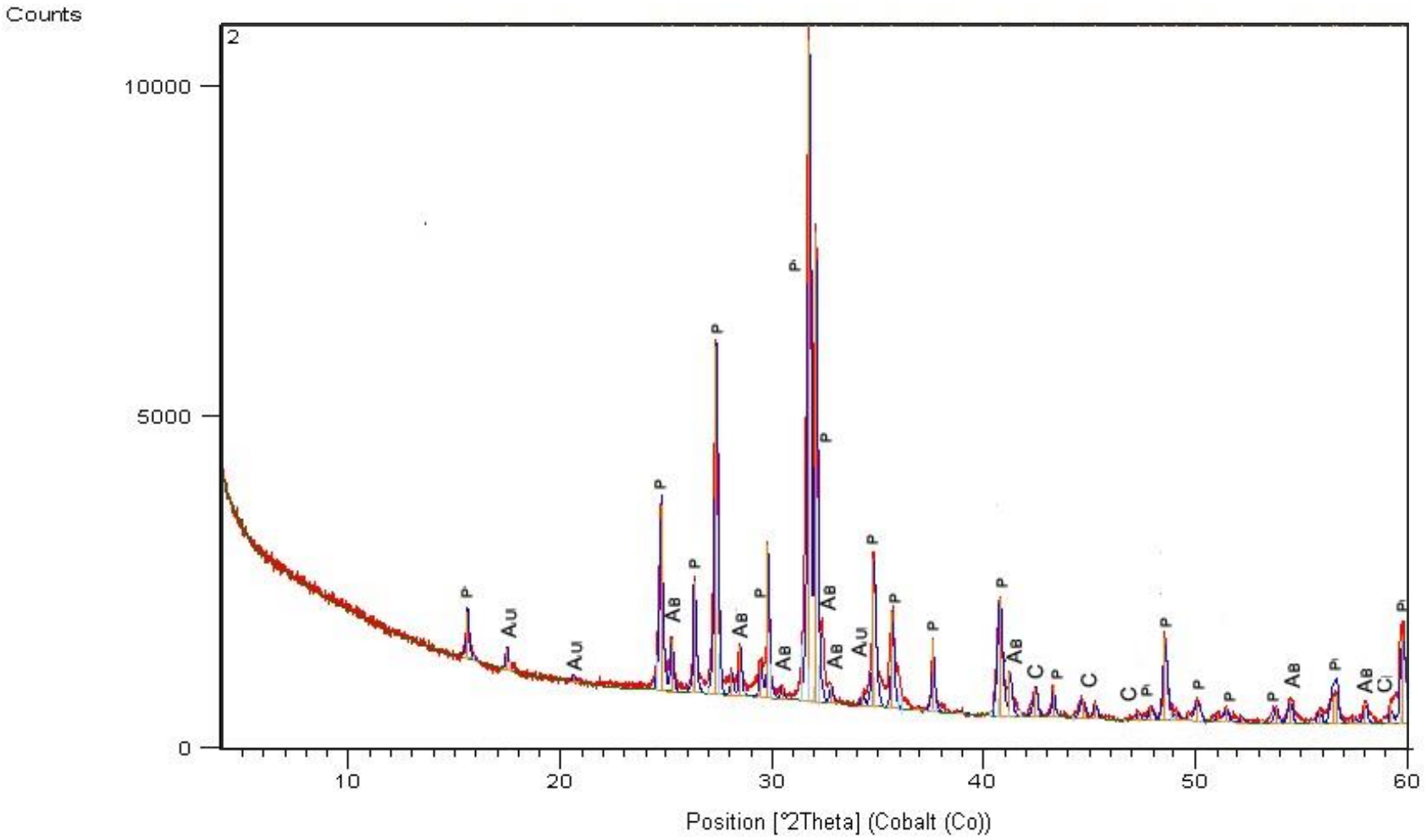

Figure C 8 X-ray diffractionof *Fu17* and *Fu17_2* (Au: Alunite, An:Anorthite)

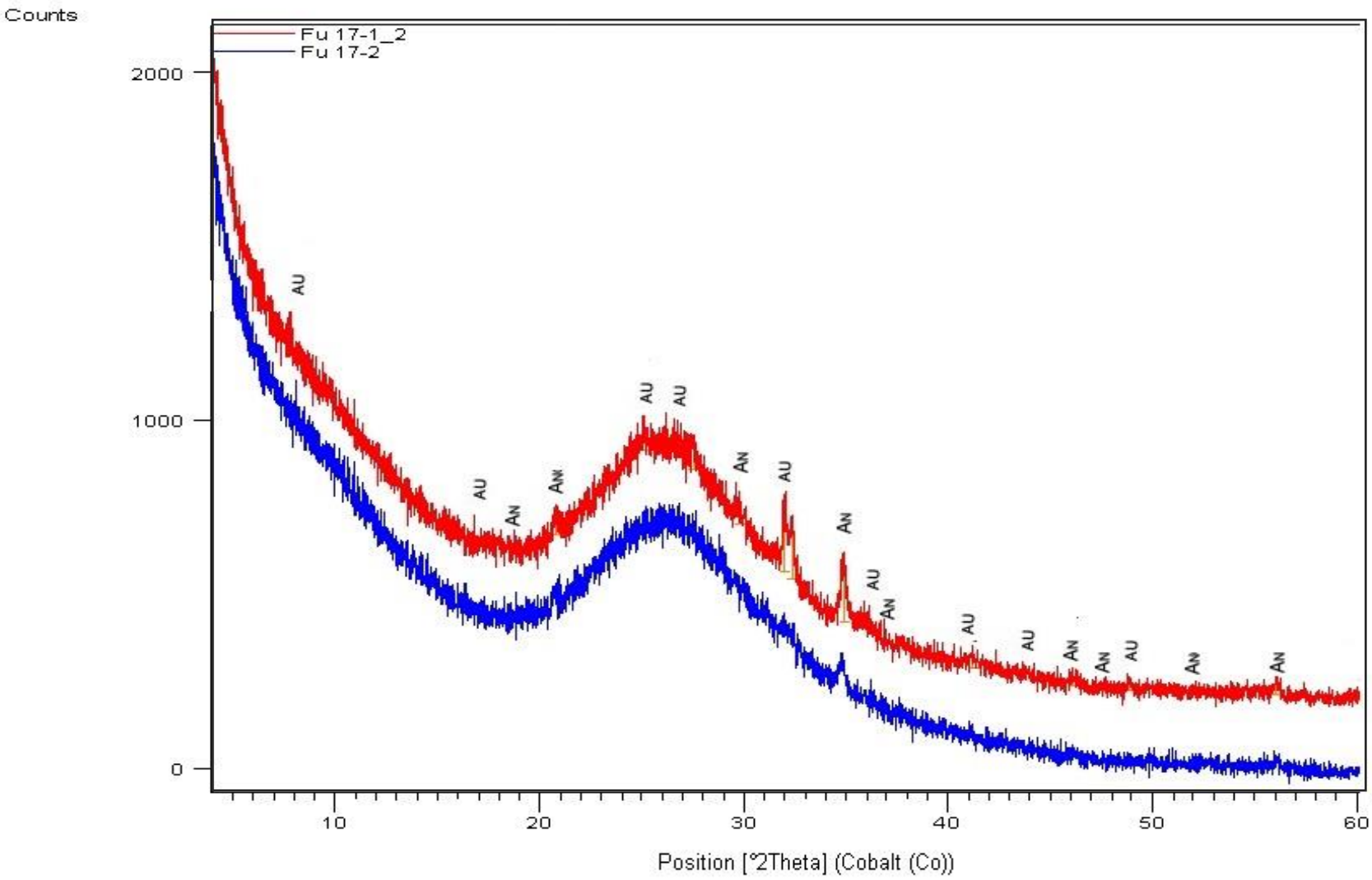

Figure C 910 IR vibrations of sampleof *SW* (H: Hornblende)

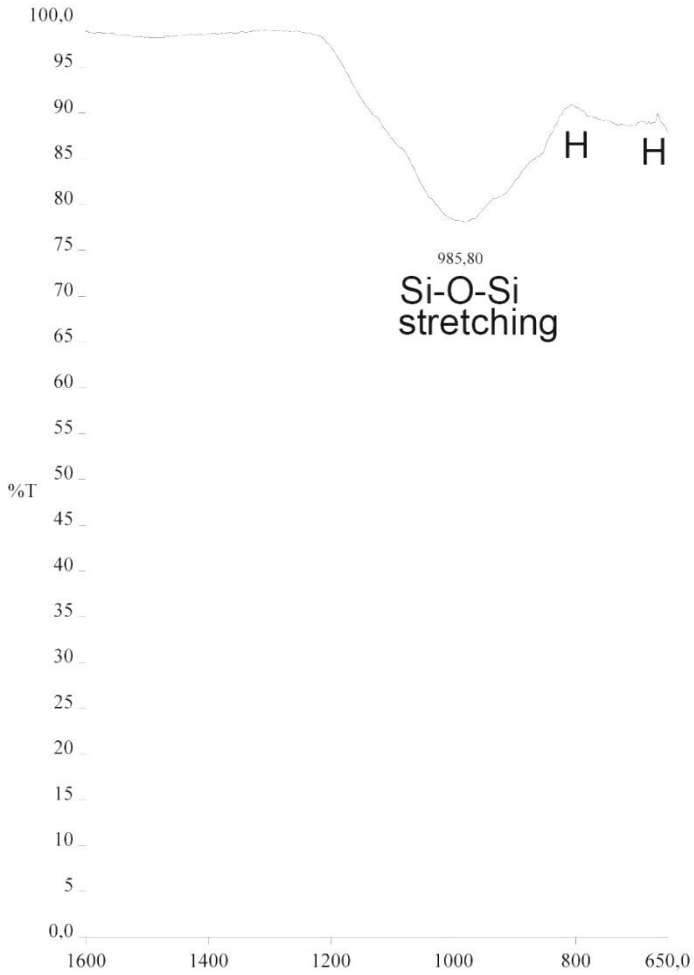

Figure C 9 IR vibrations of sampleof *Fu9* (A: Alunite)

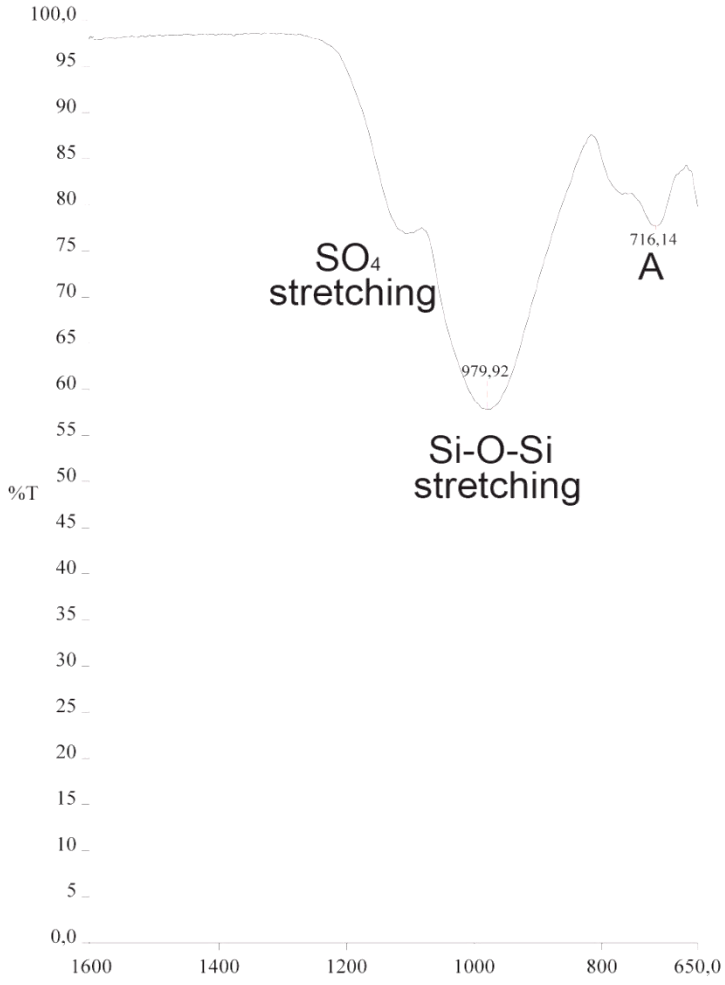

Figure C 11 IR vibrations of sample *Fu17_1* (A: Alunite)

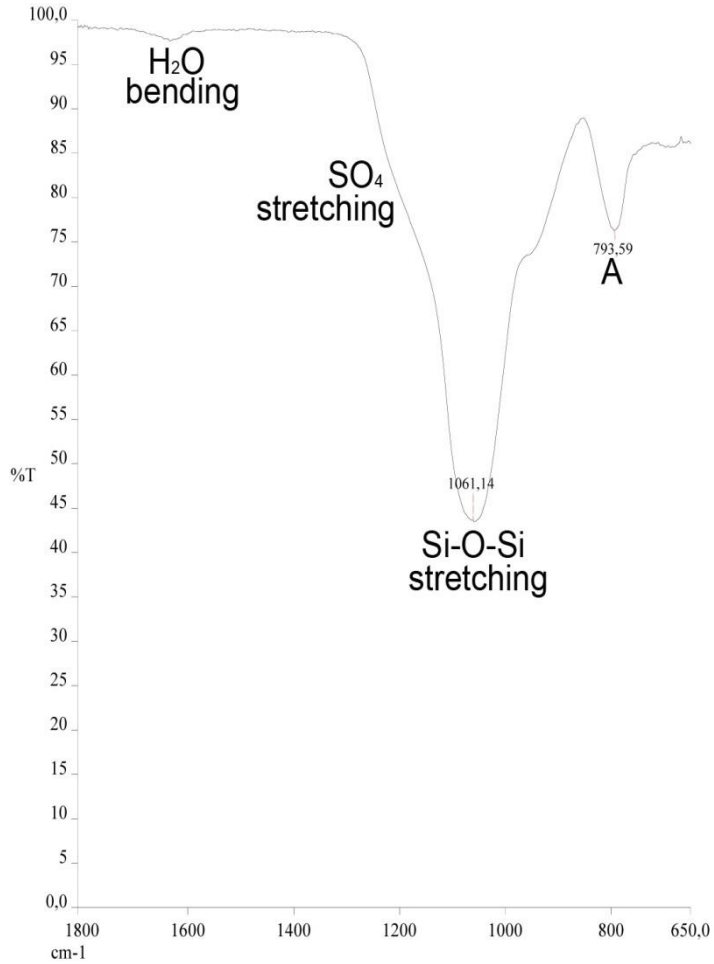

Figure C 12 IR vibrations of sample *Fu17_2* (An: Anorthite)